

8. SITE 720¹

Shipboard Scientific Party²

HOLE 720A

Date occupied: 29 August 1987

Date departed: 2 September 1987

Time on hole: 4 days, 11 hr, 30 min

Position: 16°07.796'N, 60°44.621'E

Water depth (sea level; corrected m, echo-sounding): 4037.5

Water depth (rig floor; corrected m, echo-sounding): 4048

Bottom felt (m, drill pipe): 4045.4

Penetration (m): 414.3

Number of cores: 43

Total length of cored section (m): 414.3

Total core recovered (m): 89.4

Core recovery (%): 21.6

Oldest sediment cored:

Depth sub-bottom (m): 414.3

Nature: turbiditic silt, sand, and mud

Age: Pleistocene (NN 19?)

Measured velocity (km/s): 1.9

Principal results: Site 720 is located on the westernmost part of the middle Indus Fan. The sediments drilled at Site 720 consist of turbiditic clastic sediments intercalated with pelagic nannofossil ooze; the entire sequence is Pleistocene in age (NN21 to NN19) and has been subdivided into two lithologic units.

Unit I: Nannofossil ooze from 0 to 17.2 mbsf (Holocene to upper Pleistocene) was deposited during a phase (about 0.5 Ma long) of pelagic deposition following abandonment of the major turbidite channel. Pelagic deposition persisted during several sea-level cycles of the late Quaternary. The nannofossil ooze has variable carbonate content and was deposited at a rate of approximately 32 m/m.y.

Unit II: Clastic sediments of turbiditic origin include silty clays, silty sands, sands, and clays and dominate the section from 17.2 mbsf to total depth of 414.3 mbsf. The turbidite sequence is intercalated with numerous thin nannofossil ooze layers (<10 m thickness) observed in the cores and in downhole log data. They are thought to represent intervals of pelagic deposition related to changes in turbidite flux, which possibly is associated with sea-level changes and abandonment of channels with subsequent deposition on elevated levees. The rate of sedimentation of the turbidite sequence varies from 137 to 944 m/m.y.

BACKGROUND AND OBJECTIVES

Site 720 is located at 16°07.80'N and 60°44.62'E, on the westernmost part of the middle Indus Fan in a water depth of 4045 m. The Indus Fan is 1500 km long, 960 km across at its widest point, covers an area of over 1.1×10^6 km² and is the dominant physiographic feature of the Arabian Sea (Whitmarsh et al., 1974; Kolla and Coumes, 1984). The fan is primarily fed

by the Indus River, which drains the Himalaya mountains and crosses the fluvial basins and lowlands of Pakistan.

Initiation of Indus Fan deposition is thought to have begun in Oligocene-early Miocene time as the result of collision between the Indian and Asian plates which caused major uplift of the Himalaya (Whitmarsh et al., 1974). A coincident lowering of sea level is also thought to have contributed to the onset of fan deposition (Kolla and Coumes, 1987). Sediments characteristic of the Indus drainage, which is illite-rich (Kolla et al., 1981a; Emeis, 1985), began to accumulate on the distal Indus Fan (DSDP Site 221) in the late Oligocene (Kolla and Coumes, 1987; Weser, 1974). Although major uplift of the Himalaya occurred during the early and middle Miocene, the most recent phase of accelerated uplift may have begun in the late Pliocene and has continued to the present (Mercier et al., 1987).

Previous drilling of the western Indus Fan (DSDP Site 222) penetrated 1300 m, and recovered alternating facies of gray carbonate-rich and green nannofossil-rich detrital silty clays (Whitmarsh et al., 1974). Sediment accumulation rates at Site 222 were very high (greater than 600 m/m.y.) in the late Miocene, and decreased in the early and late Pliocene (135-300 m/m.y.) and in the Pleistocene (40 to 50 m/m.y.). The entire Pleistocene section was dominated by a more pelagic (green) facies and has slower accumulation rates. Hence, the apparent increase in uplift rate of the Himalaya during the Pliocene-Pleistocene is not reflected in the accumulation rates at Site 222. The lower rates of deposition in the Pleistocene, however, may result from channel- and canyon-switching at the head of the fan (McHargue and Webb, 1986). Although deposition at Site 222 is related to sediment flux from the Indus, only about 10% of the recovered section is coarse-grained (Weser, 1974). The depositional processes responsible for these dominantly fine-grained facies are not clear, but Jipa and Kidd (1974) concluded that traditional turbidite mechanisms were not responsible for depositing such facies. Some of the sediment at Site 222 may have come from the Oman coast via downslope and eolian transport. Kolla and Coumes (1987) emphasized the roles of channel abandonment, channel avulsion, and overbank spilling in developing mud-rich deposits, although they did not directly consider the lithologic section from Site 222. On the basis of echo characteristics (Type I) and near-surface sediment samples, Kolla and Coumes (1987) devised a depositional model for the fan that predicts the sediments of the middle fan to lower fan transition should be primarily fine-grained muds with only a few sand-silt beds deposited by overbank flow.

Site 720 is located about 360 km south-southwest of Site 222, at a water depth of 4045 m (Fig. 1). The site lies on the western edge of the Indus Fan, near the boundary between the middle and the lower fan (Kolla and Coumes, 1987). Sediment thickness at Site 720 is greater than 2000 m (Leg 117 Site Survey; Kolla and Coumes, 1987). The site lies near magnetic anomaly 25 (Whitmarsh, 1974), which indicates a Paleocene basement age of about 60 Ma. The site is about 5 km east of a meandering channel that is about 1.5 km wide, 50 m deep, and has a levee elevation of about 30 m above the surrounding seafloor (Fig. 1B). This location was selected to avoid channel deposits,

¹ Prell, W. L., Niitsuma, N., et al., 1989. *Proc. ODP, Init. Repts.*, 117: College Station, TX (Ocean Drilling Program).

² Shipboard Scientific Party is as given in the list of Participants preceding the contents.

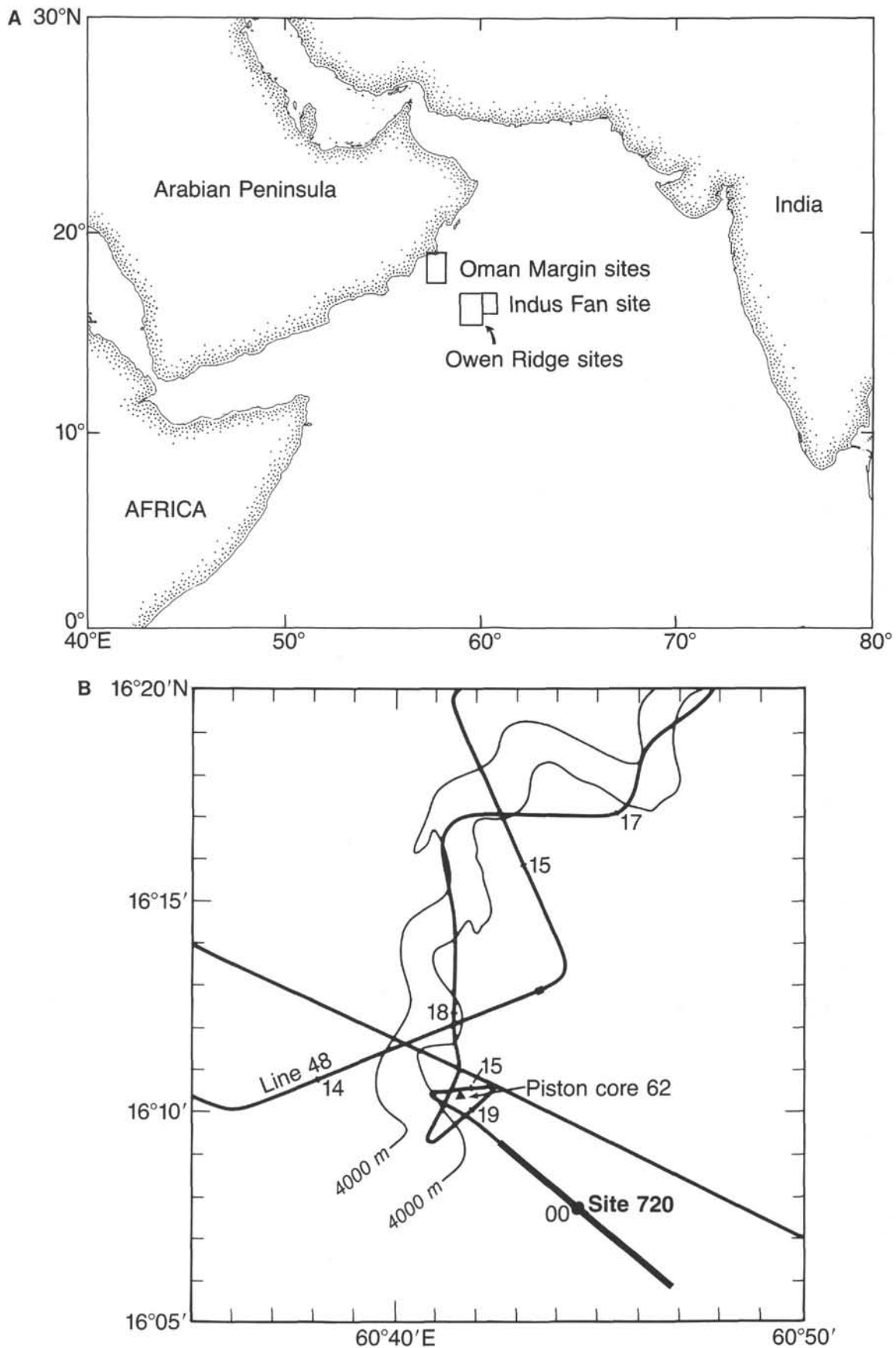


Figure 1. A. Location of Site 720 and operation area of Leg 117 in the northwest Indian Ocean. B. Tracks of RC2704 seismic lines 48 and 49, location of piston core 62, and position of Site 720 in relation to channel. Thick line denotes part of seismic line 49 depicted in Figure 2.

thereby maximizing the opportunity to collect a relatively continuous depositional record that can be related to uplift and sea-level changes. Hence, the site was located on the middle fan in the western portion of the fan away from known depocenters of sand. The site was selected on the SCS (single channel seismic) track of RC2704 (Line 49, 6-09-86, 0000 hr; Fig. 2) on the basis of the uniformity of reflectors and the lack of strong acoustical facies associated with coarse channel fill. A 12-m piston core near the site (RC2762) revealed relatively high (30%–70%) carbonate content, no distinct turbidites, and mostly silty sediment with an average accumulation rate of about 25 m/m.y (Prell, W. L., unpubl. data).

Objectives

The principal objectives of Site 720 were: (1) to recover a continuous upper Neogene section of fine-grained overbank deposits from the middle fan region of the western Indus Fan; (2) to identify the depositional facies, their composition, and their accumulation rates for comparison to other Indus Fan and Ganges Fan (Leg 116) sites; and (3) to interpret the depositional history of the Indus Fan sediments in terms of uplift of the source region (Himalaya), changes in sea level, changes in climate, circulation, and weathering processes.

OPERATIONS

Leg 117 departed Colombo, Sri Lanka, on 23 August 1987 at 2200 hr and set out to transit for the first operational area on the middle Indus Fan at Site 720. During the transit of 1234 nmi and traveling at an average speed of 9.9 kt, continuous magnetometer and 3.5-kHz profiles were obtained. Upon approach to Site 720, the ship slowed down, seismic gear was deployed on 29 August at 0615, and the site was selected on the basis of a single-channel seismic profile obtained on the second pass (see Figs. 2 and 3).

The beacon was dropped at 0930, the seismic gear was retrieved, and the ship maneuvered back to the beacon. The Global Positioning Satellite (GPS) established the position of Site 720 as being 16°07.796'N and 60°44.621'E. Water depth recorded by the Precision Depth Recorder (PDR) was 4,048.3 m. Pipe was being tripped by 1115 hr and the mud line was established at 4045.3 m around 2400 on 29 August.

Three Advanced Hydraulic Piston Corer (APC) cores were recovered with excellent recovery of 99.4%, until 40,000 pounds of overpull in sands below Core 117-720A-3H made Extended Core Barrel (XCB) coring necessary. Recovery declined dramatically in silty sands and sands retrieved in Cores 117-720A-4X to -43X, and average recovery dropped to 15.7%. Overall rate of recovery of Hole 720A, drilled to a total depth of 414.3 mbsf with Core 117-720A-43X, was 21.6% (see Table 1).

In the light of poor recovery coring was terminated at 1130 hr on 1 September. The hole was conditioned for logging by sweeping with 30 bbls of gel and a wiper trip to 70 mbsf. Maximum overpull at this stage was 20,000 pounds. On 1 September at 2230 hr, the pipe was set at 70 mbsf and the three-string Schlumberger tool was rigged and lowered. After a very successful run with the DIT, LSS, and GR combination in the interval from 4,458 to 4,152 m below sea level, the tool became stuck on the way out by a bridge 20 m below the bottom-hole assembly (BHA). An attempt to crimp the tool and cut the logging wire to retrieve the tool with the pipe failed, and the tool was lost with about 2,600 m of logging wire. Hole 720A was cleared by 1430 hr on 2 September, and the ship was underway to Site 721 by 2100.

LITHOSTRATIGRAPHY

The stratigraphic sequence recovered at Site 720 is Quaternary in age and consists predominantly of interbedded silty clays,

clayey silts, silts, and sandy silts, with lesser amounts of sand and nannofossil ooze. This sequence has been subdivided into lithologic units and lithologic facies on the basis of visual core description (color and physical and biological structures), sediment composition determined by smear slide analysis, and carbonate content. A more detailed discussion of the carbonate and organic carbon contents at this site is located in the "Organic Geochemistry" section (this chapter). Sediment residues from nine interstitial water samples were analyzed by X-ray diffractometry (XRD) on the shipboard Philips system, providing qualitative mineralogical information.

Lithologic Units

The stratigraphic sequence recovered at Site 720 has been subdivided into two lithologic units, as shown in Figure 4 and Table 2. Lithologic Unit I is relatively uniform, while lithologic Unit II is heterogenous. Because of this heterogeneity, three distinct facies have been recognized within Unit II. The characteristics and general occurrences of these units and facies are summarized in Table 2.

Unit I (Depth: 0–17.22 mbsf; Age: Holocene–Pleistocene)

Core 117-720A-1H to 117-720A-2H-6, 32 cm.

Lithologic Unit I is composed of nannofossil ooze and foraminifer-bearing nannofossil ooze, with colors of light olive gray (5Y 6/2) to gray (5Y 6/1) and light greenish-gray (5GY 7/1) to grayish-green (5G 5/2). Faint color banding on a scale of several centimeters is common throughout this interval, and the unit is slightly to moderately bioturbated.

Smear slide analyses indicate that Unit I contains 70%–85% nannofossils, 5%–20% foraminifers, 1%–5% radiolarians, trace diatoms, and 1%–5% each of quartz, volcanic glass, clays, and accessory minerals. The smear slide data do not indicate any consistent trends in composition through this interval. Carbonate content (Fig. 5 and Table 3) ranges from 35.5% to 68.4%, supporting the classification of these sediments as carbonate oozes. The residue of one interstitial-water sample from this interval (117-720A-1H-4, 145–150 cm) was analyzed by X-ray diffractometry. Calcite, quartz, and kaolinite peaks were identified on the diffractogram, with the calcite peaks dominant.

Unit II (Depth: 17.22–414.3 mbsf; Age: Pleistocene)

117-720A-2H-6, 32 cm, to Core 117-720A-43X.

Lithologic Unit II is dominated by interbedded silty clays, silts, silty sands, and sands, which form alternating bands of light and dark color, and minor occurrences of nannofossil ooze. A silty zone with abundant charcoal occurred at 117-720A-12X-2, 21–28 cm. The discontinuous recovery at Site 720 and the heterogeneous nature of this stratigraphic interval complicate the identification of stratigraphically-continuous and unique subunits. Three facies, however, can be identified, and their repeated occurrences characterize lithologic Unit II (Table 2).

Calcareous Facies

The calcareous facies is composed of nannofossil ooze, nannofossil-rich mud, and associated muds and clays, generally showing slight to moderate bioturbation. The calcareous facies ranges in color from light gray (5Y 7/1) to very dark gray (5Y 3/1) and greenish-gray (5GY 6/1) to dark greenish-gray (5GY 4/1). In its thickest occurrences, such as Core 117-720A-30X, the calcareous facies shows color banding on a scale of 20–30 cm.

The composition of the nannofossil oozes in the calcareous facies is similar to that of lithologic Unit I, although nannofossil abundances increase to as much as 90%, and detrital (inorganic) carbonate occurs at abundances up to 20%. The associated clays and muds contain 0%–10% nannofossils, 0%–5% radiolarians, 55%–95% clay, 10%–30% inorganic carbonate,

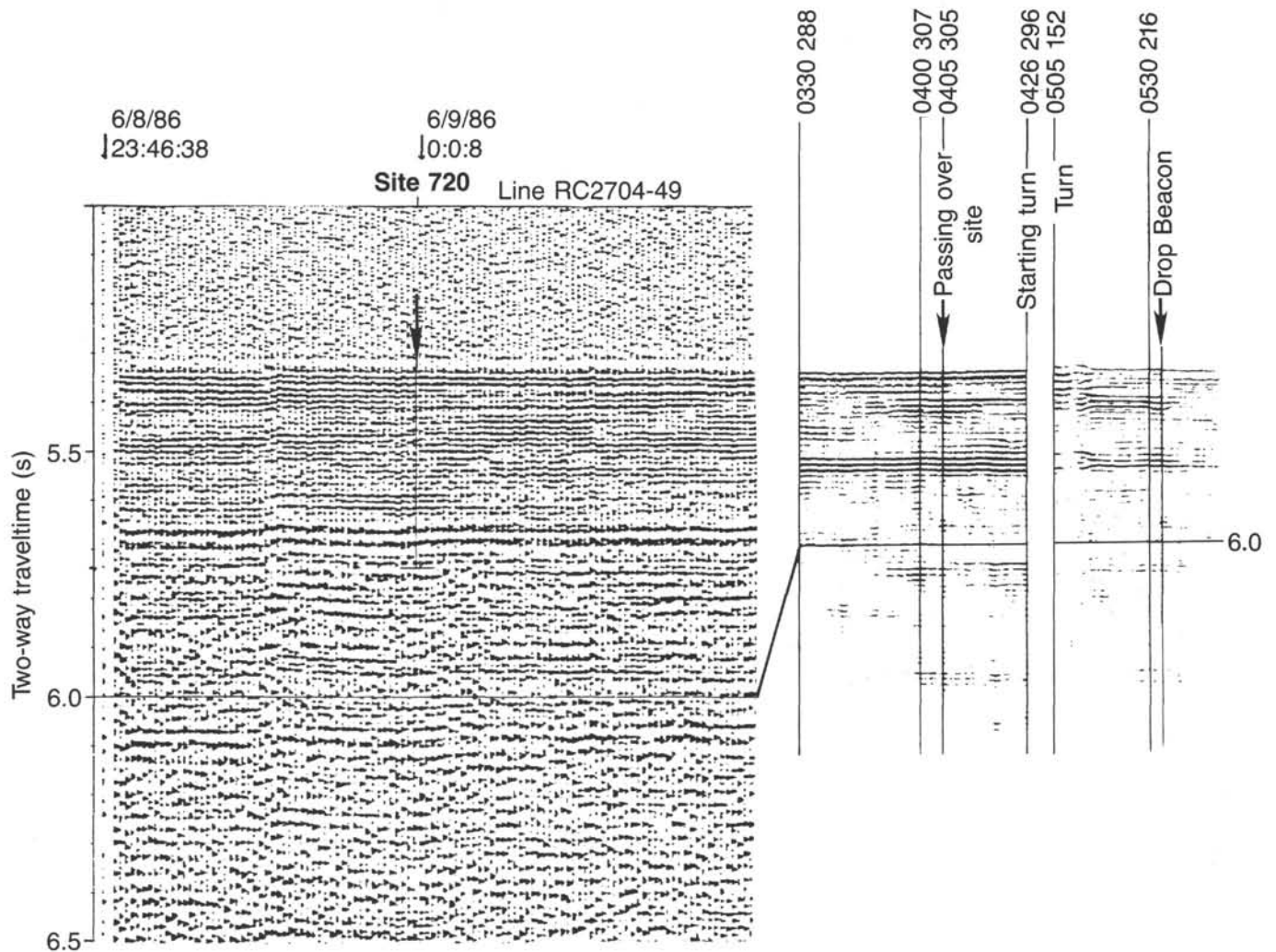


Figure 2. The location of Site 720 on the single channel seismic lines from the site survey (RC2704, Line 49, 6-09-0000 hr) and the *JOIDES Resolution* (8-29-0805).

0%–30% quartz and feldspar, and 0%–5% accessory minerals. Carbonate contents (Table 3, Fig. 5) exceed 50% in the nannofossil oozes, similar to the values obtained for lithologic Unit I. The nannofossil-rich muds, muds, and clays of the calcareous facies have carbonate contents of 9%–20%, reflecting the importance of detrital carbonate in those intervals. Qualitative XRD analysis of three samples from the calcareous facies confirms the importance of carbonate. Muds of the calcareous facies also contain quartz, plagioclase feldspar, mica (biotite, muscovite, illite), and kaolinite/chlorite (undifferentiated).

Thin- to Thick-bedded Facies

The thin- to thick-bedded facies is composed of silty clays, clayey silts, silty sands, and sands, with colors generally ranging from dark gray (5Y 4/1) and olive gray (5Y 4/2) to very dark gray (5Y 3/1) and black (5Y 2.5/1). Within the thin- to thick-bedded facies, these lithologies are characteristically combined to produce light/dark color alternations and fining-upward beds. The thin- to thick-bedded facies is defined by the presence of fining-upward beds with coarse-grained bases of variable thickness, ranging from <1 to approximately 50 cm. These fining-upward beds generally have sharp bases, rarely with scour or load structures, and grade from a coarse component (sand or silt) at the base to clayey silts or silty clays at the top. The fine-grained tops generally show little or no bioturbation. The coarse

component at each base is generally ungraded and structureless, so that the interbedding of coarse and fine lithologies is required to identify the fining-upward nature of the bed.

The composition of the thin- to thick-bedded facies varies significantly with the grain size sampled. Compositions range from 0% to 75% clay, 0% to 50% quartz and feldspar, 0% to 20% volcanic ash, 5% to 30% detrital carbonate, 0% to 10% nannofossils and foraminifers, and 0% to 10% accessory minerals. Carbonate contents in this facies range from 9% to 20%, indicating the presence of detrital and minor biogenic carbonate. XRD analyses of four samples from the thin- to thick-bedded facies indicate the presence of quartz, plagioclase feldspar, mica (biotite/muscovite/illite), calcite, chlorite, and kaolinite(?). Traces of dolomite and pyrite are also present. The pyrite is interpreted as authigenic, while the dolomite may have both detrital and authigenic sources (see "Inorganic Geochemistry" section, this chapter). No consistent downhole compositional trends are apparent from these data.

Thick-bedded Facies

The thick-bedded facies is compositionally similar to the thin- to thick-bedded facies, consisting of interbedded silty clays, clayey silts, silty sands, silts, and sands that form fining-upward beds with sharp lower contacts, uniform bases of silt or sand, and gradational fine-grained tops. The thick-bedded facies dif-

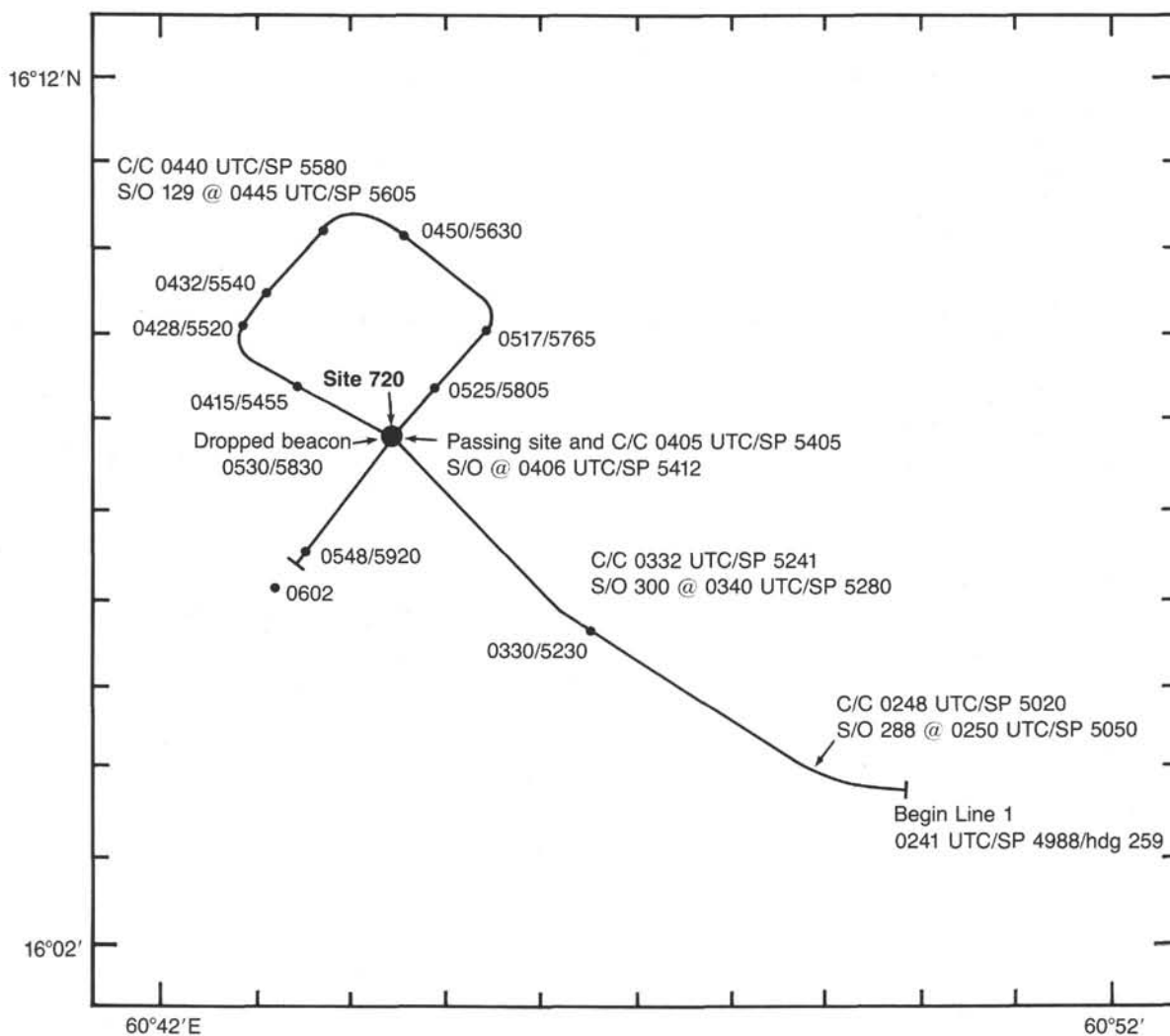


Figure 3. Track chart of approach to Site 720.

fers from the thin- to thick-bedded facies, however, by only containing sequences with coarse-grained bases more than 5 cm thick. Colors range from dark gray (5Y 4/1) and olive gray (5Y 4/2) to very dark gray (5Y 3/1) and black (5Y 2.5/1).

Abundances of sedimentary components in the thick-bedded facies are generally similar to those of the thin- to thick-bedded facies. Carbonate contents in the thick-bedded facies range from 7% to approximately 17% (Table 3, Fig. 5). Qualitative XRD analysis of one sample from the thick-bedded facies indicates the presence of quartz, plagioclase feldspar, calcite, mica, chlorite, kaolinite(?), and dolomite. Mineralogical compositions are generally similar for the thin- to thick-bedded facies and the thick-bedded facies.

In summary, the stratigraphic section recovered at Site 720 has been divided into two lithologic units, with Unit II further subdivided into three facies. Lithologic Unit I and the calcareous facies of lithologic Unit II both contain biogenic and fine-grained terrigenous components, while the thin- to thick-bedded facies and the thick-bedded facies of lithologic Unit II are dominated by fining-upward beds of coarse to fine terrigenous material.

Discussion

The subdivisions of the stratigraphic sequence at Site 720 generally reflect variations in the relative importance of marine

processes and terrigenous sediment supply. As such, these sediments may carry signals related to regional and hemispheric conditions, including surface water productivity, deep-water dissolution, continental uplift, regional tectonism, and climate. The recognition and interpretation of such records, however, is complicated by the poor recovery at this site, which directly influences the lithostratigraphic divisions presented here.

As summarized above, lithologic Unit I and the calcareous facies of lithologic Unit II are similar in composition, while the major difference between the thin- to thick-bedded facies and the thick-bedded facies in lithologic Unit II is the scale of the coarse basal intervals of the fining-upward sequences. Limited core recovery at this site, however, leaves open the question of how representative the recovered lithologies are of the entire stratigraphic section at Site 720. To assess this question, downhole logging data (see "Downhole Measurements" section, this chapter) were visually compared to the recovered intervals to establish log responses for different lithologies. Log data from the unrecovered intervals were then inspected for similar signatures. This inspection supports the following conclusions: (1) two possible occurrences of the calcareous facies in Unit II were not recovered, as indicated at approximately 150 and 170 mbsf in Figure 4; and (2) the other unrecovered intervals in Unit II are consistent with the log signatures of the thin- to thick-bedded facies and the thick-bedded facies. As a result, we interpret the entire

Table 1. Coring summary, Site 720.

Core no.	Date (1987)	Time	Depth (mbsf)	Cored (m)	Recovered (m)	Recovery (%)
117-720A-						
1H	Aug 30	0145	0.0-9.4	9.4	9.42	100.0
2H	30	0300	9.4-19.0	9.6	9.48	98.8
3H	30	0430	19.0-28.6	9.6	9.54	99.4
4X	30	0715	28.6-38.2	9.6	0.01	0.1
5X	30	0830	38.2-47.9	9.7	8.38	86.4
6X	30	0945	47.9-57.6	9.7	0.70	7.2
7X	30	1100	57.6-67.3	9.7	2.76	28.4
8X	30	1215	67.3-77.0	9.7	0.00	0.0
9X	30	1315	77.0-86.7	9.7	0.00	0.0
10X	30	1430	86.7-96.4	9.7	0.24	2.5
11X	30	1545	96.4-106.0	9.6	4.96	51.6
12X	30	1645	106.0-115.7	9.7	2.39	24.6
13X	30	1745	115.7-125.4	9.7	0.42	4.3
14X	30	1900	125.4-135.0	9.6	0.63	6.6
15X	30	2015	135.0-144.7	9.7	0.00	0.0
16X	30	2115	144.7-154.4	9.7	2.79	28.7
17X	30	2245	154.4-164.0	9.6	0.03	0.3
18X	30	2330	164.0-173.7	9.7	0.00	0.0
19X	31	0050	173.7-183.4	9.7	4.26	43.9
20X	31	0215	183.4-193.0	9.6	4.52	47.1
21X	31	0315	193.0-202.7	9.7	0.99	10.2
22X	31	0425	202.7-212.4	9.7	1.06	10.9
23X	31	0540	212.4-222.0	9.6	0.21	2.2
24X	31	0645	222.0-231.7	9.7	1.85	19.1
25X	31	0800	231.7-241.4	9.7	0.00	0.0
26X	31	0925	241.4-251.0	9.6	0.67	7.0
27X	31	1100	251.0-260.5	9.5	0.98	10.3
28X	31	1215	260.5-270.1	9.6	1.54	16.0
29X	31	1315	270.1-279.8	9.7	0.52	5.4
30X	31	1430	279.8-289.4	9.6	9.47	98.6
31X	31	1600	289.4-299.0	9.6	1.01	10.5
32X	31	1730	299.0-308.6	9.6	3.01	31.3
33X	31	1900	308.6-318.2	9.6	0.43	4.5
34X	31	2045	318.2-327.8	9.6	0.00	0.0
35X	31	2215	327.8-337.4	9.6	0.00	0.0
36X	31	2345	337.4-347.0	9.6	0.78	8.1
37X	Sep. 1	0115	347.0-356.6	9.6	0.57	5.9
38X	1	0250	356.6-366.2	9.6	0.30	3.1
39X	1	0415	366.2-375.9	9.7	0.66	6.8
40X	1	0540	375.9-385.2	9.3	2.17	23.3
41X	1	0730	385.2-394.9	9.7	1.10	11.3
42X	1	0935	394.9-404.6	9.7	0.35	3.6
43X	1	1130	404.6-414.3	9.7	1.18	12.1
				414.3	89.38	

stratigraphic section at Site 720 in terms of the lithostratigraphic divisions established above. Given their similarity, Unit I and the calcareous facies of Unit II are interpreted to indicate similar depositional conditions. The thin- to thick-bedded facies and the thick-bedded facies of Unit II are interpreted as recording one basic mechanism of deposition, with variations in scale.

Pelagic Deposits

The abundance of biogenic carbonate and the variety of microfossils in Unit I and the calcareous facies of Unit II indicate that these are pelagic deposits (Fig. 4), formed during periods of increased surface-water productivity and/or decreased clastic influx. The uniformity of Unit I and its age (~0.5 Ma at its base) indicate that the conditions controlling pelagic deposition have not changed drastically during late Pleistocene climatic fluctuations, although a more subtle record may be preserved by minor changes in clastic content and magnetic susceptibility (see "Paleomagnetism" section, this chapter). The linear sedimentation rate in Unit I is approximately 32 m/m.y. (see "Accumulation Rates" section, this chapter), suggesting that clastic influx was low during deposition of this ooze. The dominant control on clastic influx may be large-scale (i.e., climatic or tectonic) or

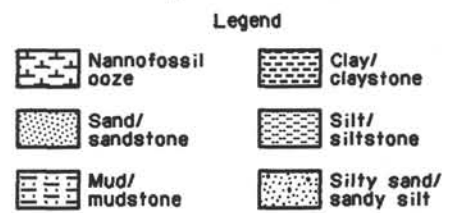
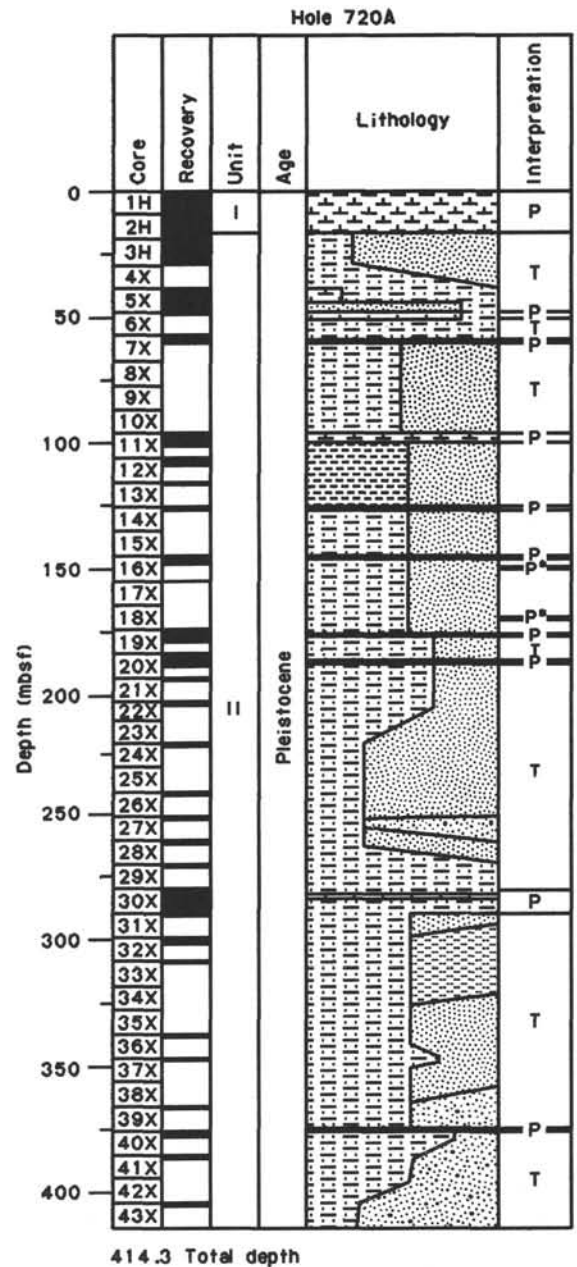


Figure 4. Lithostratigraphic summary, Site 720. Lithology is inferred between recovered intervals. T = turbidite section, P = pelagic section, and P* = possible pelagic section inferred from downhole logs.

more localized, such as depositional patterns on the upper (Kolla and Coumes, 1987), middle, or lower Indus Fan, or differential uplift/subsidence between the Owen Ridge and the western Indus Fan (see "Seismic Stratigraphy" section, this chapter). These controls must be examined by detailed shore-based studies to outline their effects more clearly.

Table 2. Lithostratigraphic summary, Site 720.

Lithologic Unit	Depth	Cores and section
I Nannofossil ooze	0.0-17.2	1H to 2H-6
II Silty clays, silts, sands, with minor nannofossil ooze	17.2-414.3	2H-6 to 43X

Facies	Best developed in core and section
Calcareous facies—Nannofossil ooze	6X, 11X-1 to 11X-3, and 30X-2
Thin- to thick-bedded facies—Interbedded silty clays, silts, and sands	3H, 11X-4 to 11X-CC, and 32X
Thick-bedded facies—Thickly-interbedded silty clays, silts, and sands	22X and 24X

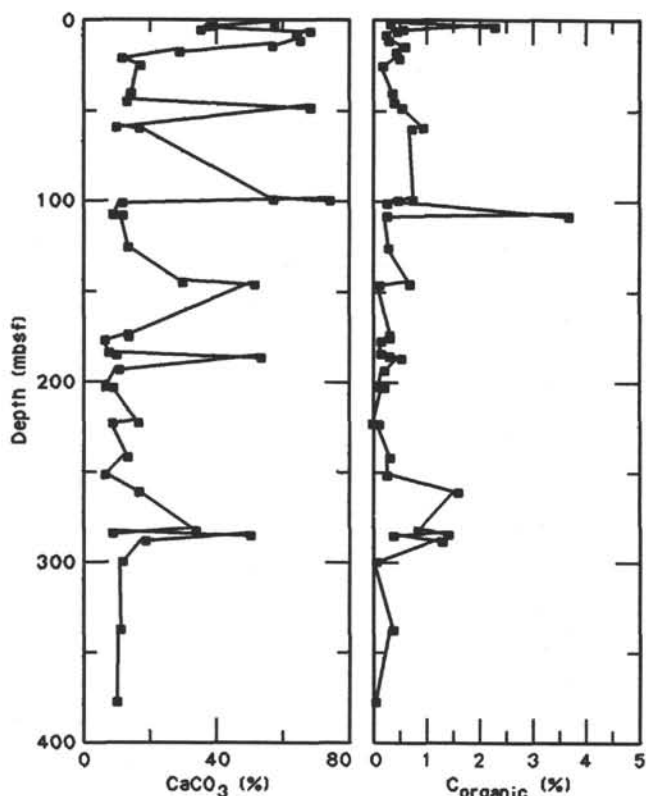


Figure 5. Carbonate and organic carbon profiles, Site 720.

The presence of the calcareous facies within Unit II indicates that similar conditions of increased marine or decreased clastic importance were repeatedly established at Site 720 prior to 0.5 Ma. By including the two pelagic zones recognized on the down-hole logs, a total of 11 such intervals are identified (Fig. 4). The pelagic units are distributed irregularly downcore, however, with 9 of the 11 located above 200 mbsf. By using the sedimentation rates presently available (see "Accumulation Rates" section, this chapter), these 9 pelagic intervals were deposited between 1.0 and 0.5 Ma, while only 2 pelagic layers were deposited prior to 1.0 Ma.

Several lines of evidence indicate that changes in terrigenous sedimentation on the Indus Fan were the major control on the lithologic variations observed in Unit II:

1. The dominance of terrigenous sediments in Unit II, their interpretation as turbidites (see below), and the high rate of sed-

Table 3. Carbonate and organic carbon abundances, Site 720.

Core, section interval (cm)	Depth (mbsf)	Total carbon (%)	Inorganic carbon (%)	Organic carbon (%)	CaCO ₃ (%)
117-720A-					
1H-2, 40-42	1.90	7.24	6.91	0.33	57.6
1H-3, 34-35	3.34	6.90	4.60	2.30	38.3
1H-4, 40-42	4.90	4.84	4.26	0.58	35.5
1H-4, 144-145	5.94	8.67	8.21	0.46	68.4
1H-6, 40-42	7.90	7.98	7.73	0.25	64.4
2H-2, 40-42	11.30	8.16	7.86	0.30	65.5
2H-4, 40-42	14.30	7.45	6.84	0.61	57.0
2H-6, 40-42	17.30	3.95	3.51	0.44	29.2
3H-2, 24-26	20.74	1.95	1.44	0.51	12.0
3H-4, 144-145	24.94	2.31	2.11	0.20	17.6
5X-2, 36-38	40.06	2.14	1.76	0.38	14.7
5X-5, 85-87	45.05	2.02	1.61	0.41	13.4
6X-1, 16-18	48.06	8.80	8.25	0.55	68.7
7X-1, 144-145	59.04	2.20	1.24	0.96	10.3
7X-2, 49-51	59.59	2.79	2.05	0.74	17.1
11X-2, 109-111	98.99	7.71	6.93	0.78	57.7
11X-2, 144-145	99.34	9.47	8.97	0.50	74.7
11X-CC, 0-1	101.07	1.78	1.48	0.30	12.3
12X-2, 25-26	107.75	4.83	1.13	3.70	9.4
12X-2, 56-58	108.06	1.74	1.46	0.28	12.2
14X-1, 29-31	125.69	1.99	1.67	0.32	13.9
16X-1, 64-66	145.34	4.35	3.63	0.72	30.2
16X-1, 144-145	146.14	6.39	6.23	0.16	51.9
19X-1, 34-36	174.04	2.01	1.67	0.34	13.9
19X-1, 149-150	175.19	2.06	1.71	0.35	14.2
19X-3, 34-36	177.04	0.98	0.81	0.17	6.8
20X-1, 45-47	183.85	1.17	0.98	0.19	8.2
20X-2, 63-64	185.53	1.59	1.26	0.33	10.5
20X-3, 45-47	186.85	7.03	6.47	0.56	53.9
21X-1, 51-53	193.51	1.60	1.35	0.25	11.3
22X-1, 0-1	202.70	0.97	0.86	0.11	7.2
22X-1, 52-54	203.22	1.38	1.14	0.24	9.5
24X-1, 90-92	222.90	2.06	2.03	0.03	16.9
24X-1, 139-141	223.39	1.23	1.10	0.13	9.2
26X-1, 31-33	241.71	2.01	1.67	0.34	13.9
27X-1, 40-42	251.40	1.13	0.84	0.29	7.0
28X-1, 40-42	260.90	3.71	2.07	1.64	17.2
30X-2, 111-113	282.41	4.97	4.09	0.88	34.1
30X-4, 1-2	284.31	2.56	1.11	1.45	11.6
30X-4, 98-100	285.28	6.52	6.10	0.42	50.8
30X-6, 100-102	288.30	3.65	2.31	1.34	19.2
32X-1, 77-78	299.77	1.58	1.48	0.10	12.3
32X-1, 93-95	299.93	1.70	1.34	0.36	11.2
33X-1, 25-27	308.85	1.15	1.00	0.15	8.3
36X-1, 0-1	337.40	1.80	1.39	0.41	11.6
36X-1, 60-62	338.00	1.89	1.62	0.27	13.5
37X-1, 19-21	347.19	1.90	1.62	0.28	13.5
39X-CC, 10-11	366.71	6.60	6.06	0.54	50.5
40X-1, 24-26	376.14	1.93	1.53	0.40	12.7
40X-1, 139-140	377.29	1.29	1.23	0.06	10.3
41X-1, 46-48	385.66	1.32	1.15	0.17	9.6
43X-1, 57-59	405.17	2.23	1.88	0.35	15.7

imentation are all characteristic of a fan setting. The long-term importance of the terrigenous source is indicated by the presence of detrital illite and chlorite throughout Unit II, recording input from a Himalayan source during both clastic and carbonate deposition (Weser, 1974).

2. Seismic reflection records from the study area are interpreted (see "Seismic Stratigraphy" section, this chapter) as indicating that sedimentation on the western Indus Fan is controlled by channel migration. Near the Owen Ridge, channel migration may respond to differential tectonics, which creates depressions subject to rapid sedimentary infilling. Each phase of infilling ends with deposition of a major pelagic drape, while minor pelagic drapes are deposited during channel switching.

3. Pelagic units, similar in appearance and composition to those described here, were recognized at DSDP Site 222, also located on the deep Indus Fan (Whitmarsh et al., 1974). At that

site, an 80-m-thick pelagic unit of Pleistocene age was underlain by 1220 m of interbedded pelagic and terrigenous sediments of Pliocene to late Miocene age. The presence of a thinner Pleistocene pelagic unit at Site 222 and a thicker, terrigenous-dominated Pleistocene unit at Site 720 supports the hypothesis that deposition of the calcareous facies in Unit II at Site 720 was controlled by decreased clastic influx.

These data all suggest that variations in clastic supply controlled the deposition of Unit II more directly than changes in marine conditions. Further investigation will be required, however, to fully understand such controls.

Turbidites

The predominance of terrigenous components, their grain sizes, and the abundance of fining-upward sequences in the thin- to thick-bedded facies and the thick-bedded facies of lithologic Unit II support the interpretation of these facies as deposits of low-density mass-transport events. These sediments are interpreted as turbidites in a general sense, but vary somewhat from the idealized model of a complete turbidite (Bouma sequence): (1) the coarse basal zones generally do not show visible grading; (2) primary sedimentary structures are absent in the thicker basal sands; and (3) the upper portions of these sequences lack both a distinct interturbidite layer (Bouma E interval) and significant bioturbation. Explanations can be advanced for each of these differences. The absence of grading may reflect a uniform grain size of the coarse fraction in transport, perhaps because of the distal to middle fan location of Site 720. The absence of primary sedimentary structures could be caused by subtle coring disturbance of the sands. Some interturbidite layers may have been eroded by subsequent events, while others may be indistinguishable from the underlying, fine-grained turbidite tops.

The differences between these sequences and the idealized turbidite, however, may also record important variations in transport and deposition mechanisms. Jipa and Kidd (1974) used textural, compositional, and sedimentary structure data to investigate similar lithologies in the older clastic unit at DSDP Site 222. Some of the intervals considered at Site 222 also lacked basal grading, sedimentary structures, pelagic intervals, and bioturbation. Jipa and Kidd (1974) concluded that the classic model of fan construction, dominated by episodic sand deposition by turbidity flows, was inadequate for the Indus Fan. Instead, they concluded that several processes were active. Turbidity flows probably supplied coarse silt and fine sand episodically, while more semipermanent bottom-following turbidity flows deposited finer sediments derived from reworking on the shelf. Similar processes may also have influenced deposition at Site 720, although interpretations of seismic reflection data emphasize channel levee deposits in this area (see "Seismic Stratigraphy" section, this chapter).

Variations in turbidite-type deposits on the Indus Fan have also been discussed by Kolla and Coumes (1987), who use varying importance of channelized flow, unchannelized flow, channel avulsion, and overbank flow to account for changes in sediment character (see "Seismic Stratigraphy" section, this chapter). According to their model, the thin- to thick-bedded facies at Site 720 contains both overbank (thin, mud-dominated) and channelized to unchannelized (thicker, sand-dominated) deposits, while overbank deposits are absent in the thick-bedded facies. The poor recovery of both clastic facies in Unit II limits our ability to trace these depositional histories in detail, but further study may provide insight into these depositional sequences.

BIOSTRATIGRAPHY

Introduction

Hole 720A consisted of a short pelagic sequence in Cores 117-720A-1H and -2H, followed by a long sequence of turbidites interrupted by short pelagic intervals (e.g., Core 117-720A-30X). Calcareous fossils (planktonic and benthic foraminifers and nannofossils) are abundant, moderately well preserved, and fairly diverse in the upper pelagic sequence. Radiolarians are present, but rare, and show signs of dissolution. Within the turbidite sequence, radiolarians are absent while the calcareous fossils become increasingly impoverished, dissolved, and reworked with depth. In the pelagic sequence of Core 117-720A-30X (279.8-289.4 mbsf) a reasonable calcareous assemblage (mostly planktonic foraminifers and nannofossils) was found along with a robust radiolarian fauna. A correlation of microfossil zones for Site 720 is presented in Figure 6; for a detailed listing of these data points see Table 4.

Planktonic Foraminifers

In general the core catcher samples of Hole 720A contained poorly preserved planktonic foraminifers that show dissolution and have been reworked by turbidites.

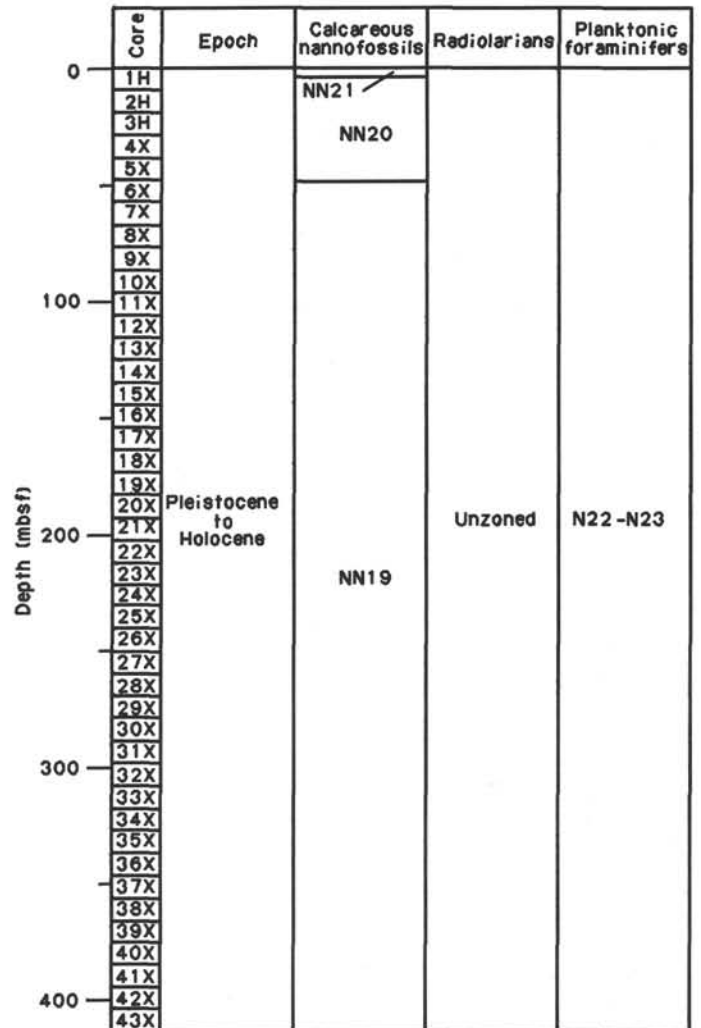


Figure 6. Correlation of biostratigraphic zones for Hole 720A. See Table 4 for a listing of events.

Table 4. Chronological listing of faunal events and paleomagnetic reversals for Hole 720A.

Event	Core, section interval (cm)	Depth (mbsf)	Age (Ma)	Source of age
B <i>Emiliana huxleyi</i>	1H-3, 100-101	4.00	0.19	3
	1H-5, 100-101	7.00		
T <i>Pseudoemiliana lacunosa</i>	5X-CC	46.56	0.49	3
	6X-1, 32-33	48.22		
Brunhes/Matuyama	7X-2, 68-70	59.78	0.73	6
	11X-1, 99-101	97.39		
T <i>Reticulofenestra</i> sp. A	17X-CC	154.42	0.82	3
	19X-2, 33-34	175.53		
B <i>Gephyrocapsa parallela</i>	19X-CC	177.94	0.89	4
	20X-2, 70-71	185.60		
T Jaramillo	20X-2, 96-98	185.86	0.91	6
	20X-3, 95-97	187.35		
B Jaramillo	22X-1, 48-50	203.18	0.98	6
	26X-1, 36-38	241.76		
T <i>Gephyrocapsa</i> "large" ^a	23X-CC	212.60	b ^{1.10}	4
	24X-CC	223.83		
T <i>Helicosphaera sellii</i> ^c	30X-3, 100-101	283.80		
	30X-5, 100-101	286.80		

Note: T = upper limit and B = lower limit. Sources of age: 3 = oxygen isotope data for Site 723 (N. Niitsuma, unpubl. data); 4 = Takayama and Sato, 1987; and 6 = Berggren et al., 1985.

^a Long axis greater than 6 μ m.

^b North Atlantic data.

^c No consistent ages recorded; event appears to be diachronous.

The calcareous pelagic part of the sequence (Sections 117-720A-1H, CC, and 117-720A-2H, CC) yields abundant planktonic foraminifers. *Globorotalia menardii* and *Neogloboquadrina dutertrei* dominate the foraminiferal assemblages along with *Globigerina bulloides*, *Globigerinoides trilobus*, *Globigerinoides ruber*, and *Globigerinita glutinata*. The presence of rare *Globorotalia truncatulinoides* indicates a Pleistocene age for these sediments (Zone N22). These pelagic oozes are late Pleistocene or Holocene (N23) as suggested by the occurrence of rare *Globigerinella calida calida* specimens (Blow, 1969).

From Section 117-720A-3H, CC, downhole, the planktonic foraminifers are diluted by terrigenous particles or are totally absent in the sandy turbidites thus making age assignments difficult. However, the occurrence of *Globorotalia truncatulinoides* in some samples (117-720A-13X, CC; 117-720A-14X, CC, and 117-720A-20X, CC) indicates that these sandy layers are of Pleistocene age (Zone N22). The presence of *Globorotalia tosaensis* in Section 117-720A-20X, CC, indicates that the sample is older than 0.6 Ma.

Core catcher Sections 117-720A-21X, CC, to 117-720A-43X, CC (202.7-414.30 mbsf), are essentially barren with only some reworked specimens present. This interval probably can also be referred to Zone N22 as no upper Pliocene species could be found.

Benthic Foraminifers

The benthic foraminiferal fauna of Hole 720A is for the most part sparse, poorly to moderately preserved, and shows signs of reworking from older and/or shallower sediments.

The upper part of the sequence, which consists of pelagic oozes (Samples 117-720A-1H-2, 52-54 cm, through -2H-2, 56-58 cm, 117-720A-2H-4, 56-58 cm), and the uppermost part of the turbidite sequence (Section 117-720A-2H, CC) yield an abundant, well-preserved, and relatively diverse benthic fauna. The number of benthic foraminifers per 10 cm³ of wet unsieved sediment was approximately 300. Below Section 117-720A-2H-2, the abundance of benthic foraminifers decreases (0 to approximately 100 specimens per 10 cm³ sediment) and the preservation is usually moderate to poor.

The most abundant species are *Chilostomella oolina*, *Cibicides wuellerstorfi*, *Epistominella exigua*, *Oridorsalis umbonatus*, and *Pullenia subcarinata* (relative abundance generally between 10% and 20%). Minor components are *Eggerella bradyi*, *Fissurina* spp., *Melonis* spp., *Pyrgo* spp., *Siphotextularia* spp., and *Uvigerina* spp. Sections 117-720A-11X, CC, 117-720A-12X, CC, 117-720A-22X, CC, 117-720A-24X, CC, 117-720A-26X, CC, 117-720A-27X, CC, 117-720A-30X, CC, 117-720A-33X, CC, 117-720A-38X, CC, 117-720A-41X, CC, and 117-720A-43X, CC, are completely barren.

The samples in the turbiditic section often contain poorly preserved specimens of *Ammonia beccarii* (a shallow-water form; Murray, 1976) and/or *Nuttallides truempyi* (with a stratigraphic range of Late Cretaceous to Eocene; van Morkhoven et al., 1986), which indicates reworking.

Calcareous Nannofossils

Coccoliths occur throughout Hole 720A and they range from abundant to rare. Pelagic oozes contain well-preserved, diverse assemblages of nannofossils. Unfortunately, most of the core catcher material recovered consisted of turbiditic sequences, in which the nannofossils were moderately to poorly preserved and present in low concentrations. Due to these circumstances age assignments for many samples have low confidence.

The general zonation used in this section is that of Martini (1971), and the Quaternary zonation of Takayama and Sato (1987) was used to further refine the biostratigraphy. The ages assigned fossil datums are derived from Berggren et al. (1985) and from Takayama and Sato (1987).

Emiliana huxleyi is present in Core 117-720A-1H down to Sample 117-720A-1H-3, 100-101 cm, but is not present in 117-720A-1H-5, 100-101 cm (4.0-7.0 mbsf). Therefore, its first occurrence at 0.19 Ma is located somewhere within this interval. The sediments containing *E. huxleyi* are assigned to Zone NN21. Sediments which contain neither *E. huxleyi* nor *Pseudoemiliana lacunosa* are assigned to Zone NN20. The last occurrence of *P. lacunosa*, at 0.49 Ma, is between Section 117-720A-5X, CC, and Sample 117-720A-6X-1, 32-33 cm (46.56-48.22 mbsf). All cores down to Section 117-720A-39X, CC, contain *Gephyrocapsa oceanica* and/or *G. caribbeanica*, which have their first occurrences at 1.57 Ma and 1.66 Ma within Zone NN19, respectively.

A trace of Cretaceous and Tertiary reworked specimens such as *Chiaetozygus litterarius*, *Cretarhabdus* spp., *Eiffelithus turiseiffelii*, *Micula decussata*, *Prediscosphaera* spp., *Tranolithus phacelosus*, *Watznaueria barnesae*, *Dictyococcites bisecta*, *Discoaster barbadiensis*, *D. saipanensis*, *Ericsonia formosa*, *Cycliargolithus floridanus*, and *Sphenolithus heteromorphus* also occur throughout the recovered section.

Radiolarians

At Site 720A, radiolarians were found only in Cores 117-720A-1H through 117-720A-3H (0-28.6 mbsf), in Section 117-720A-17X, CC (164.0 mbsf), and in Core 117-720A-30X (279.8-289.4 mbsf). In Cores 117-720A-1H through 117-720A-3H, radiolarians are generally rare and show signs of dissolution; both abundance and preservation decline with depth, and there is considerable masking by terrigenous material throughout. The fauna consists mainly of Spumellaria and age-diagnostic forms are sparse. *Pterocorys hertwigii* and *Lamprocyrtis nigrinae* were found in Section 117-720A-1H, CC, thus placing the sample in the upper Pleistocene. The Quaternary zonation of Nigrini (1971) could not be applied. A sparse, moderately well preserved fauna was found in Section 117-720A-17X, CC, but age-diagnostic taxa are lacking. Single specimens of *Eucyrtidium acuminatum*

and *Pterocanium praetextum eucolpum* suggest a cool-water fauna.

The most robust and diverse radiolarian fauna found at this site occurred within two samples from pelagic layers within Core 117-720A-30X (117-720A-30X-2, 80–82 cm, and -30X-4, 74–76 cm). This fauna also suggests a cool-water fauna with very robust specimens of *Lamprocyrtis neoheteroporos* and *Eucyrtidium calvertense*. A single specimen of *Anihocyrtdium angulare* places Sample 117-720A-30X-4, 74–76 cm, in the *A. angulare* Zone of Nigrini (1971), while the presence of *L. neoheteroporos* means that the sample is older than 1.1 Ma, but younger than 1.5 Ma (Johnson et al., in press).

PALEOMAGNETISM

Introduction

Hole 720A was cored using the APC to 28.6 mbsf and then the XCB to 414.3 mbsf. The lithologies recovered included calcareous ooze and silt/sand turbidites. We measured the natural remanent magnetization (NRM) of the archive halves of the APC cores and of discrete samples obtained from the ooze and silt, in order to establish a paleomagnetic chronology for the Site 720 sediments.

Coring/Corer-Induced Remanence

Because of the very poor recovery, the high degree of core disturbance and the frequent occurrence of coarse-grained intervals, we concentrated our efforts on measuring discrete samples. However, we did use the pass-through cryogenic magnetometer to measure the NRM of the archive halves of all APC cores (117-720A-1H, -2H, -3H) and some XCB cores (117-720A-6X, -7X). This did not produce any significant magnetostratigraphic results but it did illustrate the remanence induced by APC coring described on previous legs, in particular on Legs 115 and 116. Figure 7 shows the results of pass-through measurements for Core 117-720A-2H at demagnetizing fields of 0, 5, and 9 mT. The undemagnetized inclination values generally are greater than 70°, greatly exceeding the expected axial dipole value (30°) for this latitude, and indicating the presence of a steep downward overprint which is only partially removed after alternating field (AF) cleaning at 5 and 9 mT. There is also some evidence of anhysteretic remanent magnetization acquisition in the upper 1 m of the core after the 9 mT step, shown by the increased intensity. The Zijdeveldt plot for a discrete sample from Core 117-720A-2H (Fig. 8) also illustrates the effect of coring-induced magnetization, although in this case it appears to be removed completely at 5 mT. A strong, steep, low-coercivity overprint did not appear to be a feature of the XCB-recovered sediments at this site.

Previous shipboard paleomagnetists have attributed this steep overprint to an induced remanent magnetization (IRM) acquired from the stainless-steel APC barrel. We measured the magnetization of the core barrel after the Site 720 APC cores had been taken and found that it gave “off-scale” values on a crude portable magnetometer with a range of 2 mT. We learned subsequently that the procedure used for checking for flaws in the drill string involves magnetizing it, and that from Leg 115 onwards a much higher field (100 vs. 18 mT) has been used for this purpose. This undoubtedly has the effect of magnetizing the APC barrel. Demagnetization of the APC barrel can be performed onboard the ship; however, the Leg 116 paleomagnetist (see “Paleomagnetism” sections in Cochran, Stow, et al., in press) states that the barrel is quickly remagnetized in the drill string. The low maximum AF field of the cryogenic demagnetizer means that it may be difficult to obtain reliable results from whole APC cores. We recommend (1) that the drill string sections be demagnetized routinely after the flaw-checking pro-

cedure, and (2) that the demagnetizer power supply for the cryogenic magnetometer be enhanced as quickly as possible to give a peak AF of at least 15 mT.

Magnetostratigraphy

We measured a total of 49 discrete samples using the Minispin fluxgate magnetometer. We avoided sampling obviously disturbed and/or coarse-grained intervals. Low NRM intensities (mostly less than 5 mA/m) prevented our using the discrete sample measuring mode on the cryogenic magnetometer, since the noise level of the Z channel was high (about 10 mA/m). The noise level of the Minispin was much lower (about 0.02 mA/m). All of the samples were stepwise AF demagnetized and Figures 9–13 show Zijdeveldt plots of some of the results, both for well-behaved (Figs. 9–11 and 13) and poorly-behaved samples (Fig. 12).

The stable magnetic directions of some of the better-behaved samples are listed in Table 5, and Figure 14 shows a histogram of the distribution of inclinations. Although the number of samples is small, there is a tendency to conform to the expected axial dipole value. Figure 15 shows the inclinations plotted against depth downhole, together with a tentative and partial correlation with the reversal time-scale. The location of the chron C1N/C1R (Brunhes/Matuyama chronozones) boundary between Samples 117-720A-7X-2, 68–70 cm, and 117-720A-11X-1, 99–101 cm (59.78–97.39 mbsf), is in good agreement with the nanofossil stratigraphy (“Biostratigraphy” section, this chapter). Our assignment of two samples to subchron C1R-1 (Jaramillo subchronozones) is more tentative, but again is in reasonable agreement with the nanofossil stratigraphy. If this correlation is correct then the C1R-1 upper boundary lies between Samples 117-720A-20X-2, 96–98 cm, and 117-720A-20X-3, 95–97 cm (185.86–187.35 mbsf). The lower boundary is not so well constrained, occurring between samples 117-720A-22X-1, 48–50 cm, and 117-720A-26X-1, 36–38 cm (203.18–241.76 mbsf), ignoring the anomalously steep normal sample at about 223 mbsf. Below about 300 mbsf a combination of too few stable samples and lack of biostratigraphic control prevents any reliable correlations with the reversal time scale.

Magnetic Susceptibility

The volume magnetic susceptibility of Hole 720A cores was measured using a Bartington Instruments susceptibility meter and M.S.1 sensor. The cores were measured at 5-cm intervals using the low-frequency (0.47-kHz) and high sensitivity (0.1) settings. Downcore susceptibility profiles can be interpreted as reflecting fluctuations in the volume concentration of magnetic particles. A total of 1475 measurements were made over the entire depth range of Hole 720A, although 571 of these were measured for the upper 30 m of core due to the good recovery of that interval. The measured values ranged from 25×10^{-6} to 75×10^{-4} SI units, over two decades of variation, which suggests that the susceptibility data are reflecting the dynamic depositional setting of the Indus fan. The susceptibility record from Hole 720A is best interpreted in two parts, the first part being shallower than 30 mbsf where recovery was good, and the second part below 30 mbsf where recovery was poor and only general observations are appropriate.

The upper 30 m of Hole 720A showed marked variations in susceptibility which could be generally related to varying lithologies (Fig. 16). Sections 117-720A-1H-1 through -5 contain an apparently pelagic unit with cyclic susceptibility variations. Comparison of the susceptibility values with the core descriptions indicates that the lower-valued susceptibility units are light gray in color, have higher percent carbonate content, and generally contain less clay than those units of relatively higher susceptibility which are commonly olive-green in color. An example of a high

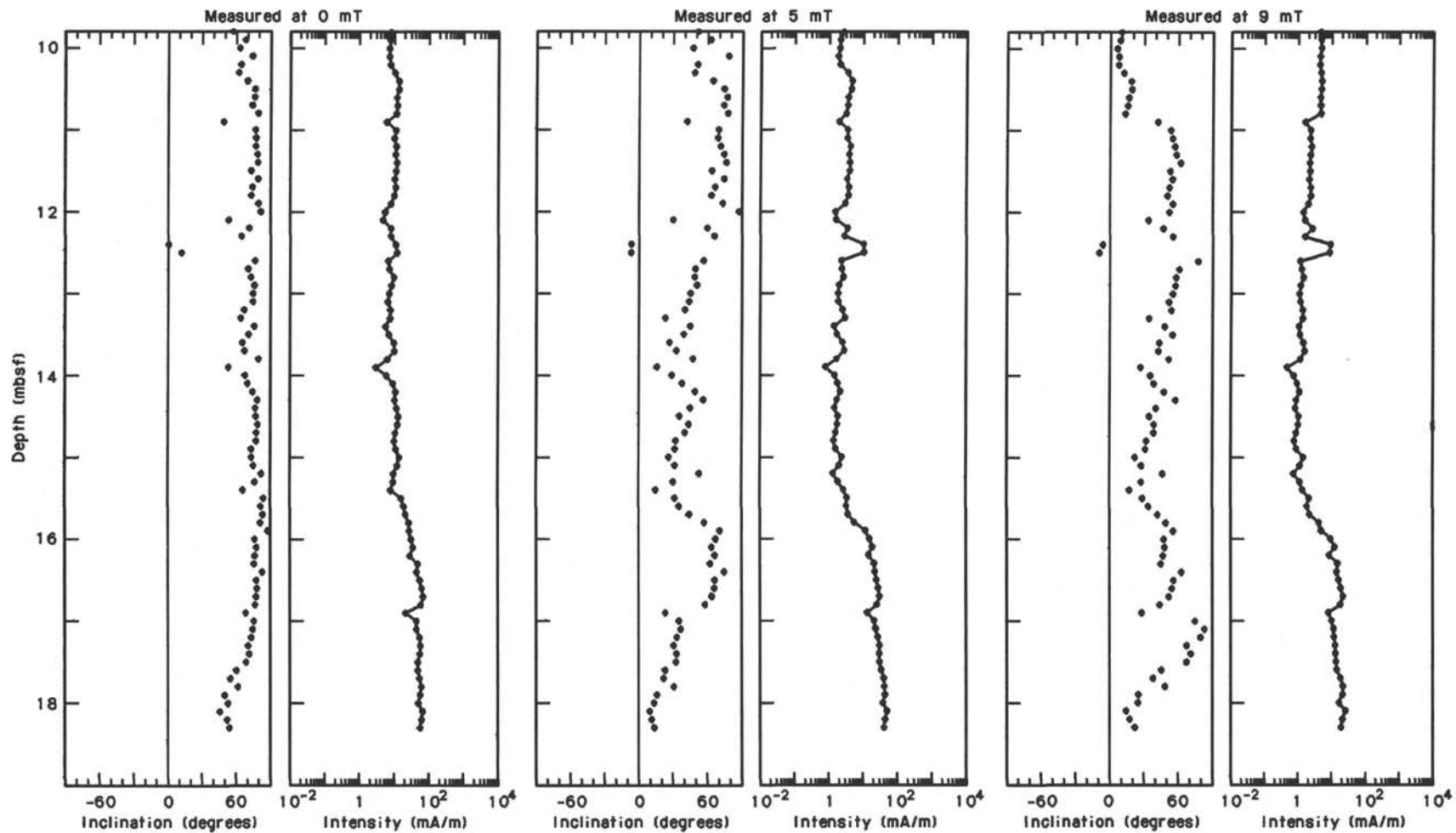


Figure 7. Plots of magnetic inclination and intensity of Core 117-720A-2H, measured on the pass-through cryogenic magnetometer after alternating field (AF) demagnetization at 0 mT (left pair), 5 mT (middle pair), and 9 mT (right pair).

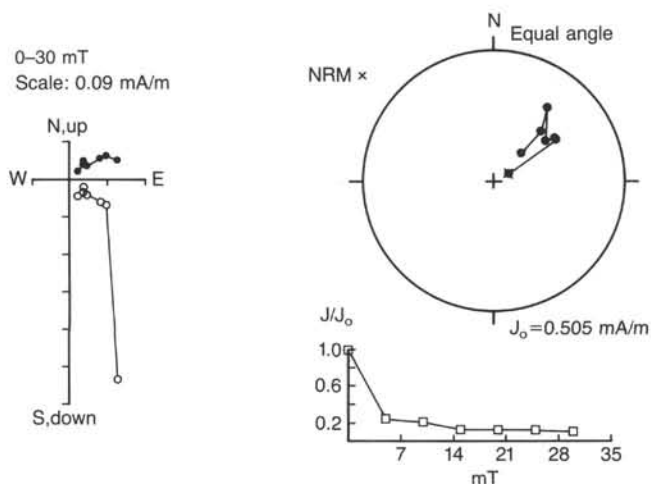


Figure 8. Results of stepwise alternating field (AF) demagnetization of Sample 117-720A-2H-1, 119–121 cm, plotted on a Zijderveld diagram and an equal-area projection.

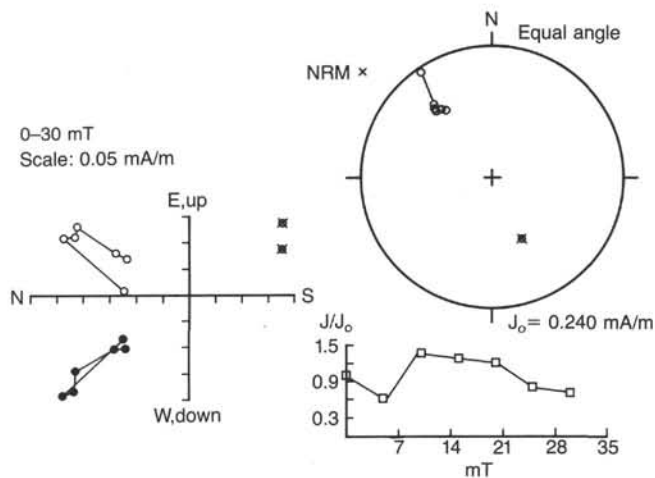


Figure 10. Results of stepwise alternating field (AF) demagnetization of Sample 117-720A-11X-1, 99–101 cm, plotted on a Zijderveld diagram and a equal-area projection.

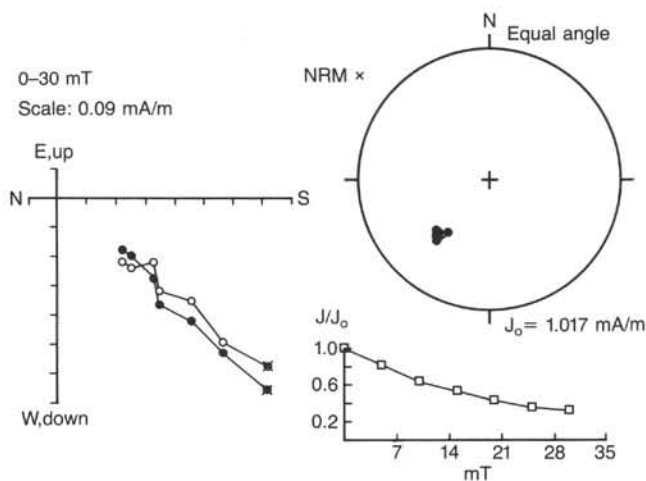


Figure 9. Results of stepwise alternating field (AF) demagnetization of Sample 117-720A-6X-1, 24–26 cm, plotted on a Zijderveld diagram and a equal-area projection.

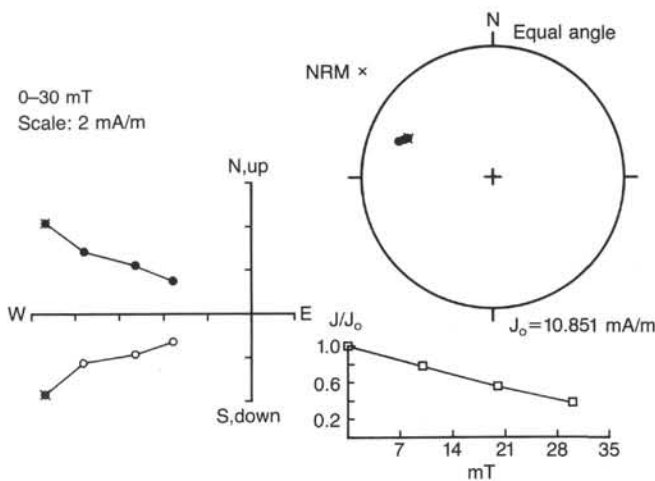


Figure 11. Results of stepwise alternating field (AF) demagnetization of Sample 117-720A-22X-1, 48–50 cm, plotted on a Zijderveld diagram and a equal-area projection.

susceptibility and low carbonate sequence is Section 117-720A-1H-4, 0–77 cm (4.50–5.27 mbsf); an example of the lower susceptibility, high carbonate unit is Section 117-720A-1H-4, 77–150 cm (5.27–6.00 mbsf; see “Lithostratigraphy” section, this chapter). Although the carbonate percentages were determined from smear slide analyses, an inverse correlation between susceptibility and carbonate is apparent for the upper 7.50 m of Hole 720A. A preliminary correlation of high susceptibility intervals with even (glacial) isotope stages (Niitsuma and Oba, unpubl. data) yields an age model for the first 600 k.y. that is consistent with the paleomagnetic and biostratigraphic data. We are uncertain whether this relation is due to dilution (from changing productivity) or magnetic mineral dissolution effects.

Underlying the pelagic unit below Section 117-720A-2H-5 (17.2 mbsf) is another unit composed of interbedded normally-graded clayey-silt sequences of variable thickness which extends to the base of Section 117-720A-3H-6 (28.4 mbsf; Fig. 17). Susceptibility values over this interval are generally much higher and are much more variable than the overlying pelagic unit. Given the depositional environment on the Indus fan and the

graded appearance of the unit, these sediments are interpreted as turbidites. Recovery deteriorates below 117-720A-3H, which is almost certainly a consequence of the poorly consolidated nature of the turbidites. The progression of these clayey-silt units from 28.4 to 17.2 mbsf is from generally thick to thin units. This upward-thinning is apparent not only in the core descriptions (see “Lithostratigraphy” section, this chapter), but also can be seen in some of the susceptibility data as well (Fig. 17). Numerous thin (less than 1 m) graded units were encountered between 17.0 and 21.0 mbsf; below this, more massive units dominate (exceeding 2 m thickness). A general feature of all turbidites is that they show a strong susceptibility maximum at the base and gradually decline in susceptibility toward the top. Presumably, this is a reflection of the grading process, whereby the densest minerals and largest grains are concentrated at the basal part of the turbidite.

An interesting correlation was noted between the whole-core Gamma Ray Attenuation Porosity Evaluator (GRAPE) density values and the susceptibility data for the uppermost 30 m. The susceptibility data appear to correlate well with the GRAPE

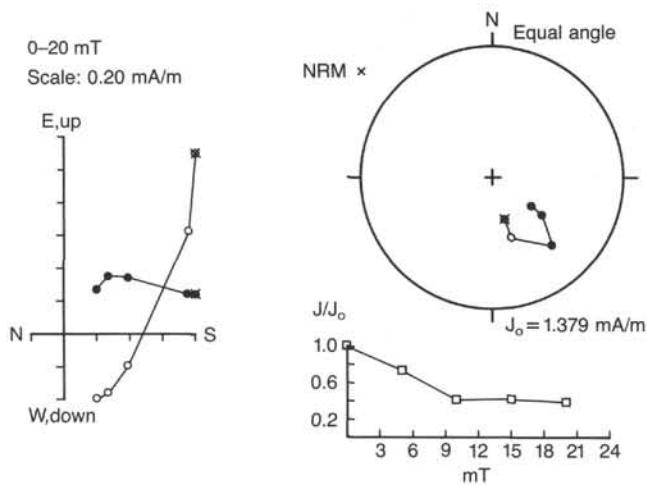


Figure 12. Results of stepwise alternating (AF) demagnetization of Sample 117-720A-29X-1, 10–12 cm, plotted on a Zijderveld diagram and an equal-area projection.

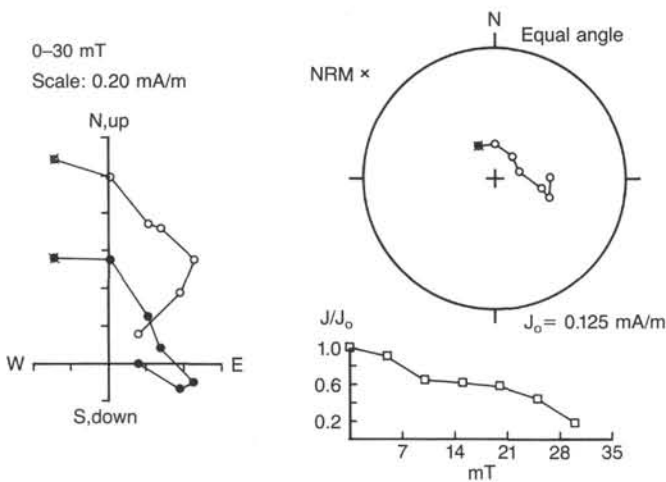


Figure 13. Results of stepwise alternating field (AF) demagnetization of Sample 117-720A-30X-3, 94–96 cm, plotted on a Zijderveld diagram and an equal-area projection.

density values, suggesting that there may be a causal link between the two parameters (Fig. 18). The highest densities and susceptibilities occur within the turbidite units, so that changes in grain size may be the common cause.

A final observation about the general trend of the data with respect to the susceptibility data from Holes 717C and 719A from the Bengal Fan region (Leg 116) suggests that the Indus and Bengal fan depositional histories may have differed over the past ~2.0 Ma. The Leg 116 susceptibility data (Cochran, Stow, et al., in press) indicate that the Bengal Fan experienced two episodes of increased magnetic particle influx at Holes 717C and 719A, ~0.9–3.5 Ma and ~5.0–5.6 Ma (Fig. 19), which the authors (S. Hall and W. Sager) tentatively interpret as reflecting increased influx of terrigenous material. Although the oldest sediment of Hole 720A was deposited at only ~1.5 Ma, a comparison of Indus and Bengal Fan sites suggests that the increased magnetic influx to the Bengal Fan sites from ~0.9–3.5 Ma did not occur at Site 720. Even though the data of Hole 720A are

sparse, so that interpretation is at best tentative, we found no evidence for the very high susceptibilities seen at the Bengal Fan sites in the poorly-recovered coeval sediments of Site 720. The reasons for this may be geological (sediment diversion), diagenetic (Fe^{3+} reduction), or technical (poor turbidite recovery).

ACCUMULATION RATES

The sediment accumulation rates for Site 720 (Fig. 20) are based on five calcareous nannofossil and three paleomagnetic datum levels (Table 4). The upper nannofossil ooze unit (0–17 mbsf) has a mean rate of 32 m/m.y. which is similar to recent pelagic deposits on the nearby Owen Ridge (see “Site 721,” “Site 722,” and “Site 731” chapters, this volume). This suggests that clastic influx to this site was low during the past 200,000 years.

The rate of sedimentation within the turbidite sequences averages more than a factor-of-ten higher than the pelagic deposits and ranges from 137 to 944 m/m.y. over the last million years. Because of poor recovery and a lack of diagnostic microfossils in the deeper cored interval (>225 mbsf), sedimentation rates could not be determined in sediments older than ~1 m.y. However, the older cored sections are dominantly turbidites (see “Lithostratigraphy” section, this chapter), and the rates calculated between 17 and 225 mbsf should be applicable to the base of the hole. Therefore, the oldest sediments cored at Site 720 are probably Pleistocene.

PHYSICAL PROPERTIES

Introduction

Physical properties measured on discrete samples of sediments recovered from Hole 720A include index properties, thermal conductivity, vane shear strength, and compressional-wave velocity (Table 6). The GRAPE and *P*-wave logger were used to measure wet-bulk density and compressional-wave velocity continuously in core sections that were 100 cm or more in length. All techniques and equipment used are described in the “Explanatory Notes” chapter (this volume).

All samples were taken from the least-disturbed, most-coherent intervals of the recovered core. Sampling frequency was limited by the poor recovery and drilling-induced disturbance. Gas expansion and accompanying cracking, particularly between 50 and 300 mbsf, further hampered sampling for physical properties.

Index Properties

The transition from the pelagic carbonate ooze of lithologic Unit I to the terrigenous turbidites of lithologic Unit II is reflected in the index properties (Fig. 21). Throughout Unit I, 0–17.2 mbsf, porosity is nearly constant at approximately 70%. Water content and wet-bulk density values are also nearly constant with sub-bottom depth, averaging 45% and 1.55 g/cm³, respectively. Within the terrigenous sequence of Unit II, porosity decreases gradually from 60% at 17.3 mbsf to 46% at 376.1 mbsf (the last reliable measurement). The profiles of water content and bulk density both reflect the same gradual downsection consolidation of Unit II that is illustrated in the porosity profile. Water content decreases from 36% at the top of Unit II to 23% at 376.1 mbsf, while wet-bulk density increases from 1.70 g/cm³ to 2.03 g/cm³ over the same interval. The relatively high bulk densities and low porosities between 188 and 277 mbsf reflect the high sand content of thick-bedded turbidites that are characteristic of seismic units B-2 and B-3 (see “Seismic Stratigraphy” section, this chapter).

Grain densities of the sediments recovered from Site 720 average 2.70 g/cm³ over the entire drilled sequence (Fig. 21). The

Table 5. Results of magnetic measurements of discrete samples, Hole 720A.

Core, section, interval (cm)	Depth (mbsf)	AFD (mT)	CSD (°)	Declination (°)	Inclination (°)	Intensity (mA/m)
117-720A-						
1H-1, 91	0.91	25	7.7	86.9	22.8	0.4213
1H-2, 26	1.76	20	12.4	116.0	17.2	1.3733
1H-3, 26	3.26	20	4.9	147.8	22.5	1.8383
1H-4, 11	4.61	20	7.2	195.8	28.9	0.7218
1H-5, 20	6.20	20	4.7	223.1	21.5	0.3908
2H-1, 119	10.59	5	14.6	57.4	30.9	0.1201
2H-2, 119	12.09	20	11.9	62.5	33.2	0.0914
2H-3, 119	13.59	20	4.5	84.1	29.3	0.2343
2H-4, 119	15.09	22	—	91.0	13.9	0.2807
2H-5, 119	16.59	20	2.4	85.9	38.2	4.9185
5X-6, 39	46.09	20	2.7	268.5	30.9	2.5914
6X-1, 24	48.14	10	5.4	222.3	29.5	0.6461
7X-1, 24	57.84	20	15.0	284.8	15.8	16.3038
7X-2, 68	59.78	15	5.2	356.7	22.7	3.7679
11X-1, 99	97.39	20	6.3	325.6	-26.6	0.2872
11X-2, 99	98.89	30	8.5	4.5	-11.2	0.2630
11X-3, 92	100.32	25	10.1	191.7	-14.8	1.6036
12X-1, 95	106.95	20	4.4	250.3	-10.1	1.2054
16X-1, 95	145.65	30	—	201.1	78.2	1.4484
16X-2, 38	146.58	20	12.5	255.8	64.6	2.5797
19X-1, 36	174.06	20	6.8	170.3	-36.0	6.6931
19X-2, 42	175.62	20	12.6	81.6	-22.2	3.8985
20X-2, 96	185.86	20	25.4	279.6	-68.3	0.1235
20X-3, 95	187.35	20	5.3	310.2	19.7	1.8479
21X-1, 35	193.35	20	4.0	179.3	5.7	6.5672
22X-1, 48	203.18	20	7.3	292.6	18.0	5.9603
24X-1, 124	223.24	20	7.6	339.1	85.0	0.8900
26X-1, 36	241.76	20	5.0	164.1	-58.5	1.5948
28X-1, 109	261.59	10	3.6	258.6	-30.1	1.4794
30X-3, 94	283.74	25	23.1	109.5	-42.8	0.0551
32X-2, 55	301.05	10	5.8	181.8	-39.0	0.6018
33X-1, 20	308.80	5	4.0	38.7	26.3	0.7397
36X-1, 20	337.60	20	3.7	240.8	38.5	3.0011
37X-1, 10	347.10	10	4.9	47.8	-61.4	0.8197
39X-1, 14	366.34	10	3.3	325.6	44.7	2.3075
40X-1, 93	376.83	20	54.8	194.4	-30.0	0.4797
41X-1, 48	385.68	10	12.1	4.1	-76.6	2.4173

only notable trend is a difference in degree of scatter of the data from the two lithologic units. Grain densities within Unit I quite consistently range from 2.65 to 2.75 g/cm³. Within Unit II the grain density values showed considerable scatter (2.54 to 2.90 g/cm³) but most values lie between 2.65 and 2.75 g/cm³.

Compressional Velocity Measurements

P-wave velocity measurements were limited by the condition of recovered sediment at Site 720. At depths less than 100 mbsf the sediments were too soft to allow determination of *P*-wave velocities in the Hamilton Frame Velocimeter. At depths greater than 100 mbsf, the gas expansion inhibited signal transmission through sediment samples. Only two measurements were made, both perpendicular to bedding (Fig. 22). The velocity at 7.8 mbsf, 1461 m/s, is less than that of seawater but is not unusual for seafloor sediments (Hamilton, 1974). At 60.1 mbsf, the measured velocity is unusually high, 1960 m/s, and is possibly not reliable.

Thermal Conductivity

Thermal conductivity of the sediments increases gradually from 1.20 W/m·K near the seafloor to 1.35 W/m·K at 400 mbsf (Fig. 22). The increase in thermal conductivity with depth tracks the increase in wet-bulk density with depth.

Vane Shear Strength

Drilling-induced core disturbance limited the number of vane shear strength determinations. Only three measurements are considered reliable because at depths greater than 105.5 mbsf

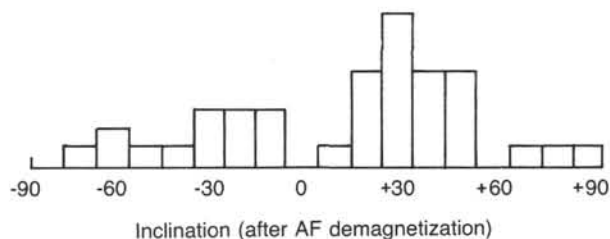


Figure 14. Histogram of inclination values of discrete samples after alternating field (AF) demagnetization. Values grouped in 10° steps.

(Core 117-720A-11X), failure occurred by fracturing rather than shearing of the sediment. The brittle behavior of the sediments is likely the result of gas expansion within the sediments. The maximum measured shear strength was 50 kPa at 99 mbsf (Fig. 22).

GRAPE and *P*-Wave Logs

Reliable continuous records from the GRAPE and *P*-wave logging devices are limited to depths shallower than 30 mbsf. *P*-wave logs were not obtained for cores deeper than Core 117-720A-5X because of signal transmission failure resulting from incompletely filled cores and gas-expanded sediments. GRAPE data quality decreases below Core 117-720A-5X as a consequence of nonuniform core diameter. GRAPE logs for the interval 0–30 mbsf show the increase in wet-bulk density that marks the boundary between lithologic Units I and II (Fig. 23). Cyclic density

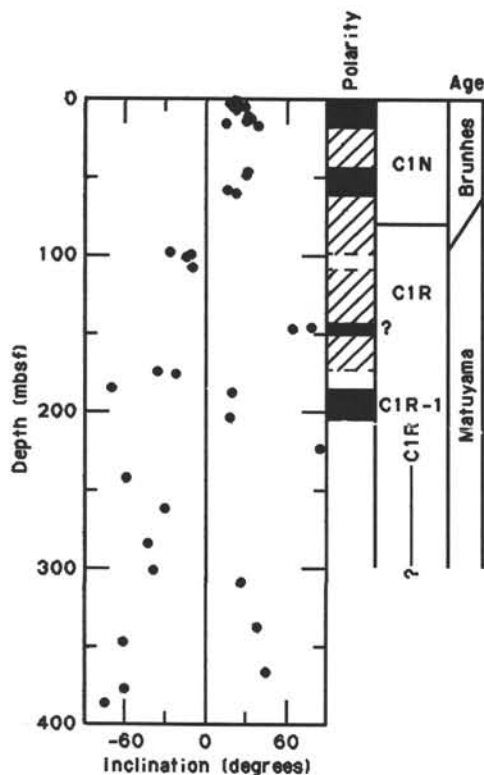


Figure 15. Plot of magnetic inclinations against sub-bottom depth. Magnetic polarity log (black = normal, white = reversed, hatched = undetermined) and its tentative assignment to the polarity time-scale are shown on the right.

variations in Unit I are in phase with variations of magnetic susceptibility interpreted to represent glacial-interglacial fluctuations in the supply of calcium carbonate and magnetic minerals (see "Paleomagnetism" section, this chapter).

SEISMIC STRATIGRAPHY

Introduction

Site 720 is located on the western margin of the Indus Fan near the transition from middle fan to lower fan (Kolla and Coumes, 1987). Based on modern depositional patterns on this fan (Kolla and Coumes, 1987), the lithology of Site 720 was expected to consist of: (1) sands and silts of channel levee deposits, (2) silty clays and mud turbidites of overbank deposits from more distant channels, (3) sand sheet deposits from unchannelized flows occurring at the terminations of channels, and (4) pelagic sediments from times when channels are so distant or inactive that no turbidites reach the site.

In this section we discuss the cored sequence at Site 720 in the context of regional seismic stratigraphy, in order to determine the lateral implications of observed downhole variations. Our approach is based on a sequence analysis of two *Robert Conrad* site survey lines which cross the Indus Fan in roughly northwest-southeast directions: RC 2704 Line 1, which is 3 km northward of Site 720, and RC 2704 Line 49, which crosses the site. We then compare the seismic sequences to core and log data, based on depth-to-time conversion through a synthetic seismogram.

Seismic Sequences

The surface morphology of the Indus Fan in the vicinity of Site 720 is characterized by several meandering channels (e.g.,

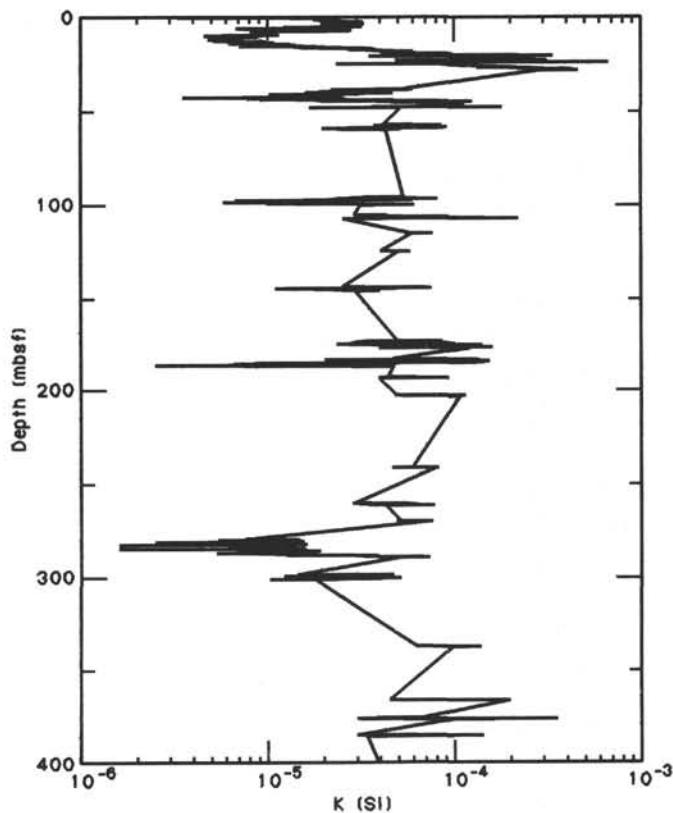


Figure 16. Log-normal plot of magnetic susceptibility as a function of sub-bottom depth. Note that the data range over two decades of variation in the upper 30 m.

Fig. 1). Two major surface channels that are observed on seismic profiles or precision depth records are within 200 km of the site. The nearest surface channel is only 5 km northwest of the site. These channels are about 1.5 km wide, 50 m deep, and have levee elevations about 30 m above the surrounding fan surface. Thus, the surface of the fan has slight depth variations caused by the depositional levees and erosional channels. On the basis of the site survey data, the levees in the vicinity of the site have characteristic widths of 15-20 km.

The digitally recorded single-channel seismic data for this area show a variety of subsurface features that are most likely related to turbidite flux and levee building, channel migration, and abandonment. The subsurface levee/channel complexes are characterized by convexly inclined reflectors that converge and pinch out away from the central channel area that has diffuse, irregular reflectors. According to McHargue and Webb (1986) and Kolla and Coumes (1987), the inclined reflectors are interpreted as levee deposits and the diffuse patterns are thought to represent a mixture of channel sands, slumped levee deposits, and fine-grained channel fill accumulated after abandonment of the channel.

A study of the major regional sedimentary and tectonic processes on the lower part of the western Indus Fan was possible due to a long seismic line collected during the *Robert Conrad* site survey cruise in 1986 (Leg 2704, Fig. 24). Line 1 runs 3 km north of Site 720 in a roughly northwest-southeast direction and shows the major depositional patterns found at Site 270 in both the lithostratigraphic and downhole logging record. Tracing of laterally distinctive reflectors permits the identification of three major seismic sequences, which we refer to as A, B, and C (downsection).

Changes in the small-scale depositional patterns associated with channel migration can be tentatively identified on seismic

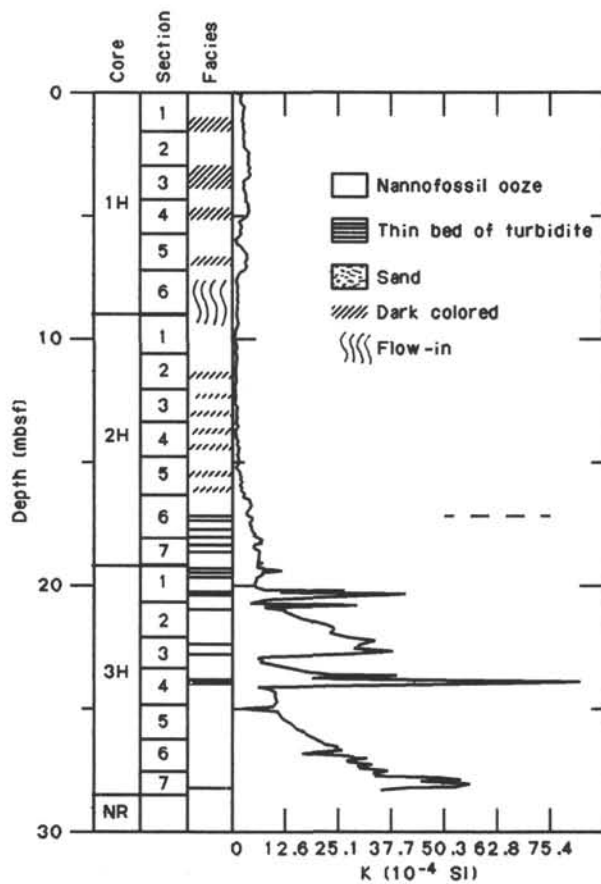


Figure 17. Plot of volume magnetic susceptibility as a function of depth for the upper ~30 mbsf of Hole 720A. Turbidite facies dominates the sediments between 18–30 mbsf, pelagic facies dominates the upper 18 mbsf.

line RC7204-49 (Fig. 25), based on the seismic sequence analysis techniques of Vail et al. (1977). In nearly flat-lying sequences such as these, the terms “onlap” and “downlap” are interchangeable; we use the term “downlap” here because of the assumed small initial downward slope away from each levee. Traveltimes to sequence boundaries discussed below refer to the sub-bottom two-way traveltime of these boundaries at Site 720. On the section across Site 720 (Fig. 25), we identify seven subunits of the three major seismic sequences found on Figure 24. The seismic processing used for Figure 25 is very different than that for Figure 24; the former is preferable for determining continuity of reflectors, while the latter is more appropriate for identifying variations in reflection strength and, indirectly, importance.

Sequence A is at the western margin of the Indus Fan, 75–200 m thick (102 m thick at Site 720), and has three subunits. Sequence A shows abundant development of medium and small channels which are spaced about 20 km apart. The sequence shows abundant channel switching, often with eastward migration of channels (see also McHargue and Webb, 1986; Kolla and Coumes, 1987), and also stable or intermittent positions of channels. Phases of channel switching are followed by well-established reflectors which drape the former channel and channel levee deposits (Fig. 25).

In Sequence A, the highest rates of deposition occur at the portion of the fan closest to Owen Ridge (Fig. 24) where young tectonic movements caused a 100–150 m relative uplift of the eastern margin of the Owen Ridge, accompanied by a relative downward movement of the western Indus Fan sediments. This

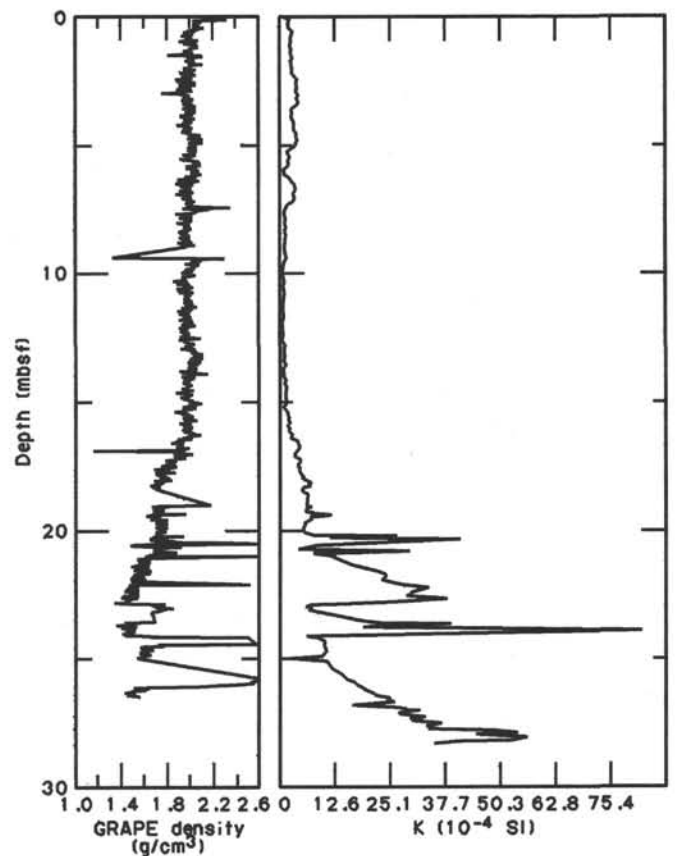


Figure 18. GRAPE bulk density estimates and magnetic susceptibility plotted as a function of depth for the upper 30 mbsf. Note the covariance of the two parameters.

uplift is inferred from the narrower spacing of the seismic reflectors above the Owen Ridge margin, the major increase in thickness of Sequence A between Site 720 and the margin of the uplift zone, and the concentration of buried channels within Sequence A just east of the uplift zone. A major tectonic episode occurred during the deposition of Sequence A (around 0.75 Ma, see below).

The newly accumulated sediment wedge of Sequence A is draped at the surface with a thin transparent layer, Subsequence A-1 (coincident with lithologic Unit I). This unit is too thin (0.02 s) to be detectable on the digital seismic lines, because of interference with the bottom reflector (0.07 s in duration). Subsequence A-1 is evident on the higher frequency 3.5-kHz records. Draping of the subunit over pre-existing topography indicates a recent period of inactivity which followed the period of rapid infill. This layer also drapes the uplifted part of Owen Ridge. A similar but much thicker pelagic layer caps the section penetrated at DSDP Site 222, on the portion of the Indus Fan west of Owen Ridge.

Subsequence A-2 (0.02–0.07 s) consists of generally parallel reflectors (Fig. 25), with some eastward downlap evident at the base of the subsequence just to the east of the site. The sequence exhibits a gradual decrease in traveltime width to the east, probably caused by an eastward thinning associated with pinch-outs of the lowest horizons. At Site 720 this subsequence is likely to consist of overbank deposits from the modern channel just to the left (west) of the seismic section of Figure 25.

Subsequence A-3 (0.07–0.10 s) is a thin unit of strongly progradational reflectors, clearly associated with a buried channel at 0.05–0.11 s sub-bottom. The sequence thickens substantially to the east (right on Fig. 25). The characteristic convex upward

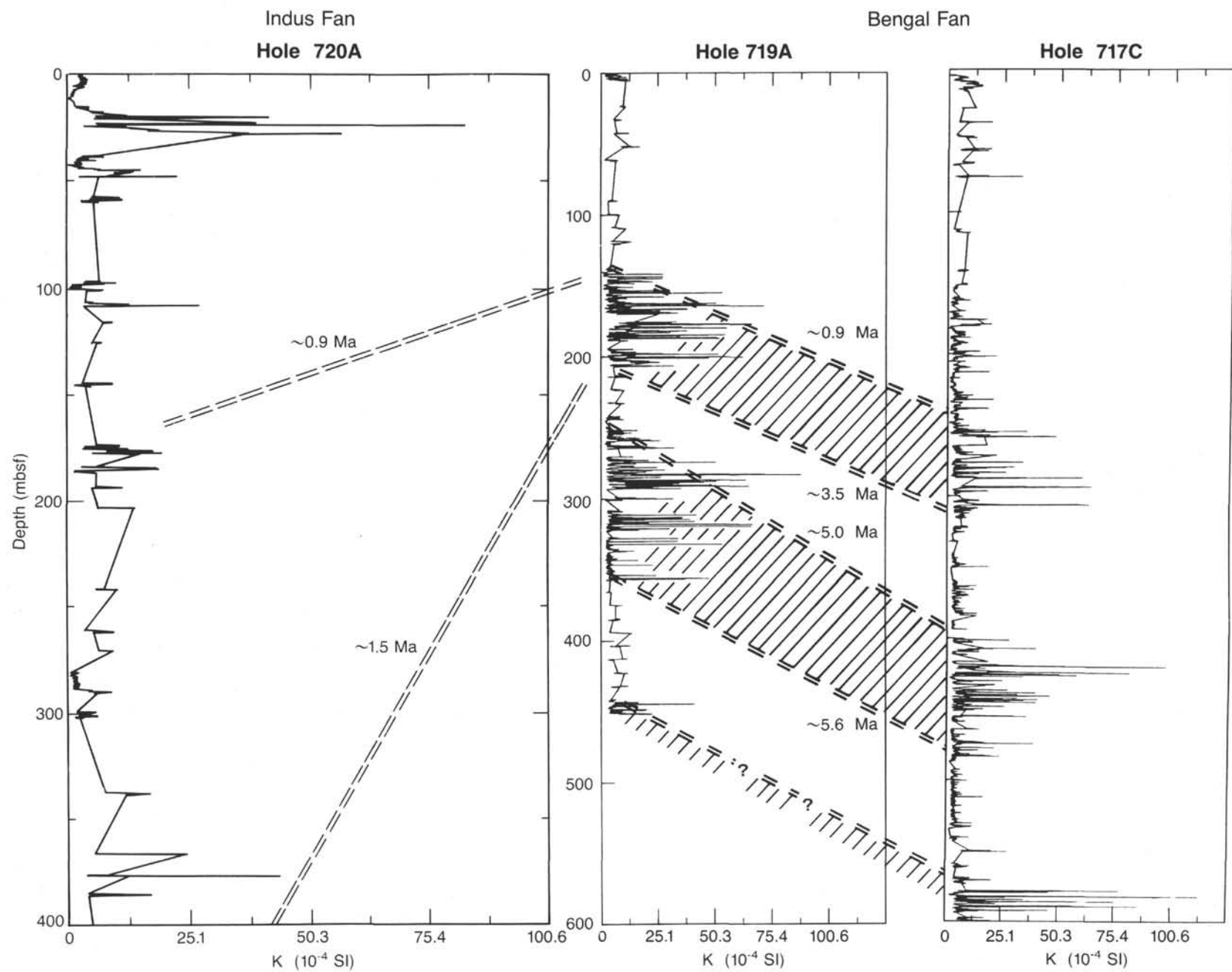


Figure 19. Magnetic susceptibility data for Hole 720A compared to Holes 717C and 719A from the Bengal fan. Tie lines indicate approximate time-correlative horizons. Note that Hole 720A does not display the high susceptibility values apparent in the Bengal fan sites during the 0.9–1.5 Ma interval.

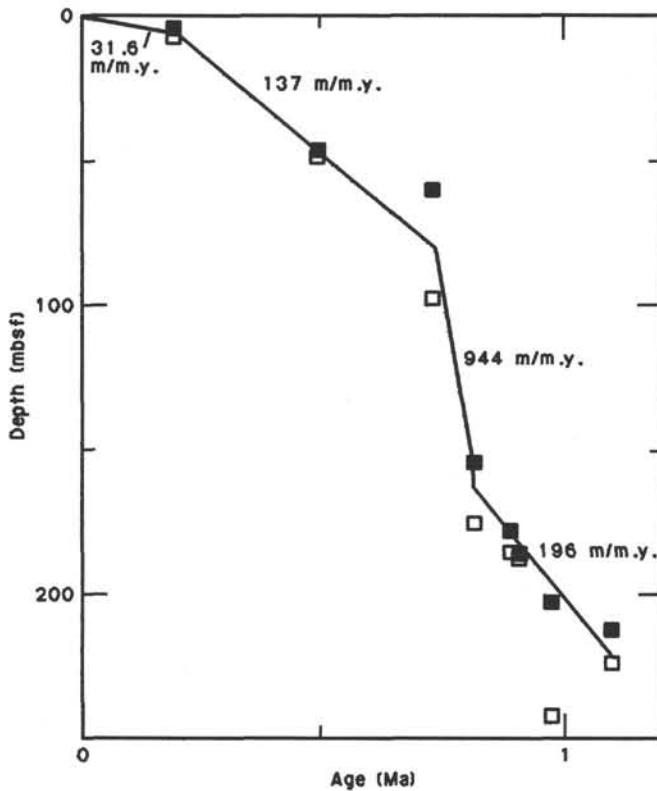


Figure 20. Sedimentation rate curve for the top 250 mbsf of Site 720. The indicated sedimentation rates are based on a best fit of the stratigraphic datum levels (Table 4). Filled and open boxes are the respective upper and lower depths of the datum levels.

shape of the levee is evident just west of the channel. Both downlap and toplap patterns are evident in this subsequence; the toplap is probably caused by later erosion or thinning of the levee beds toward the crest of the levees.

Sequence B displays a constant thickness of 180–200 m over a distance of 150 km, although some syndepositional uplift of the Owen Ridge may be inferred from the closer spacing of reflectors on the ridge margin. The lower part of Sequence B shows a rather uniform pattern with no major channel visible, while the upper half of this package displays three large channels within a lateral distance of 150 km. The top of Sequence B is defined by a nearly continuous reflector. Based on unconformities identified on seismic Line 49 near the site, we subdivide Sequence B into three units.

Subsequence B-1 (0.10–0.22 s) is a thick, fairly uniform sequence of mostly parallel reflectors. No pinchouts are visible at the top of the sequence. Gradual eastward downlap of basal horizons is seen, probably accounting for the slight thickening of the section to the west. A long-lived or volumetrically important channel is implied by the thickness and uniformity of the sequence. The downlap pattern and thickening to the west suggest that the channel was to the west; it gradually flattened out the initially substantial slope of the underlying B-2 levee system.

Subsequence B-2 (0.22–0.25 s) is a thin unit of reflectors prograding strongly to the west (Fig. 25). Its seismic signature is very similar to Subsequence A-3, and the corresponding buried channel is clearly evident at 0.2–0.25 s sub-bottom on Figure 25, almost immediately below the channel of Subsequence A-3. The levee of the channel's west bank appears to be visible beneath the A-3 channel. This "levee" could be an artifact and actually be "velocity pullup," caused by higher-velocity sediments in the channel of Subsequence A. If so, the levee deposits of A-3

would need to be more clay-rich and therefore have a higher velocity than the channel fill. Subsequence B-2 exhibits the same westward downlap and eastward toplap as Subsequence A-3. Again, the downlap is likely to be constructional (levee and overbank deposits), and the toplap is probably erosional or caused by wedge-shaped overbank beds. Subsequence B-2 thins to the west with increasing distance from the source channel.

Subsequence B-3 (0.25–0.36 s) is a fairly uniform sequence of parallel reflectors, with no toplap and almost no basal downlap. A single toplap pinchout may be present near the Subsequence B-2 channel, and possible downlaps may be present at and slightly east of Site 720. No significant thickness changes are evident within the portion of Subsequence B-3 shown in Figure 25. A source from the same channel as Subsequence B-2 is possible but the identification of a channel of Subsequence B-3 on Figure 25 is highly tentative.

Sequence C is about 300 m thick. The upper part of Sequence C shows only one well-developed, large channel along a 150-km section (Fig. 24). Levee deposits associated with this channel are more than 20 km wide, and the channel apparently remained active and stationary throughout the upper part of Sequence C. A distinctly developed reflector can be traced over the top of this channel and laterally for more than 200 km, suggesting a major draping period of pelagic sediments after a phase of rapid deposition. This prominent reflector, which crosses Site 720 at a sub-bottom time of 0.33 s, appears to be conformable with the upper portion of Sequence C. The reflector is well displayed on Figure 24 but much less prominent on the heavily clipped section of Figure 25. We pick the top of Sequence C at 0.36 seconds sub-bottom, which represents the top of the major channel which was responsible for much of the Sequence C deposition. Sequence C contains at least two units.

The top of Subsequence C-1 (0.36–0.42 s) is clearly associated with the top of a channel fill and its western levee system. One toplap pinchout and one downlap of the overlying unit is visible to the west of the channel. The bottom of the sequence is marked by a pinch-out (downlap) to the east and toplap of the underlying unit.

Subsequence C-2 (0.42–0.47 s) is the lowest seismic sequence likely to have been encountered at Site 720. This sequence has conformable bottom reflectors, overlying a deeper sequence whose top boundary is defined on the basis of toplap pinchouts to the west. The top of Subsequence C-2 is also marked by toplap of several horizons, but to the east. This toplap probably is caused by erosion associated with establishment of the nearby Subsequence C-1 channel. The channel source for Subsequence C-2 is uncertain.

Depth-to-time Conversion for Site 720

The velocity log at Site 720 provides a continuous and representative curve of velocity variations, which can be used to link core depth to seismic traveltime. We used the velocity log of Figure 32 and a pseudodensity log based on porosity to calculate a synthetic seismogram for the site. Density logs seldom have much effect on ODP synthetic seismograms, because both density and velocity are responding primarily to porosity changes. A possible exception to this generalization occurs at major lithologic boundaries such as between turbidites and pelagic clays. The velocity contrast between these two lithologies is relatively small in comparison to the porosity contrast, so the density contrast at these boundaries may be more effective in creating seismic reflectors than is the velocity contrast.

The synthetic seismogram was calculated using a convolutional model, with internal multiples. For calculation of a synthetic comparable to the site survey line of *Robert Conrad* across the site, we used a wavelet appropriate for the *Robert Conrad*. Rather than utilizing a near-field wavelet recorded by hydro-

Table 6. Physical properties summary for Site 720.

Core, section, interval (cm)	Depth (mbsf)	Wet-bulk density (g/cm ³)	Porosity (%)	Water content (%)	Grain density (g/cm ³)	Velocity ^a (m/sec)	Thermal conductivity (W/mK)	Vane shear strength (kPa)
117-720A-								
1H-2, 40-42	1.90	1.553	69.6	45.9	2.695		1.20	
1H-4, 40-42	4.90	1.514	74.1	50.1	2.713		1.12	7.1
1H-6, 35-38	7.85					1461		
1H-6, 40-42	7.90	1.553	68.6	45.3	2.647		1.21	
2H-2, 40-42	11.30	1.549	67.7	44.8	2.664		1.26	
2H-4, 40-42	14.30	1.554	70.1	46.2	2.684		1.22	9.6
2H-6, 40-42	17.30	1.704	60.5	36.4	2.747		1.39	
3H-2, 23-25	20.73	1.888	59.1	32.1	2.896			
3H-4, 40-42	23.90				2.845			
5X-2, 38-40	40.08	1.846	55.9	31.0	2.541		1.33	
5X-4, 40-40	43.10						1.46	
5X-5, 85-87	45.05	1.928	57.2	30.4	2.796			
7X-1, 48-48	58.08						1.36	
7X-1, 52-54								17.6
7X-2, 49-51	59.59	1.791	57.8	33.1	2.590		1.20	
7X-2, 106-108	60.06					1960		
11X-1, 110-110	97.50						1.23	
11X-2, 110-112	99.00	1.806	69.3	39.3	2.684		1.21	
11X-3, 98-100	100.38							50.3
11X-3, 110-110	100.50						1.35	
12X-1, 56-56	106.06						1.09	
12X-2, 56-58	108.06	1.984	45.0	23.2	2.539		1.41	
14X-1, 30-32	125.70	1.837	54.4	30.4	2.551		1.47	
16X-1, 64-66	145.34	1.842	55.6	30.9	2.598			
16X-2, 20-20							1.32	
19X-1, 34-36	174.04	1.883	52.5	28.6	2.639		1.01	
19X-1, 42-44	174.12							23.2
19X-3, 34-36	177.04				2.722		1.92	
20X-1, 45-47	183.85				2.733		1.40	
20X-3, 45-47	186.85	1.826	53.2	29.9	2.591		1.40	34.6
21X-1, 51-53	193.51	2.114	53.3	25.8	2.708			22.8
21X-1, 58-60	193.58							
22X-1, 34-34	203.04						1.35	
22X-1, 52-54	203.22				2.690			
24X-1, 90-92	222.90	2.029	46.6	23.5	2.738			
24X-1, 110-110	223.10						1.24	
26X-1, 31-33	241.71	1.974	50.3	26.1	2.778			
27X-1, 40-42	251.40				2.671			
28X-1, 40-42	260.90				2.719		1.22	
30X-2, 100-100							1.43	
30X-2, 112-114	282.42	1.841	54.4	30.3	2.750			
30X-4, 98-100	285.28	1.766	57.3	33.2	2.634		1.20	
30X-6, 100-102	288.30	1.781	53.4	30.7	2.544		1.34	
32X-1, 50-50	299.50						1.39	
32X-1, 93-95	299.93	1.889	50.4	27.3	2.691			
32X-2, 50-50	301.00						1.21	
33X-1, 25-27	308.85				2.703			
36X-1, 60-62	338.00	1.882	52.1	28.4	2.711			
37X-1, 19-21	347.19	1.938	48.3	25.5	2.691			
39X-CC, 11-13	366.72	1.897	48.4	26.2	2.589			
40X-1, 24-26	376.14	2.027	46.3	23.4	2.779		1.31	
41X-1, 46-48	385.66				2.677			
43X-1, 50-50	405.10						1.61	
43X-1, 57-59	405.17				2.731			

^a Velocity measurements perpendicular to bedding.

phone (which may differ from the actual far-field wavelet), we used an average of the seafloor returns obtained at shotpoint 540 on RC2704 Line 19 and shotpoint 1692 on RC2704 Line 35 (Fig. 26). Selection of these particular shotpoint numbers is not important; both are in regions of very stable seafloor returns over long intervals. examination of site survey lines suggests that these two line portions show both a high signal-to-noise ratio and, more significantly, no evidence of shallow sub-bottom reflections that could contaminate the wavelet estimate. The close similarity of the two wavelet estimates for 0-75 ms confirms the suitability of this wavelet estimate (Fig. 26).

Figure 27 shows the final synthetic seismogram for the portion of the hole between 78.8 and 412.4 mbsf. No synthetic seis-

mogram was possible for the interval 0-78.8 mbsf, because the sonic log does not work through pipe in uncompacted sediments and because gas traces caused Hamilton Frame velocity measurements on cores to be unreliable (see "Physical Properties" section, this chapter).

In Figure 27, the synthetic seismogram is compared to a 10-trace average of the *Robert Conrad* seismic data at the site, as well as to a portion of the same line processed as in Figure 25. The latter is heavily clipped and shows only peaks (with troughs blanked); this processing is useful for regional seismic correlation but is of limited usefulness for comparison to the synthetic. In contrast, the composite seismic trace is unclipped and shows both peaks and troughs; this display is best for comparison to

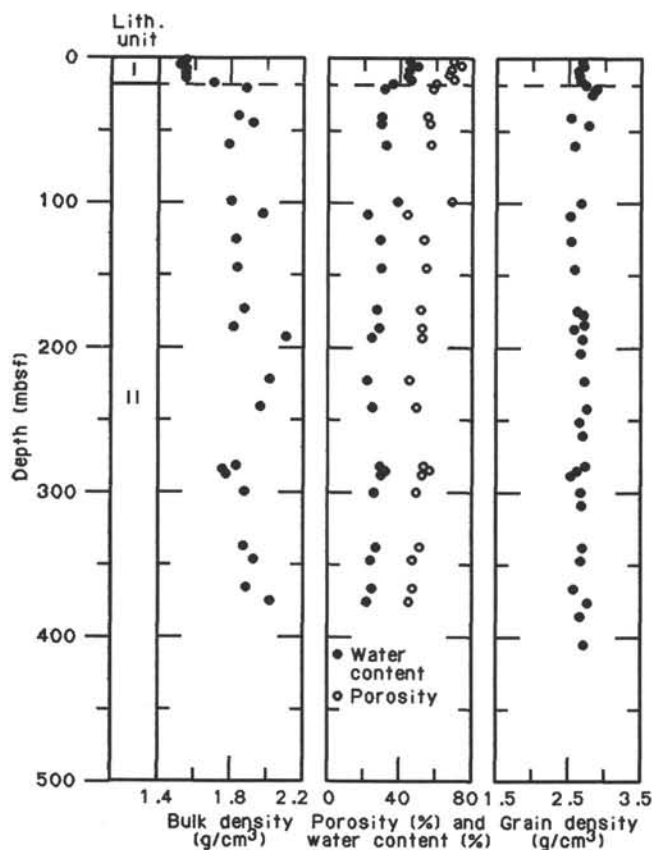


Figure 21. Index properties (wet-bulk density, porosity, water content, and grain density) at Site 720.

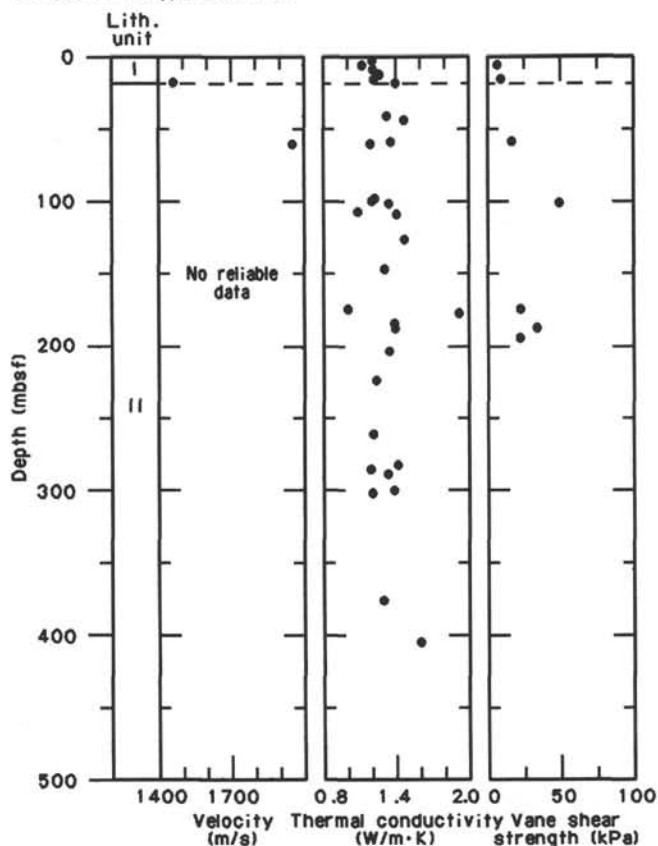


Figure 22. Compressional-wave velocity, thermal conductivity, and vane shear strength measured on discrete samples at Site 720.

the synthetic seismogram but provides no information on the lateral continuity of peaks and troughs, information essential to distinguishing signal from local noise.

Initial comparison of the synthetic seismogram to the seismic traces showed a fair correlation, but traveltimes between the few readily correlatable reflectors were about 8% longer on the seismic trace than on the synthetic. Therefore sonic traveltimes were increased by 8%, in spite of the high replicability found for sonic log data at this site. The revised synthetic shows not only a consistency with seismic traveltimes between reflectors, but also a much better character correlation with the composite seismic trace (Fig. 27). Small-scale features show only a moderate correlation, but major reflectors are readily identified. The peak/trough pair at 100 mbsf on the synthetic seismogram corresponds with a similar pair at 0.11–0.12 s sub-bottom on seismic, the packet of four peaks and central major trough at 213–247 mbsf corresponds with a similar packet at 0.25–0.29 s, and the large peak at 390 mbsf corresponds to a seismic peak at 0.46 s sub-bottom. The most significant mismatch is that the trough on the synthetic seismogram centered on the pelagic unit of 278–290 mbsf occurs in a featureless portion of the seismic trace. However, this trough is the largest sub-bottom reflector on Figure 24 so the composite seismic trace must be contaminated by noise at this location.

Table 7 shows the depths of sequence boundaries at Site 720, based on the correlation between seismic and synthetic seismogram in Figure 27. The A-1/-2 and A-2/-3 boundaries lie above the logged interval, so their depths are based on the assumption of a linear velocity increase between the seafloor and the start of the synthetic seismogram.

SYNTHESIS OF SEISMIC AND STRATIGRAPHIC SEQUENCES

The cored interval at Site 720 is divided into two units based on lithostratigraphy (see "Lithostratigraphy" section, this chapter). Lithologic Unit I, from 0 to 17.22 mbsf, is composed of pelagic nannofossil ooze, with a noncarbonate component of primarily quartz and clay minerals. Lithologic Unit II, from 17.22 mbsf to the bottom of the hole, includes some pelagic beds similar to Unit I but is dominated by turbidite facies: interbedded silty clays, silts, silty sands, and sands which commonly occur in fining-upward sequences on scales of <2 to >50 cm. Unit II has been further subdivided into at least four informal subunits based on downhole log responses (see "Downhole Measurements" section, this chapter).

In the synthesis that follows, an exact match of the estimated depths of sequence boundaries with log depths is not expected: most seismic reflectors are interference patterns that resulting from convolution of the 70-ms long wavelet with a depth interval of about 12 m. In comparing the approximate sequence boundaries with sedimentary facies interpretations from logs, we have used the logs to revise the depths of sequence boundaries by an average of 11 m (Table 7).

The most distinctive relationship between seismic sequences and the lithostratigraphy of Site 720 is in the occurrence of pelagic beds. Both Sequences A and B, as well as five or six of the eight subsequences, have pelagic units at their tops. The two thickest pelagic units in the logged interval (78.8–412.4 mbsf) are at the top of Sequences B and C (3 and 12 m thick, respectively). Subsequence A-1 is the pelagic drape of Subsequence A-2, whereas Subsequence A-3 may have a pelagic top, but limited core recovery precludes precise depth determination for the pelagic bed of Core 117-720A-7X. Only the tops of Subsequence C-1 and the strata below C-2 have no detected pelagic beds. Probably few if any of these sub-bottom pelagic beds are as laterally continuous as the modern sediments of Subsequence A-1. We often identified toplap of underlying beds by the initial ero-

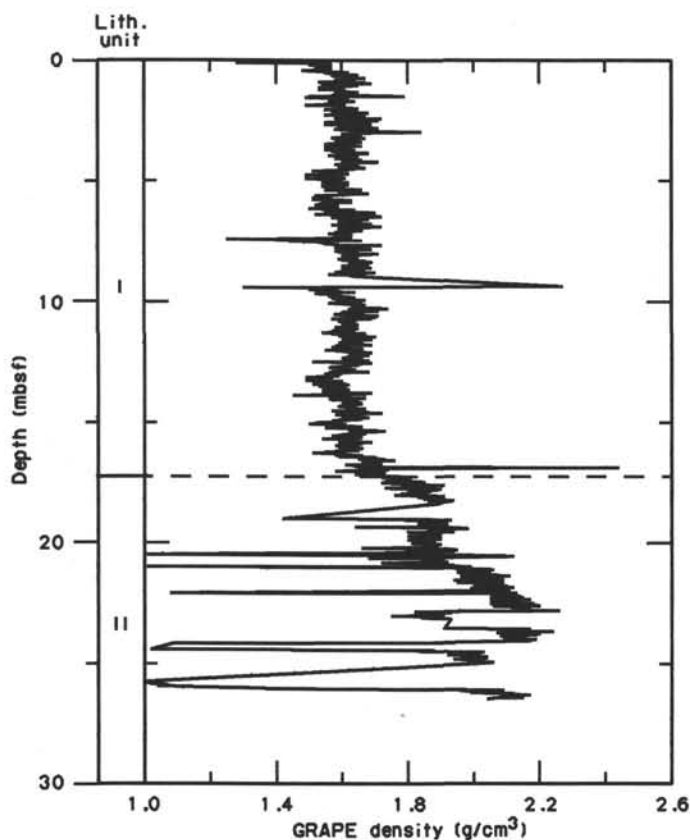


Figure 23. Wet-bulk density as measured by GRAPE for sediments recovered in the interval 0-30 mbsf.

sive stage of channel formation, or by lateral levee migration. Only at the boundary between Sequence B and C is the pelagic bed thick enough to create a prominent seismic reflector (Fig. 24). For the other sequence boundaries, the seismic reflector is created by the velocity contrast between the uppermost clay-rich turbidites of one sequence and the basal, sandy turbidites of the overlying strata.

The top portion of Sequence A (Subsequence A-1) is correlated with lithostratigraphic Unit I, a 17.2-m thick pelagic bed which is 0.5 Ma old. Unit I is the thickest of the many pelagic beds penetrated at Site 720. Its occurrence at Site 720 results from a major late Pleistocene eastward shift of active channel deposition on the Indus Fan (Kolla and Coumes, 1987). Sequence A is mainly composed of turbiditic channel-levee deposits with a high clay content. Since channel switching occurred rapidly, a suite of fining-upward sequences is expected. Due to the need to anchor the bottom-hole assembly during logging, only the lowermost part of Sequence A was logged. Paleontologic and magnetostratigraphic data indicate an age of roughly 0.75 Ma for the base of Sequence A. The most recent episode of substantial uplift of the western margin of Owen Ridge probably occurred between 0.75 and 0.5 Ma, based on the substantial subsidence and turbidite infilling in Subsequences A-2 and A-3 near Owen Ridge, and the lack of a modern seafloor slope toward the ridge in spite of pelagic sedimentation since 0.5 Ma. Two major channels supplied the sediments of Sequence A. The "modern" channel just west of the site formed Subsequence A-2, and a now-buried channel west of the site formed Subsequence A-3. Subsequence A-3 corresponds to an interval of virtually zero core recovery.

On the interpreted thorium log (Fig. 27), the upper part of Sequence B (Subsequence B-1) displays two suites of fining-upward sequences (25 and 60 m thick, respectively), which are composed entirely of small-scale, 5-m thick fining-upward sequences. The two large fining-upward sequences are interpreted to reflect the gradual build-up of levee deposits interrupted by a phase of channel switching, whereas the small-scale fining-upward sequences probably reflect activity periods in the channels. Seismic progradational patterns suggest that both channels were west of the site. The lower part of Sequence B shows large-scale fining- and coarsening-upward sequences on the thorium log, related to the build-up and retreat of unchanneled sheet sands associated to terminated channels (Kolla and Coumes, 1987).

Seven to nine pelagic beds in Sequence B have been identified from logs, and the presence of five has been confirmed in cores, in spite of the 18% average core recovery for Sequence B. Based on comparison of core lithology with logs from Sequence B, core recovery was about 80% for pelagic sediments and about 10% for turbidites. Generally, pelagic intervals may be related to two sources:

1. Major periods of channel switching which occurs after tectonically induced periods of rapid infill. An example is the pelagic Subsequence A-1, which comprises several glacial and interglacial times.
2. Pleistocene sea level variations which largely influence the sediment input to the fan (e.g., Shanmugam and Muiola, 1982). On seismic sections, draping of channel levee deposits occurs when the position of the channel is stable, indicating active and passive periods in channel deposition.

In the interpreted thorium log (Fig. 27), Sequence C exhibits a set of small-scale fining-upward sequences of turbiditic levee deposits. The consistent pattern of thorium log responses throughout the penetrated portion of Sequence C is most easily interpreted as related to a constant position of the nearby large channel. However, as previously discussed, the seismic data are ambiguous concerning the source channel for sediments of Subsequence C-2. No pelagic interbeds are detected in logs from Sequence C, however a single thin bed was identified in Core 117-720A-40X.

INORGANIC GEOCHEMISTRY

Introduction

The results from interstitial water analyses of nine samples from Hole 720A are summarized in Table 8 and displayed in Figure 28. No *in-situ* interstitial water samples were recovered at this site for analysis.

Salinity, Chloride, and pH

The concentration profiles of salinity and chloride in Hole 720A together with the measured pH are shown in Figure 28. Overall, a slight decrease in salinity from 34.3 to 30.6 g/kg to ~300 m was observed, with most of the decrease (about 2.5 g/kg) occurring in the top 50 mbsf. In contrast, the chloride content decreases over the same interval by only ~10 mmol/L (about 0.3 g/kg) from a value at 5.95 mbsf of 554 mmol/L. The salinity decrease can be accounted for by the loss of Mg^{2+} and SO_4^{2-} from solution; a roughly 25-mmol/L decrease in the Mg^{2+} concentration and total depletion of sulfate within the top 50 m at this site (see below) would reduce the salinity by roughly 3 g/kg which approximately accounts for the observed difference. Hole 720A has a mean pH value of 7.77 and displays little significant variation with depth.

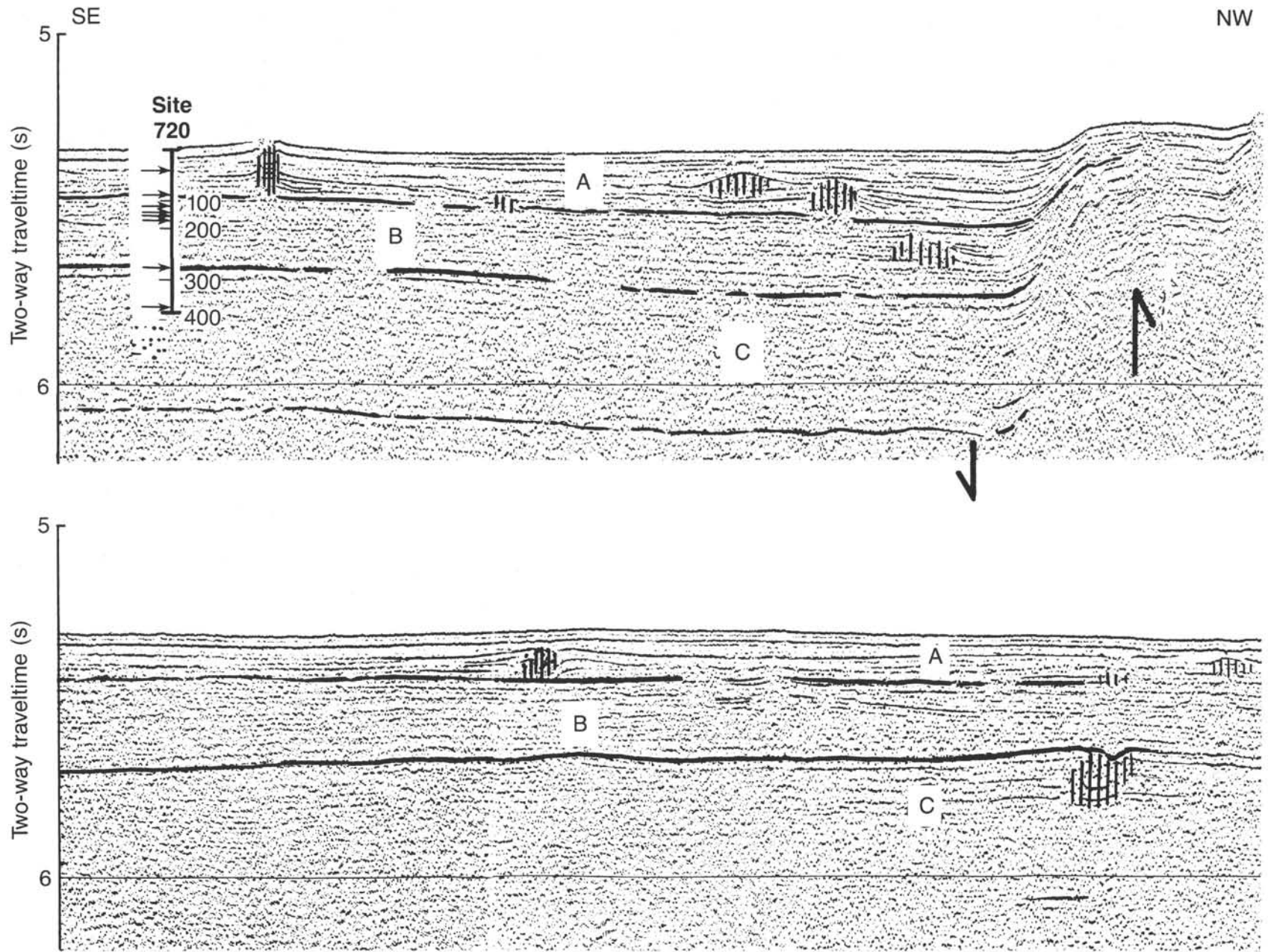


Figure 24. Cross section through the western part of the Indus Fan and the eastern margin of Owen Ridge. A, B, and C tie to major depositional sequence boundaries. Arrows (->) on Site 720 section point to pelagic horizons as identified by the lithologic sequence recovered (from seismic line RC2704 Line 1, 1986). Section is 150 km long.

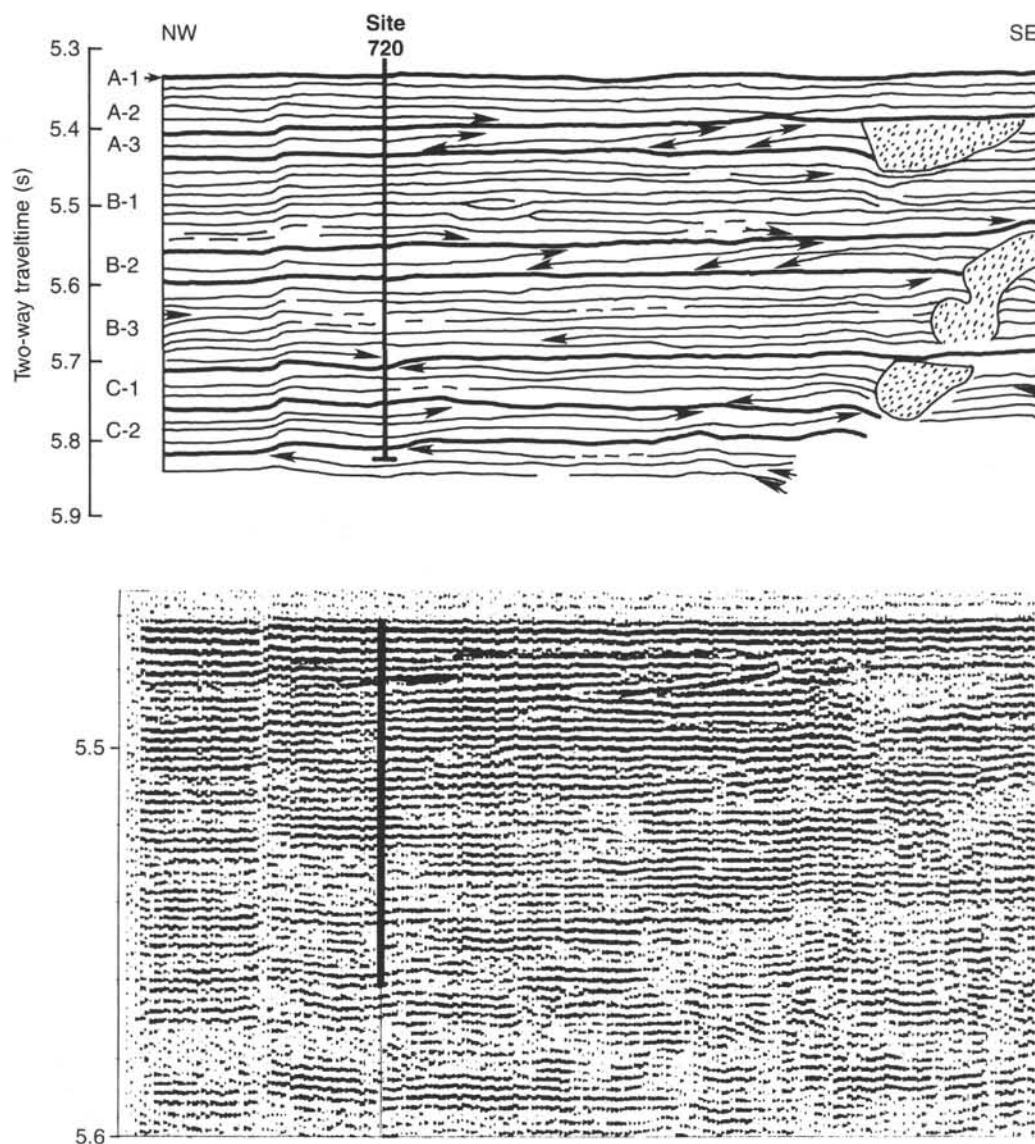


Figure 25. Interpretation of seismic section at Site 720 displays major depositional sequences (A, B, and C), which are divided into subsequences (from seismic line RC2704 Line 49, Leg 2704, 1986).

Sulfate and Alkalinity

Figure 28 indicates that sulfate reduction is complete by 59 mbsf. This is not surprising considering that the turbidites contain substantial organic matter (see "Organic Geochemistry" section, this chapter) and accumulate very rapidly (see "Biostratigraphy" section, this chapter). The amount of oxygen which can diffuse into the sediments to replenish that lost during bacterial degradation of the organic component is thus strongly limited, and sulfate is depleted as a consequence. The production of sulfide in these sediments and the associated reduction and removal of iron from clay minerals and oxide grain-coatings leads to the formation of pyrite (see below). Because no dissolved sulfide was present in the pore waters, an observation based entirely on the absence of the odor of H_2S , we infer that relatively large concentrations of iron must have been extracted from clay minerals or iron minerals and fixed as authigenic pyrite. Drever (1974) has suggested that Mg^{2+} replaces Fe^{3+} extracted diagenetically in this way. Such a reaction could account for some of the Mg^{2+} depletion observed at depth at this site.

Alkalinity, largely a measure of the HCO_3^- content, increases from 5.08 mmol/L at 6 m depth to 6.73 mmol/L at 23.5 mbsf

(Fig. 28). Below this depth, the alkalinity decreases to a mid-hole minimum of 3.12 mmol/L at 146 mbsf. A local maximum of 5.68 mmol/L at 284 m depth (Core 117-720A-30X) coincides with the occurrence of a pelagic nannofossil ooze sequence which is enriched in organic carbon. Dissolved ammonia, phosphate, and silicate concentrations are also anomalously higher at this depth, indicating that the pelagic unit is (or was?) a locus of diagenetic activity within the drilled fan sequence. The low value (2.50 mmol/L) at the bottom of the hole suggests that authigenic carbonate minerals are precipitating near the base of the cored section.

Calcium and Magnesium

At Site 720 both Ca^{2+} and Mg^{2+} are depleted below seawater values (Fig. 28) in the topmost sample (7.9 and 50.3 mmol/L, respectively). However, while Mg^{2+} decreases asymptotically to a value of ~ 30 mmol/L, the Ca^{2+} concentration generally rises with depth below 25 mbsf reaching a maximum of 9.36 mmol/L at the bottom of the hole. This relationship is reflected by the decreasing Mg^{2+}/Ca^{2+} ratio (Fig. 28). Maximum curvature on the depth profiles of these two cations suggests that most of the

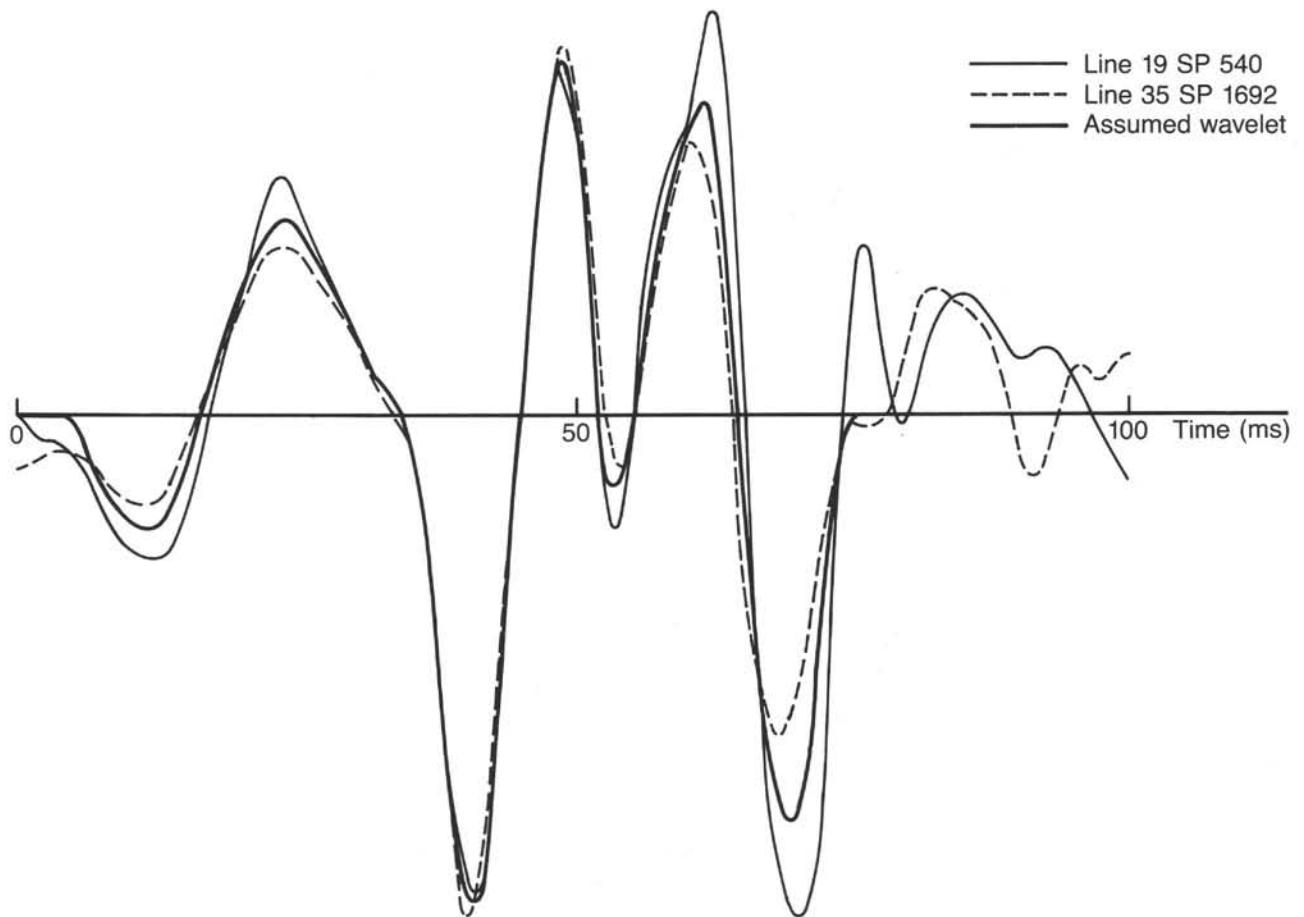


Figure 26. Greatly expanded seafloor portion of seismic traces from two regions surveyed by *Robert Conrad* for Leg 117 (RC2704). The heavy solid line is the wavelet used for the synthetic seismogram of Figure 27, based on averaging the two traces.

diagenetic reactions involving calcium and magnesium (e.g., ionic exchange in clay lattice sites such as replacement of iron by magnesium, and calcite and dolomite dissolution/precipitation reactions) occur in the top 100 m. Interestingly, the lowest Mg^{2+} and highest Ca^{2+} contents (26.3 and 9.4 mmol/L, respectively) occur in the deepest sample where the minimum alkalinity was observed. These observations are consistent with the contention that dolomite formation, perhaps by dolomitization of calcite, is occurring in this deep zone.

Ammonia, Phosphate and Silicate

Ammonia and phosphate distributions (Fig. 28) in the upper 100 m at the site are consistent with the addition of metabolites to pore water during the bacterially-mediated decomposition of organic matter. Ammonia concentrations increase from 0.58 mmol/L at 6 m depth to a relatively high maximum of 3.12 mmol/L at 284 mbsf. Although phosphate values reach a maximum of 13.9 $\mu\text{mol/L}$ at 23 m depth, the extremely high ammonia/phosphate ratio and the decrease in concentration at greater depths suggests that phosphate is being removed from solution by the diagenetic precipitation of minor amounts of apatite (not detectable by XRD). The silicate concentration at 6 mbsf (626 $\mu\text{mol/L}$, Fig. 28) is much higher than the predicted bottom-water value (140 $\mu\text{mol/L}$; Broecker and Peng, 1982) indicating that opaline silica is dissolving in the pelagic nannofossil ooze. Below the uppermost sample, dissolved silicate levels decrease to $\sim 150 \mu\text{mol/L} \pm 100 \mu\text{mol/L}$ except for the sample at 284 m depth which contains the highest concentration (1014 $\mu\text{mol/L}$)

measured in the hole. Relatively high levels of phosphate, ammonia, and alkalinity also occur at this depth which, as noted earlier, can be attributed to more pronounced diagenetic reactivity in the organic-carbon-rich nannofossil ooze sequence in Core 117-720A-30X. The high dissolved silica content reflects local dissolution of biogenic opal in this interval. The deficiency of dissolved silica in much of the rest of the hole may be attributed to a paucity of opal in the terrigenous turbidite facies. It is clear that interstitial waters at this site cannot be in diffusive steady state, which is a direct consequence of the extremely high sedimentation rates on the fan. Length scales for diffusion over a period of 1 Ma would be in the range of 60–90 m assuming a diffusion coefficient on the order of $10^{-6} \text{ cm}^2 \text{ s}^{-1}$.

Sediment Mineralogy

The mineralogy of the nine sediment residues remaining after extraction of interstitial waters was determined by X-ray diffractometry using the onboard Philips PW1729 diffractometer. Samples were lightly ground in a porcelain mortar and pestle and presented to the X-ray beam as pressed unoriented powders in aluminium holders. No pre- or post-diffraction treatments were performed.

The gross mineralogy of the bulk sediments varies predictably and in accord with the major lithological units: calcite dominates the pelagic nannofossil oozes and quartz the terrigenous clastics. Notable concentrations of calcite also occur in all samples comprised of terrigenous clastics which can be attributed to the presence of calcite of detrital origin in addition to biogenic

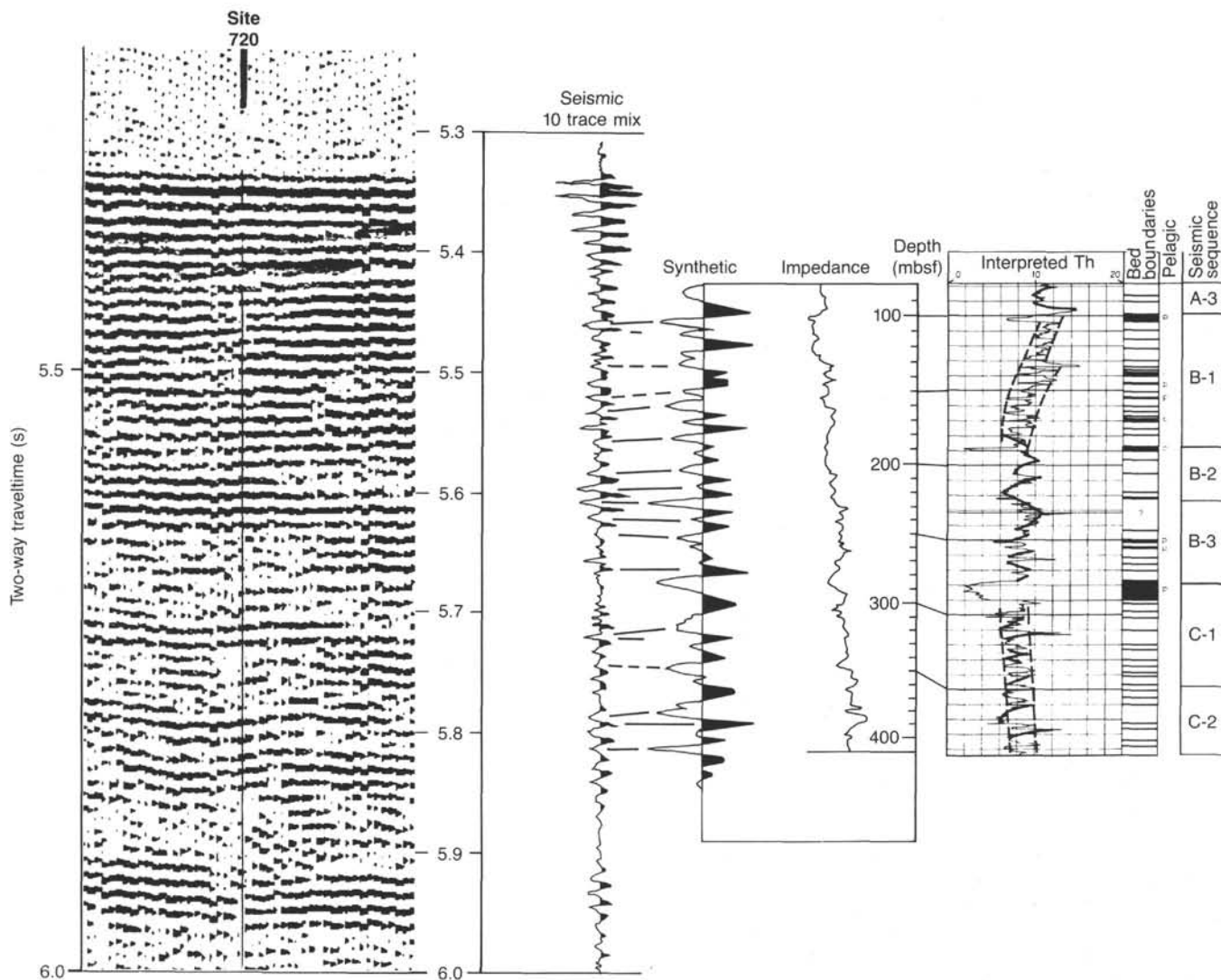


Figure 27. Fit of a synthetic seismogram into observed seismic data and into an interpreted Th log.

Table 7. Correlation of seismic sequence boundaries with depth at Site 720A.

Sequence	Seismic time	Depth from synthetic seismogram (mbsf)	Revised depth from log facies (mbsf)
A-1	0.00-0.02	0-20	0-17.2
A-2	0.02-0.07	20-65	17.2-(65)
A-3	0.07-0.10	65-90	(65)-103
B-1	0.10-0.22	90-175	103-190
B-2	0.22-0.25	175-205	190-222
B-3	0.25-0.36	205-300	222-290
C-1	0.36-0.42	300-355	290-347
C-2	0.42-0.47	355-400	347-391

CaCO_3 . The former was observed by optical microscopy (see "Lithostratigraphy" section, this chapter). Micas and illite occur in significant amounts in the terrigenous detritus of both mud- and sand-dominated facies. Muscovite and biotite were identified in smear slides and are evident in all diffractograms with the exception of the calcareous ooze samples. A small but well-defined peak at about $12.5^\circ 2\theta$ is attributed to kaolinite plus chlorite. Because the kaolinite and chlorite diffraction spectra overlap to a considerable extent, differentiating between the

two minerals is difficult. Close examination of the joint peak at about $25^\circ 2\theta$, however, suggests that reflections from both kaolinite (002) at 3.57 \AA ($24.88^\circ 2\theta$), and chlorite (003) at about 3.50 \AA ($25.30^\circ 2\theta$), are present. Although the severe chemical weathering characteristic of tropical and subtropical weathering usually precludes the occurrence of chlorite in low-latitude marine sediments, physical weathering at high elevations in the Himalaya contributes considerable amounts of detrital chlorite to the sediment load of the Indus River (Emeis, 1985) and thence to the fan. Kolla et al. (1981b) noted that chlorite was relatively abundant in the clay fraction of surface sediments in the northern and central Arabian Sea and that kaolinite was uncommon in these areas.

The occurrence of two other minerals bears mention in this summary. Dolomite occurs in trace quantities in all samples with the exception of the terrigenous mud at 294 mbsf in which a significantly larger concentration (several percent) of the mineral is present. Although the Mg^{2+} and alkalinity depletions observed in the pore waters suggest, as described above, that authigenic dolomite is forming at depth in the sediments, authigenesis is unlikely to account for the significant presence of the mineral indicated by the diffractograms. Dolomite of apparent detrital origin was noted in the sedimentological descriptions (see "Lithostratigraphy" section, this chapter) and it is probable that a continental source may account for the presence of the mineral in

Table 8. Summary of interstitial water geochemical data for Hole 720A.

Sample	Depth (mbsf)	Vol. (mL)	pH	Alk. (mmol/L)	Sal. (g/kg)	Mg (mmol/L)	Ca (mmol/L)	Cl (mmol/L)	SO ₄ (mmol/L)	PO ₄ (μmol/L)	NH ₄ (mmol/L)	SiO ₂ (μmol/L)	Mg/Ca
117-720A-													
1H-4, 145-150	5.95	70	7.54	5.08	34.3	50.28	7.85	554	21.4	9.6	0.58	626	6.41
3H-3, 145-150	23.45	35	7.80	6.73	33.0	41.19	4.73	558	8.5	13.9	1.18	162	8.71
7X-1, 145-150	59.05	28	7.68	5.58	31.8	31.40	5.91	544	0.0	1.9	2.01	218	5.31
11X-2, 145-150	99.35	39	7.55	3.88	32.2	31.22	7.29	546	0.0	1.5	2.79	391	4.28
16X-1, 145-150	146.15	29	7.79	3.12	31.7	30.88	6.35	543	0.0	1.6	3.09	233	4.86
19X-2, 140-150	176.60	29	8.00	4.09	31.0	29.98	6.55	545	0.0	1.0	2.47	116	4.58
24X-1, 140-150	223.40	40	7.97	—	31.0	31.07	6.89	548	0.0	0.6	2.43	121	4.51
30X-3, 145-150	284.25	28	7.63	5.68	30.6	28.93	6.81	543	0.0	3.8	3.12	1014	4.25
40X-1, 140-150	377.30	30	7.96	2.50	31.8	26.32	9.36	547	0.0	<0.2	2.19	80	2.88

the fan sediments. Pyrite is also present in trace quantities in most of the samples. This mineral is certainly of authigenic origin and its presence in the diffraction traces is consistent with the total depletion of dissolved sulfate observed in pore waters below about 50 mbsf.

ORGANIC GEOCHEMISTRY

The organic geochemical program at Site 720 consisted of measurements of hydrocarbon gases, total carbon and carbonate carbon, and Rock-Eval pyrolysis. The methods and instrumentation used are described in detail in the "Explanatory Notes" chapter (this volume).

Organic Matter Abundance and Character

Carbonate carbon and organic carbon, measured as total carbon minus carbonate carbon, were determined by coulometry on 52 samples. These samples had been previously used for either headspace analyses or physical properties measurements. In addition, some samples were selected after visual inspection of the cores, because they were thought to contain charcoal.

Results of the measurements are listed in Table 3 and the CaCO₃ depth profile is shown in Figure 5 (see "Lithostratigraphy" section, this chapter). Organic carbon values are relatively high for open marine sediments; approximately 50% of the analyzed samples have an organic carbon content above 0.40%. Most pelagic marine sediments have organic carbon concentrations less than 0.2% (Degens and Mopper, 1976). In general, organic carbon values in Hole 720A do not exceed the 1% level. The terrestrial nature of the organic matter in Hole 720A, as evident from Rock-Eval pyrolysis measurements, is in accord with the largely turbiditic and land-derived nature of the sediments. Generally, organic carbon values are higher at ODP Site 720 than those measured in sediments from DSDP Site 222, Leg 23 (Bode, 1974).

Most likely, the relatively high organic carbon content of sediments from the Indus fan is the result of rapid sedimentation, which enhances preservation, in combination with an high input of terrigenous organic matter (see below). The sedimentary sink of continental-derived organic matter is normally in nearshore environments, but the major river systems of southeast Asia, such as the Indus, are known to have depositional centers extending several thousand kilometers offshore (Kolla et al., 1981b).

The Rock-Eval pyrolysis method was used to characterize the type and maturity of the organic matter. The results are listed in Table 9. The hydrogen index vs. the oxygen index (both calculated from the coulometric organic carbon data) of the organic matter are plotted in Figure 29. They show that oxygen-rich, cyclic, or refractory organic matter (kerogen type III) is the almost exclusive organic component in sediments of sedimentary Unit II, i.e., the turbiditic unit below 17.3 mbsf to total depth. The or-

ganic matter in sedimentary Unit I is immature, and, in spite of its marine pelagic facies, has relatively high oxygen indices. Therefore, the organic matter of Unit I can also be classified as kerogen Type III. This may be attributable to a contribution of oxygen-rich components which have not been degraded by bacteria.

Hydrocarbon Gases

During the routine safety monitoring program for hydrocarbon gas accumulations, 10 sediment samples were taken for interstitial gas analysis by the headspace technique. These samples were collected adjacent to interstitial water and geochemistry samples (Table 10) in Hole 720A. In addition, vacuater samples were taken when gas pockets were observed. The overwhelmingly predominant hydrocarbon gas is methane, which occurs in quantities ranging from 27 μL/L of sediment to 0.375 L/L of sediment. The organic carbon concentrations are relatively high and the terrestrial origin of the organic matter in the sediments recovered at Site 720 (see below) classifies the turbiditic sequence of lithologic Unit II as a gas-prone source rock. *In-situ* thermal maturation has not produced any thermogenic gas, and hence ratios of methane to C₂₊ hydrocarbons are very high (between 31 × 10³ and 19 × 10³). The methane appears to be of biogenic origin, an assumption that is corroborated by the inverse relationship of methane and interstitial sulfate (Fig. 30; see "Inorganic Geochemistry" section, this chapter). Due to high sedimentation rates and closing of the sedimentary system to diffusion from the seafloor, the interstitial sulfate is exhausted by organic matter oxidation during microbial sulfate reduction at approximately 60 mbsf. Below 60 mbsf microbial remineralization of sedimentary organic matter appears to be dominated by methane production. A generally decreasing trend of methane abundances below 100 mbsf may be attributed to exhaustion of organic matter that can be metabolized.

DOWNHOLE MEASUREMENTS

Introduction

Three Schlumberger logging runs were planned at Site 720, i.e., the seismic stratigraphic, lithoporosity, and geochemical combinations. The tool strings and their applications are described in the "Explanatory Notes" chapter (this volume). The primary logging objectives at the site were: (1) turbidite bed delineation for study of variations in source region and depositional environment, (2) determination of the thickness and location of pelagic interbeds, (3) seismic/core tie through a synthetic seismogram, (4) detailed mineralogy, and (5) major element geochemistry. Only the first three objectives were fully achieved, due to loss of the seismic stratigraphic tool string downhole and consequent curtailment of logging operations.

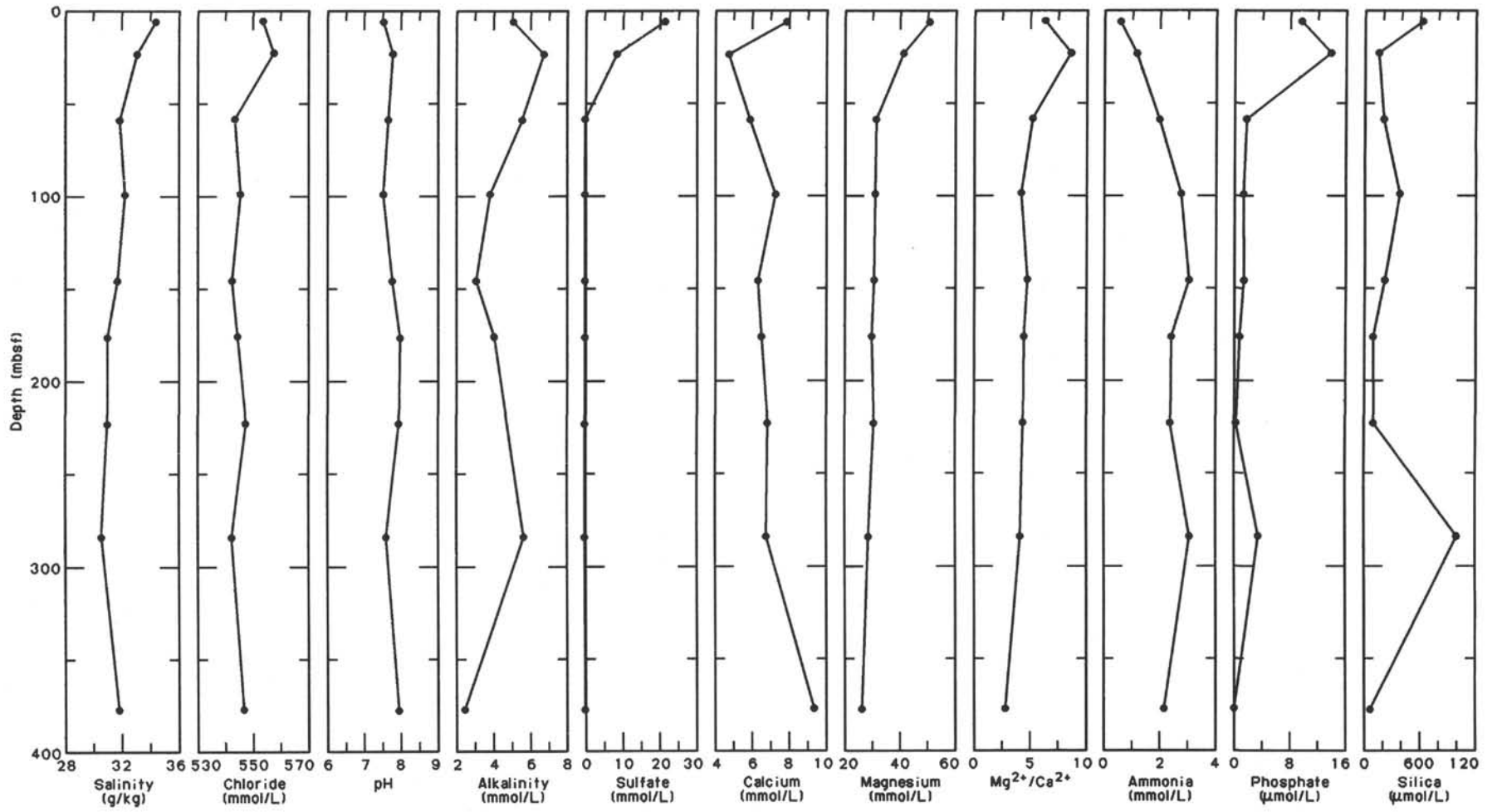


Figure 28. Concentrations profiles vs. depth for Hole 720A.

Table 9. Results of Rock-Eval pyrolysis of sediment samples from Hole 720A.

Core, section, interval (cm)	Depth (mbsf)	T _{max} (°C)	S ₁	S ₂	S ₃	S ₂ /S ₃	TOC	HI	OI
117-720A-									
1H-2, 40-42	1.90	395	0.09	0.13	0.62	0.20	0.53	40	188
1H-4, 40-42	4.90	393	0.15	0.30	0.68	0.44	0.58	52	117
1H-4, 144-145	5.94	404	0.37	0.42	0.81	0.51	0.46	91	176
1H-6, 40-42	7.90	396	0.11	0.23	0.56	0.41	0.25	92	224
2H-2, 40-42	11.30	395	0.10	0.18	0.54	0.33	0.30	60	180
2H-4, 40-42	14.30	407	0.15	0.45	0.70	0.64	0.61	74	115
3H-2, 24-26	20.74	590	0.04	0.09	0.47	0.19	0.51	18	92
5X-2, 36-38	40.06	475	0.15	0.06	0.39	0.15	0.38	16	103
5X-5, 85-87	45.05	379	0	0.06	1.35	0.04	0.41	15	329
6X-1, 16-18	48.06	419	0	0.57	1.84	0.30	0.55	104	335
7X-1, 144-145	59.04	393	0.23	0.43	0.25	1.72	0.96	45	26
7X-2, 49-51	59.59	403	0	0.17	1.30	0.13	0.74	23	176
11X-2, 144-150	99.34	415	0.19	0.54	0.69	0.78	0.50	108	138
11X-2, 109-111	98.99	418	0	0.59	2.04	0.28	0.78	76	261
11X CC, 0-1	101.07	393	0.15	0.07	0.18	0.38	0.30	23	60
12X-2, 25-26	107.75	366	1.48	2.66	0.92	2.89	3.70	72	^a 25
12X-2, 56-58	108.05	312	0	0.05	0.69	0.07	0.28	18	246
14X-1, 29-31	125.69	276	0	0.02	1.03	0.01	0.32	6	322
16X-1, 64-66	145.34	383	0	0.39	1.96	0.19	0.72	54	272
19X-1, 149-150	175.19	332	0.03	0.05	0.44	0.11	0.35	14	126
19X-1, 34-36	174.04	312	0	0.07	1.55	0.04	0.39	21	456
20X-2, 63-64	185.53	367	0.16	0.10	0.32	0.31	0.33	30	96
20X-3, 45-47	186.85	397	0	0.34	1.67	0.20	0.56	61	298
21X-1, 51-53	193.51	273	0	0.01	0.92	0.01	0.25	4	368
26X-1, 31-33	241.71	273	0	0.04	1.11	0.03	0.34	11	326
27X-1, 40-42	251.40	237	0	0	0.22	0	0.29	0	76
28X-1, 40-42	260.90	420	0	0.05	0.60	0.08	1.64	3	36
30X-2, 111-113	281.41	390	0	0.21	1.66	0.12	0.88	23	188
30X-4, 1-2	284.31	409	0	0.91	1.96	0.46	1.45	62	135
30X-4, 98-100	285.28	386	0	0.38	2.01	0.18	0.42	90	478
30X-6, 100-102	288.30	413	0	1.39	2.17	0.64	1.34	103	161
32X-1, 93-95	299.95	232	0	0.02	1.46	0.01	0.36	5	405
36X-1, 1-2	337.41	212	0	0.07	1.32	0.05	0.41	17	321
37X-1, 19-21	347.19	203	0	0.04	0.94	0.04	0.28	14	335
39X CC, 11-13	366.72	193	0	0.04	1.35	0.02	0.54	7	250
40X-1, 24-26	376.14	397	0	0.23	1.70	0.13	0.40	57	425
43X-1, 57-59	405.17	268	0	0.03	0.37	0.08	0.35	8	105

Note: HI = hydrogen index and OI = oxygen index. For a detailed description of parameters, see "Explanatory Notes" chapter (this volume).

^a Sample suspected to contain charcoal.

Operations

Thirty eight hours were allotted for logging at Site 720, including time allotted for possible use of the sidewall entry sub (SES). The SES was not used, because drilling and hole conditioning showed good hole conditions, and because capillary suction time tests on three samples (pelagic clay, turbidite clay, and turbidite clayey silt) showed only minor clay swelling.

Hole conditioning began at 1440 on 1 September 1987 and concluded at 2245. This conditioning included sweeping the hole with 30 barrels of gel mud, a wiper trip, another 30 barrel sweep, bit release, displacing the hole with polymer mud, and pulling pipe to 70 mbsf for logging. Hole conditioning was slower than anticipated because of special projects (pressure testing of the Barnes tool and treating the sand line) and because gas shows required displacing the hole with mud.

Logging tool rigup began at 2245 and concluded 1.75 hr later. The digital seismic stratigraphic combination (long spaced sonic, spectral gamma ray, and phaser resistivity) obtained open-hole logs while running down to the bottom. Hole conditions were generally good, with only one bridge encountered and broken through at about 90 mbsf. Logging upward commenced at 0342 on 2 September. Nearly the entire interval was logged, before the tool was stopped and soon stuck in the reformed bridge at 97 mbsf.

In order to free the tool, a new cutter and crimper combination was sent down the pipe at 0810. The objective was to cut and clamp the logging cable in the BHA, lower pipe through the bridge to free the tool, then pull both pipe and logging tool out

of the hole. However, the cutter/crimper fired at 1500 m below rig floor rather than 4050 m, and lowering the pipe apparently failed to break through all of the bridge and free the logging tool. When the BHA was pulled to the rig floor, 2600 m of cable and the tool string failed to accompany it.

Logging operations terminated at 1030 on 2 September, when pulling up of the drill string commenced. In all, 20 of the 38 hr allotted for logging were utilized.

Log Quality and Editing

Logs were obtained both during lowering of the tool string from pipe to total drilled depth and during raising of the tool string from total depth to the bridge at 97 mbsf. Less than 2 m of cavings were present at the bottom of the hole. A more significant data loss near the bottom of the hole results from the length of the tool string: resistivity is measured 1.8-2.9 m above the bottom of the tool, sonic response is measured 12.8-13.4 m above the tool bottom, and spectral gamma ray is measured 21.2 m above tool bottom. A 45-cm downward shift of resistivity curves was applied, as indicated by comparison of the depths of similar horizons on sonic and resistivity. A 2.6-m upward shift of downgoing logs was applied to depth-justify them with upcoming logs. The final log interval of live data was 78.8-390.9 mbsf for downgoing logs and 104.0-412.4 mbsf for upcoming logs.

Log quality was generally excellent for upcoming logs and very good for downgoing logs. Overlay of downgoing and up-

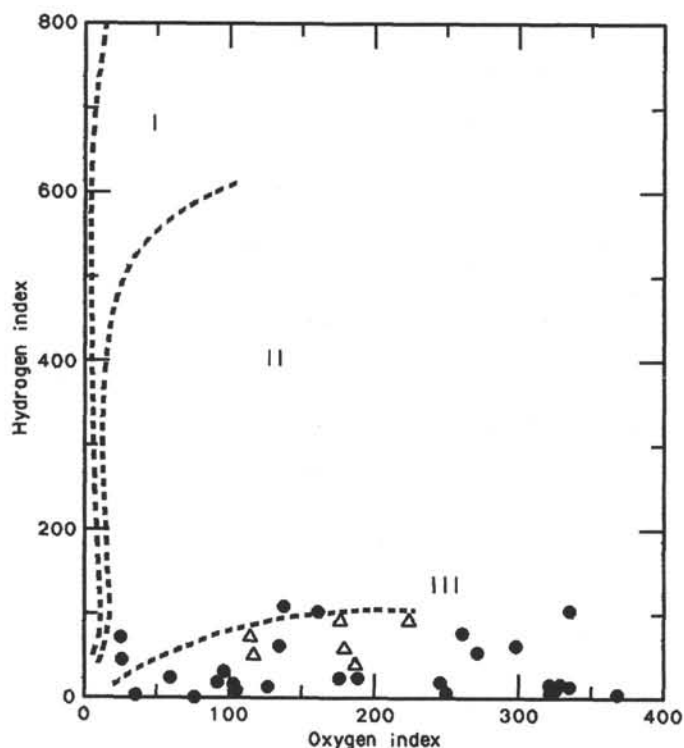


Figure 29. Oxygen vs. hydrogen indices of organic matter in Hole 720A, indicating that the organic matter is predominantly of kerogen type III. This type of diagram suggests that sediments are dominated by terrestrial and reworked residual material from erosion of the continent and transport of land-derived organic matter via turbidity currents. Explanation of symbols: triangle = Pelagic Unit 1; circle = Pelagic interval Core 30X; dot = Clastic Unit 2.

Table 10. Interstitial gas abundances and ratios of methane (C_1) to ethane (C_2) in samples of headspace gas from Hole 720A.

Core, section interval (cm)	Depth (mbsf)	C_1 ($\mu\text{L/L}$)	C_2 ($\mu\text{L/L}$)	C_1/C_2
117-720A-				
1H-4, 144-145	5.94	27		
7X-1, 144-145	59.04	110,418		
11X-2, 149-150	99.39	375,390	12	31,283
16X-1, 120-121	145.90	170,446	9	18,938
19X-1, 149-150	177.19	61,622		
22X-1, 0-1	202.70	52,364		
24X-1, 139-140	223.39	94,323	3	31,441
30X-4, 1-2	284.31	98,675	5	19,735
36X-1, 0-1	337.41	52,979		
40X-1, 139-140	377.29	27,245		

Note: Values are expressed in $\mu\text{L/L}$ (volume gas/volume wet sediment). The very high ratios of C_1/C_2 show that gas is of biogenic origin.

coming logs shows that the two are virtually identical for resistivity and sonic logs. Gamma ray logs are quite similar but differ in finest-scale features, as expected from the poorer counting statistics for the spectral gamma tool at the high logging speed used for the downgoing log. This degradation of counting statistics makes the calculated abundances of potassium, thorium, and uranium substantially less accurate in the downgoing log

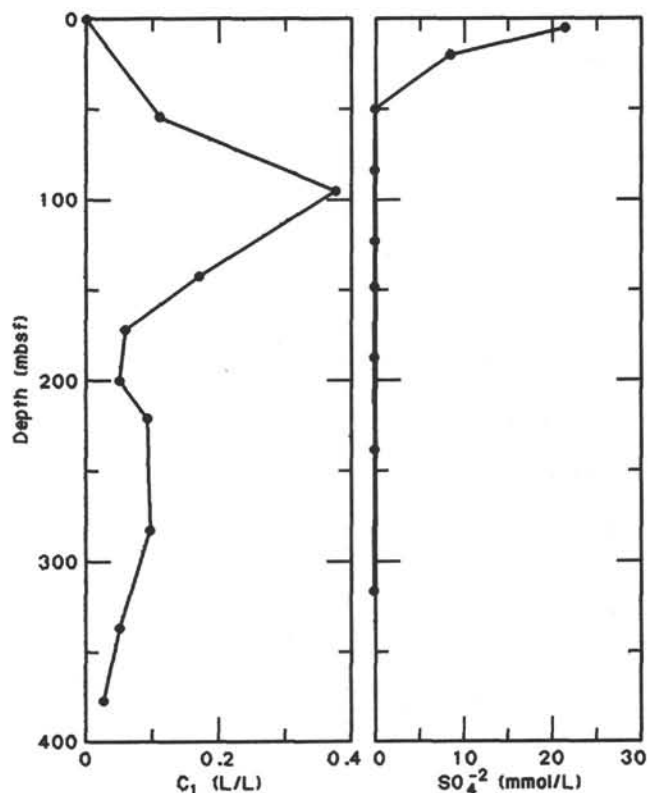


Figure 30. Methane abundances in sediments from Hole 720A. Sulfate concentrations, which determine the extent of organic matter oxidation and methane production, approach 0 mmol/L at approximately 60 mbsf. Below this depth, methane concentrations from bacterial processes rise significantly.

than in the upcoming log. Post-cruise reprocessing of spectral gamma ray logs is possible but has not yet been done.

Because of the higher accuracy of the upcoming logs, we only use these in the interval for which they are available. We did not average downgoing and upcoming logs, because slight cable stretch between and within runs is likely to cause depth mismatches of up to 30 cm; averaging then would degrade vertical resolution without significantly improving signal-to-noise ratio. Downgoing logs for the interval 78.8-104.0 mbsf were merged with the upcoming logs available below that depth, in order to provide continuous logs over the interval 78.8-412.4 mbsf. Note, however, that the spectral gamma log obtained data only for the interval 78.8-394.3 mbsf, because of its higher position in the tool string.

The only unreliable data obtained were from the spherically focussed log (SFL). Nearly all of the SFL data are consistent with the other resistivity logs, but occasional very large resistivity spikes occur. These presumably are caused by either electrical or data telemetry problems. A similar phenomenon was noted on Leg 116. No problems were encountered in bench tests.

Porosity and Velocity

In deep-sea sediments, both the sonic and resistivity logs respond primarily to porosity variations. Resistivity is relatively insensitive to mineralogy (at least for the high-porosity sediments considered here), whereas sonic velocity is somewhat sensitive to mineralogy though dominantly sensitive to porosity. Furthermore, the relationship of velocity to porosity is poorly known for high-porosity sediments. Thus resistivity can be a superior tool for porosity determination.

The relationship of formation resistivity to porosity is well known from the Archie (1942) equation:

$$S_w^a = \frac{aR_w}{f^m R_t}$$

where S_w is water saturation (equal to 1 for these virtually hydrocarbon-free sediments), R_w is resistivity of the formation water, f is fractional porosity, R_t is measured formation resistivity, and both a and m are "constants" dependent on lithology and pore geometry. We calculated porosity using the Humble formula (Winsauer et al., 1952), which assumes that $a = 0.62$ and $m = 2.15$.

We calculated R_w based on its known relationships to temperature and salinity (Keller, 1982). Measurements of interstitial water salinities at this site (see "Inorganic Geochemistry" section, this chapter) are widely spaced but suggest a gradual decrease from 31 g/kg at about 70 mbsf to 29 g/kg at the bottom of the hole. Temperature of formation water near the borehole is not known with certainty, but it is probably similar to the temperature of the borehole fluid. Temperature within the resistivity tool is continuously measured during logging. This measured temperature gradually increased from 4°C to 5°C during downgoing logging, and it decreased from 38°C to 37°C during upcoming logging. The substantial difference between the two temperature logs arises from the long delay time for the interior of the tool to reach equilibrium with ambient temperatures. Because the tool remained near bottom for about an hour, the 38°C reading probably is a good estimate of bottom-hole temperatures. We assumed a linear thermal gradient from 1°C at the seafloor to 38°C at 412 mbsf. This thermal gradient is consistent with the seafloor age and is identical to that measured at Site 646 (Arthur et al., in press), where both crustal age and sediment type are very similar to Site 720.

The resulting porosity log closely mimics the character of the measured resistivity log, while the overall trend of porosity values is controlled by the choice of a , m , and R_w . Calculated porosities were much lower than expected porosities for terrigenous sediments, probably because the values for a and m are inappropriate for these sediments. Unfortunately, these parameters have seldom been determined for high-porosity terrigenous sediments. Thus we are forced to calibrate our porosity log to either laboratory measurements on cores (see "Physical Properties" section, this chapter) or the empirical porosity/depth trend of Hamilton (1976). We used the core measurements for calibration, multiplying all calculated porosities by 1.5.

This final porosity curve (Fig. 31) may be incorrect by as much as 5% porosity, but the relative porosity changes are much more accurate, as they are controlled by measured resistivity rather than assumed values for a and m . The gradual and normal compaction profile is not evident in the resistivity log (Fig. 31), because the effect of gradual compaction on resistivity is obscured by the gradual downward decrease in fluid resistivity due to increasing temperature. The effect of the salinity correction is trivial.

Two velocity logs are measured during each logging run: a short-spaced log which measures the difference between travel-times for receivers 2.44 and 3.05 m from the transmitter, and a long-spaced log which similarly uses 3.05- and 3.66-m spacings. Both logs are virtually identical throughout each run, and the the downgoing and upcoming logs are nearly identical. Figure 31 shows the long-spaced velocity log. Velocities increase gradually from 1.7 to 2.1 km/s over the logged interval due to compaction. Substantial variations from this average trend are observed, primarily due directly to porosity changes (Fig. 31) and indirectly to changes in clay mineral content. Velocities are gen-

erally slightly higher than the empirical velocity/depth trend of Hamilton (1979) for terrigenous sediments. This observation is consistent with the finding of lower core porosities (see "Physical Properties" section, this chapter) and lower core-calibrated log porosities than Hamilton's (1976) empirical trend, suggesting that the clay mineral content at Site 720 is somewhat lower than at the sites on which the empirical trends were based.

Lithology and Mineralogy

The logged interval at Site 720 is from lithologic Unit II, a dominantly terrigenous turbidite section with rare pelagic interbeds (see "Lithostratigraphy" section, this chapter). The turbidites are primarily clayey silts and silty clays, with rare clays. Dominant minerals in the turbidites are quartz, feldspar, detrital carbonate, and clay minerals, with occasional mica. Preliminary clay mineralogy studies (see "Inorganic Geochemistry" section, this chapter) indicate that illite is the dominant clay mineral, but chlorite also occurs. Most pelagic interbeds are a few centimeters to 2 m in thickness; a single bed greater than 9 m thick was found in Core 117-720A-30X. The pelagic intervals are composed of clay minerals and nanofossils.

The gamma-ray log, which responds to K, Th, and U that are usually found primarily in clays, shows a general trend of decreasing values downhole, from 85 to 70 API units (Fig. 32). The pelagic intervals are readily visible on the gamma-ray log as downward spikes of 20–30 API units below the turbidite average. Based on the gamma-ray response, pelagic interbeds probably occur at 101–103, 139, 155–156, 170, 188–190, 201–202, and 277–290 mbsf. Several other negative spikes of lower amplitude are probably thinner pelagic units that are near the 0.5-m vertical resolution limit of the log. Separately examining the K and Th contributions to the gamma ray log (Fig. 33), we see that both Th and K are lower in the pelagic intervals than in the turbidites. The Th/K ratio is only slightly lower in the pelagics than in the turbidites (Fig. 32). U/Th (not shown) exhibits extremely large positive spikes at the two pelagic intervals 188–190 and 277–290 mbsf, indicating U enrichment in addition to the Th depletion. U/Th spikes are often caused by enrichment of organic material (Fertl, 1979).

The pelagic intervals are also visible on the porosity log (Fig. 31) as high-porosity zones, but the porosity variability within the turbidites precludes identification of pelagic units from porosity alone. The higher porosity in pelagics than in turbidites is probably attributable to the much higher clay content in the former. The high porosity in the pelagics causes only slightly lower velocities, probably indicating that higher matrix velocity in the pelagics is reducing the velocity contrast associated with porosity.

Th/K ratio is often a useful indicator of clay type. The majority of the logged interval at this site has Th/K of $5\text{--}8 \times 10^{-4}$. This ratio indicates either an illite or montmorillonite dominance (Fertl, 1979). The potassium concentrations of about 1%–2% are more consistent with illite (3.5%–8.3% for pure illite) than with montmorillonite (0%–0.6%; Serra, 1987). Mica has a high potassium content (consistent with observed values) but too low a Th/K ratio ($<0.7 \times 10^{-4}$) to be the dominant mineral. Probably the log responses result from a mixture of dominant illite and subsidiary other clay minerals. In contrast, the pelagic clays have Th/K ratios that are slightly lower ($2.5\text{--}5 \times 10^{-4}$) and very low K and Th concentrations. These changes could be partly caused by a greater proportion of montmorillonite in the clays, but dilution associated with the 50%–80% nanofossils in the pelagic units also is partially responsible for the very low K and Th concentrations.

Th/K ratio exhibits a large number of spikes to 11 to 14×10^{-4} (Fig. 32). These spikes are present but less noticeable on

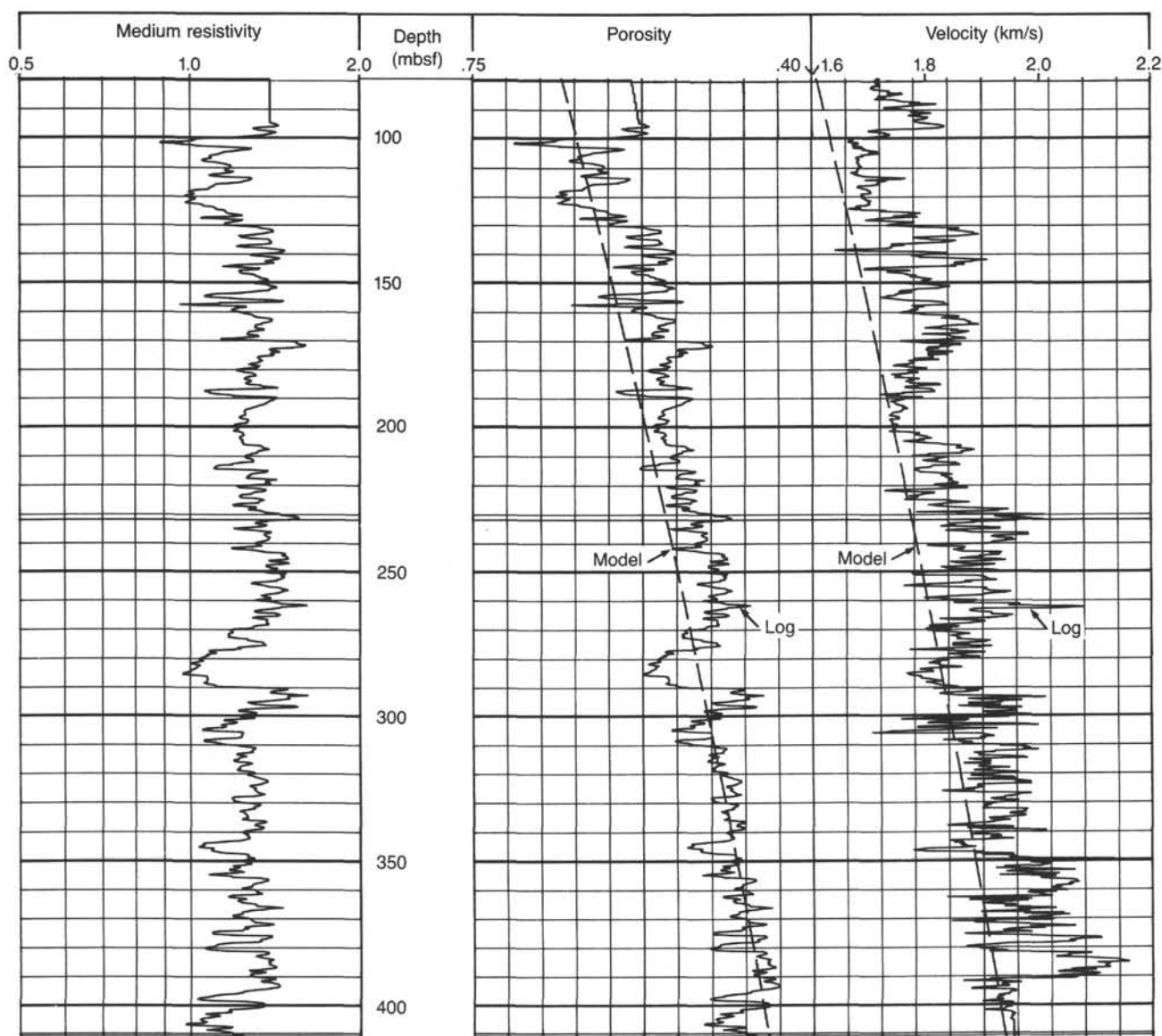


Figure 31. Left: Medium induction resistivity log (ohm-m). Center: Porosity log calculated from resistivity, compared with empirical trend of porosity vs. depth (smooth dashed curve) for terrigenous sediments from Hamilton (1976). Right: Velocity log (km/s), compared with empirical trend of velocity vs. depth (smooth dashed curve) for terrigenous sediments from Hamilton (1979).

the gamma ray log, because the increase in Th is countered by a decrease in K (Fig. 33). Chlorite and kaolinite have Th/K ratios of $10\text{--}18 \times 10^{-4}$ and low K (Serra, 1987).

The changes in clay mineralogy can also be spotlighted by principal components analysis. Using the sonic, porosity, and gamma ray logs after removal of a linear regression trend from each log to minimize the effect of compaction, the first principal component is dominated by clay abundance changes within the turbidites. The second principal component (Fig. 32), accounting for 32% of the covariance, is dominated by the gamma ray term (0.9438) and includes a slight positive correlation with porosity (0.1073) and stronger inverse correlation with velocity (-0.3124). This component appears to respond primarily to clay type. The dominance of a single clay mineral (illite?) and occasional spikes of a second clay mineral (chlorite?) are evident throughout the turbidites, and the different mineralogy of the pelagic sediments is also evident.

The principal components approach provides an independent but less effective detection of the chlorite(?) spikes than the Th/K log. The bridge that trapped the logging tool is the uppermost of these chlorite(?) spikes. More detailed tests of capillary suction time on cores would have been unlikely to detect this anomalous horizon.

Porosity and gamma-ray logs from turbidites often exhibit the characteristic sawtooth pattern of a fining-upward sequence: clay content and porosity increase gradually uphole within each bed or group of beds. Such a pattern is rare at Site 720 (Figs. 31 and 32). Thick intervals of gradually increasing gamma ray response are evident at 104–129 and 190–221 mbsf. In contrast, the Th log does show the sawtooth pattern of gradual upward increase and sharp decrease. For example, the gamma ray unit at 104–129 mbsf is seen on the Th log to be composed of three subunits. This pattern probably indicates a fining-upward sequence, in which increasing clay mineral concentration causes

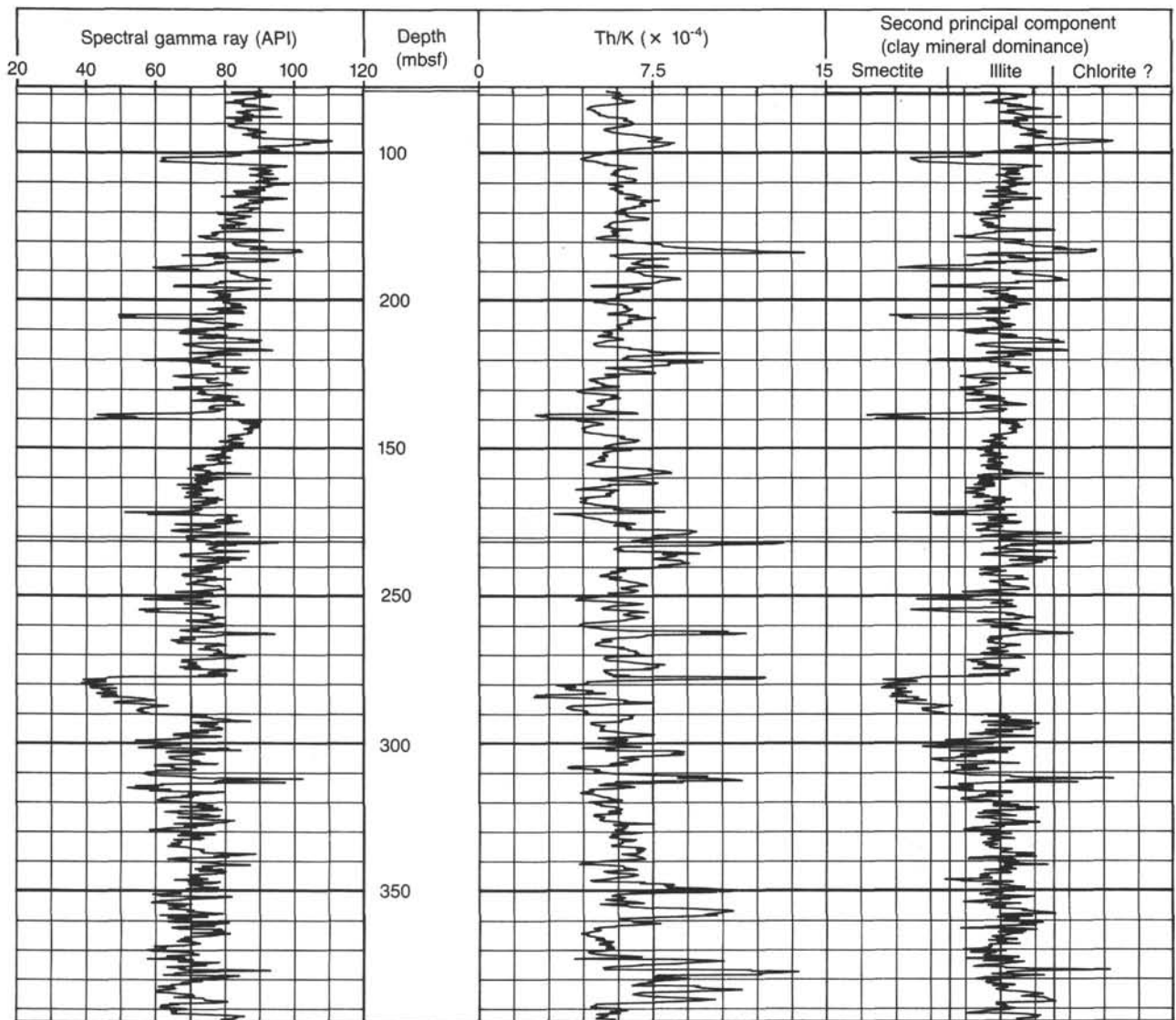


Figure 32. Left: Gamma-ray log (API units). Center: Th/K ratio ($\times 10^{-4}$). Right: Second principal component of porosity, velocity, and gamma-ray covariance. Note the pronounced gamma-ray and principal component spikes toward the left, marking the locations of pelagic beds. Also note the pronounced Th/K and principal component spikes toward the right, indicating turbidite horizons with a very different clay mineral composition (chlorite?). The minerals listed above the three zones on the principal-component log refer to the dominant clay mineral in that zone from the standpoint of log responses; actual clay mineralogy is much more complex.

increasing Th. However, Th is positively correlated with velocity at Site 720, the opposite of the usual pattern of clays being more porous and therefore lower in velocity than silts and sands.

In general, Th seems to be the most effective of the obtained logs for delineation of turbidite beds or packets. In addition to revealing fining-upward sequences, it often shows abrupt shifts to a different baseline value, indicating a significant compositional change. In Figure 33 an identification of the most obvious turbidite bed boundaries is attempted based on Th alone. Fining-upward and coarsening-upward beds are highlighted by heavy curves on the Th log, and long-term trends are highlighted by heavy dashed lines.

Depositional Environments

From near the bottom of the hole (383 mbsf) to 290 mbsf, a relatively uniform depositional environment of turbidites prevails (Fig. 33). Little change in average bed thickness, a predominance of fining-upward sequences, and two relatively well-defined limiting compositions of clayey silt and silty clay are evi-

dent. No pelagic interbeds are detected. Thin chlorite(?) beds top two of the fining-upward sequences, and several chlorite horizons may be present in the interval 373–388 mbsf (Fig. 33). Deposition was probably controlled by overflow from a stable, distant channel. A single major seismic reflector occurs just below this interval at 391 mbsf, associated with a sudden upward decrease in porosity (see “Seismic Stratigraphy” section, this chapter). Because the spectral gamma tool did not reach this depth, the cause of this porosity change cannot be determined from logs.

From 277 to 290 mbsf, a relatively thick pelagic clay interval was deposited. A facies change resulting from a sudden shift of the turbidite channel to a position far from Site 720 is implied. A small seismic reflector is associated with this pelagic unit in the synthetic seismogram (Fig. 27), but it is possible that the associated density drop is larger than assumed.

From 277 to 188 mbsf, the depositional environment at Site 720 was quite variable. Turbidite deposition resumed, interrupted by at least four thin pelagic intervals. Both fining- and coarsen-

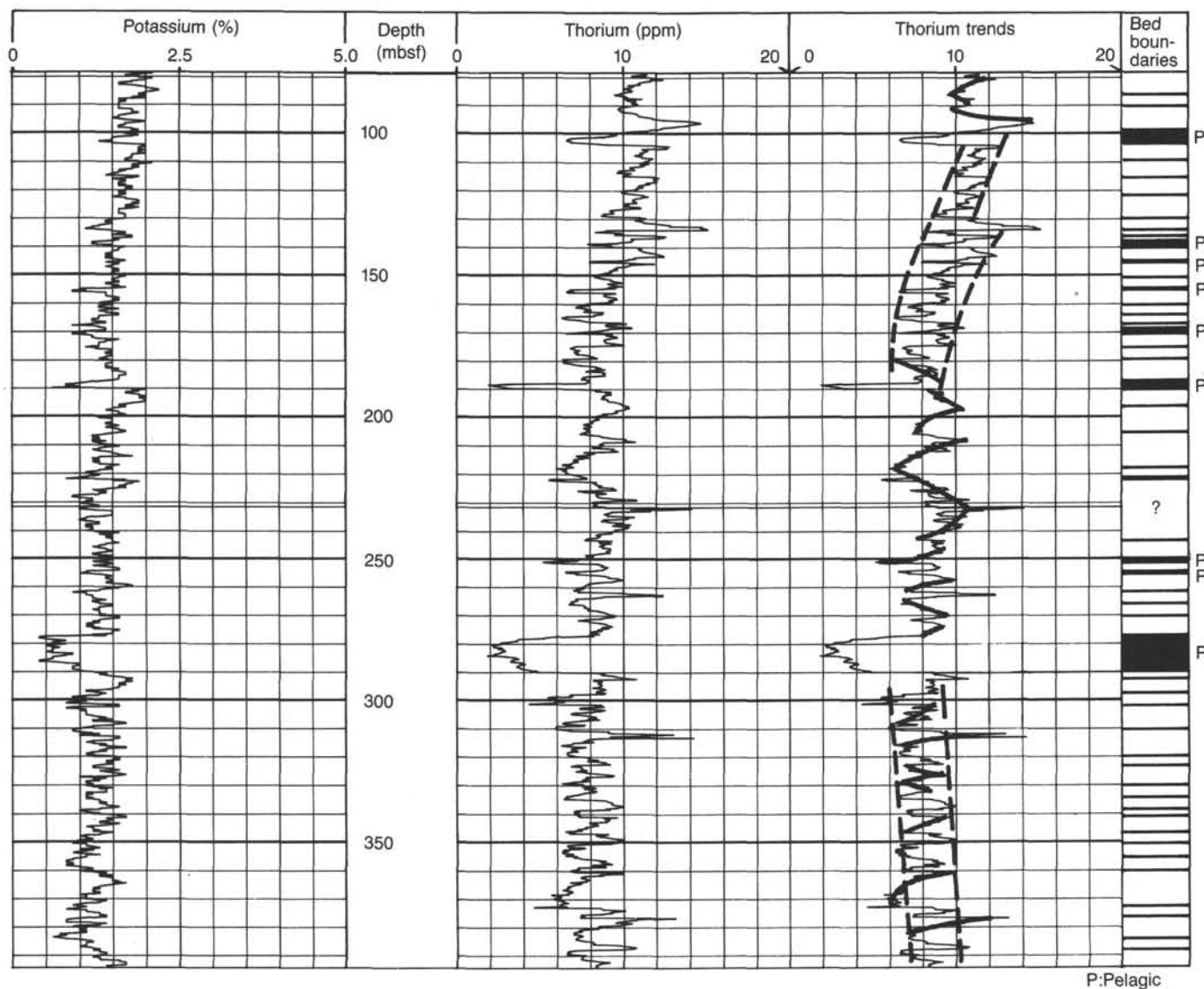


Figure 33. Left: Potassium log (weight percent). Center: Thorium log (ppm). Right: Thorium log with bold-line highlighting of interpreted patterns within a turbidite bed, and with dashed-line highlighting of interpreted long-period patterns. Far right: Probable locations of turbidite bed boundaries based on Th variations, and pelagic interbeds from Figure 32.

ing-upward sequences are present, at first similar in thickness to the lower sequence but later much thicker. Chlorite(?) interbeds occur occasionally, most notably as the first sedimentation after deposition of the pelagic unit and in the interval 226–240 mbsf. The unit is capped by a 32-m-thick claying-upward sequence (based on gamma-ray, Fig. 32) topped by a 2-m-thick pelagic unit, but the Th log shows that this sequence is more complex than a single thick turbidite.

From 188 to 103 mbsf, rhythmic turbidite deposition resumed, but with several characteristic differences from the somewhat similar interval 383–290 mbsf. Again, several thin chlorite(?) beds are present, bed thicknesses are 3–6 m, and fining-upward sequences are common. However, this entire interval shows a general trend toward increasing clay content, as indicated by the potassium and gamma ray logs. An exception is a single setback at 130 mbsf, as indicated by the Th log. The interval 188–130 mbsf, like the interval 220–190 mbsf, shows a smooth fining-upward sequence on the gamma-ray and several smaller fining-upward sequences on the Th log; both are topped by moderately thick pelagic units (2 and 3–4 m, respectively). Log responses

for the entire unit from 188 to 103 mbsf may indicate a period of variable but gradually waning supply from a distant channel. The unit is topped by a pelagic/chlorite(?) pair (like 277–290 mbsf) that creates a seismic reflector.

SUMMARY AND CONCLUSIONS

Site 720 is located on the westernmost part of the Indus Fan, near the boundary between the middle and the lower fan sectors, in a water depth of 4048 m. The Indus Fan is 1500 km long, 960 km across at its widest point, covers an area of over 1.1×10^6 km², and is the dominant physiographic feature of the Arabian Sea. Initiation of Indus Fan deposition is thought to have begun in Oligocene to early Miocene time when the Indian and Asian plates collided and caused major uplift of the Himalayas.

Sediment thickness at Site 720, inferred from seismic reflection and refraction data, is greater than 2000 m. The site lies near magnetic anomaly 25, which indicates a Paleocene basement age of about 60 Ma. The site is about 5 km east of a meandering channel that is 1.5 km wide, 50 m deep, and has a

levee elevation of about 30 m above the surrounding seafloor. Seismic reflection data from the site survey reveal levee complexes of similar size in the subsurface near Site 720 (see "Seismic Stratigraphy" section, this chapter). The location of Site 720 was selected to avoid channel deposits, and thus to maximize the opportunity to collect a relatively continuous depositional record that was related to sea-level changes and the uplift of the Indus Fan source areas in the Himalaya and in Pakistan. The principal objectives of Site 720 were: (1) to recover a continuous upper Neogene section of fine-grained overbank deposits from the middle fan region of the western Indus Fan; (2) to identify the depositional facies, sediment composition, and sediment accumulation rates for comparison with other Indus Fan and Ganges Fan (Leg 116) sites; and (3) to interpret the depositional history of the Indus Fan sediments in terms of uplift of the source region, changes in sea level, changes in climate, circulation, and weathering processes.

One APC/XCB hole was drilled at the site. Hole 720A consists of 3 APC cores that penetrated to 28.6 mbsf with a recovery of 28.44 m (99%), and 40 XCB cores that penetrated from 28.6 mbsf to 414.3 mbsf with a recovery of 60.94 m (16%). Total recovery was 21.6%. The hole was terminated due to poor recovery, and the section was logged successfully from 80 to 380 mbsf with the seismic stratigraphy logging tool.

The stratigraphic section recovered at Site 720 ranges in age from basal Pleistocene to upper Pleistocene and has been divided into two major lithologic units. Unit I (0–17.22 mbsf) is composed of nannofossil and foraminifer-bearing nannofossil ooze that is characteristic of pelagic deposition.

Unit II (17.22–414.3 mbsf) is composed of a wide range of lithologies, including interbedded silty clays, silts, silty sands, sands, and occasional nannofossil oozes; these sediment types are characteristic of turbiditic deposition. Within lithologic Unit II, three facies represent intervals that are characterized by: (1) a high abundance of pelagic (nannofossil) components; (2) fining-upward sequences of mud turbidites and thin- to thick-bedded sandy turbidites with a wide variety of bed thicknesses (<2 cm to >50 cm); and (3) sandy, relatively structureless turbidites with coarse-grained bases >5 cm thick. The pelagic intervals within lithologic Unit II occur at about 52, 62, 100, 125, 150, 179, 185, 285, and 375 mbsf. These pelagic beds are clearly identified on the gamma-ray logs (see "Downhole Measurements" section, this chapter), and some are observed in the seismic sections (see "Seismic Stratigraphy" section, this chapter). The downhole logging data also identify several pelagic intervals within Unit II that were not recovered. The logging results further indicate that most of the unrecovered section was of a turbiditic character.

Within lithologic Unit II, the fan sediments contain relatively high concentrations (average of about 0.4%) of organic carbon that is mostly derived from terrestrial sources as indicated by its pyrolysis character. The sediments are also characterized by complete sulfate reduction below 50 mbsf, its depth being largely a function of high sedimentation rates. Traces of dolomite occur throughout the sequence and are thought to reflect both detrital sources and *in-situ* precipitation. Sediments of Unit II contained 20% detrital calcite and 5% feldspar as observed in the smear slides.

Biostratigraphic and magnetostratigraphic data from the pelagic intervals indicate that the average rates of sedimentation range from 137 to 944 m/m.y. for the turbidite sequence and 32 m/m.y. for the pelagic intervals of Pleistocene age (Fig. 34). If we assume that the pelagic intervals interbedded within the turbidite sequence have the same sedimentation rate as the comparable sediments of lithologic Unit I, i.e., 20–30 m/m.y., then the plot of age vs. depth should have a step-like pattern (the dotted line in Fig. 34) indicating alternating phases of very rapid and slow sedimentation.

The pelagic intervals of nannofossil ooze, notably in lithologic Unit I, display cyclic color changes that are thought to be caused by variations in the CaCO₃ content. Measurements of the magnetic susceptibility of the sediments also detected a cyclic pattern that appears to correlate with calcium-carbonate content. Light-colored CaCO₃-rich layers generally have low susceptibility, while the darker sandy and silty turbidite layers have distinctly higher values. A transition between the pelagic and turbidite facies occurs in the lower part of lithologic Unit I, where susceptibility gradually decreases upsection (see Fig. 17 and "Paleomagnetism" section, this chapter). This trend reflects the decreasing turbidite dilution of the pelagic carbonate sedimentation. The decrease is evident from 28 to 14 mbsf and signifies decreasing turbidite activity in this section of the Indus Fan. Because the top of the ooze (light in color and low in susceptibility) probably corresponds to the last interglacial, low values in the upper 8 m of Hole 720A may be correlated with interglacial conditions. The amplitudes of the fluctuations in the susceptibility are rather large in this upper 8-m interval (Fig. 35). The good correlation of the susceptibility curve with the standard oxygen isotope curve can be used to develop a very detailed curve of sedimentation rates for the uppermost Pleistocene at Site 720 (Fig. 35). The upper and lower parts of sedimentary Unit I may have higher rates because of less compaction and dilution by turbidites, respectively.

The depositional history at Site 720 has been dominated by turbidite deposition with brief interludes that are characterized by an increase in pelagic components. The deposition of the pelagic beds clearly reflects a decrease in clastic influx to the site (see "Lithostratigraphy" section, this chapter, for a discussion) rather than an increase in pelagic sedimentation rate. A decrease in clastic influx could be caused by local, regional, or global mechanisms. For example, highstands of sea level could reduce the clastic flux to the entire fan. This pattern is observed in the Holocene age sediments of the Indus Fan, which are foraminiferal marls and oozes (Kolla and Coumes, 1987). This sea-level mechanism thus produces thin pelagic interbeds with great lateral extent on the fan. Therefore, the timing of pelagic interbeds within a generally clastic fan facies should be coincident with, and controlled by, sea-level and climate variations. Another mechanism that could produce predominantly pelagic deposits on the elevated levee deposits is the abandonment of an active channel. This mechanism would be local in extent (affecting only the active channel levee) and would allow pelagic sediments to accumulate over several sea-level cycles until the channel became active or another channel migrated into the area. The timing of channel switching and abandonment, although difficult to establish precisely, is also likely to be related to increased clastic influx during low or falling sea level. These mechanisms may act separately or in combination to produce the observed thickness and timing of the pelagic intervals observed at Site 720.

In this summary of Site 720, the term "bed" is used to refer to individual turbidites as observed in the lithologic logs. The term "sequence" refers to larger-scale trends, such as fining, that are observed in the downhole logging data and in the seismic data sections. Here, we combine the lithologic, logging, and seismic to interpret the evolution of depositional environments at Site 720.

The lower part of the section (390–290 mbsf, seismic Sequence C) is of early Pleistocene age and has no pelagic interbeds. It is mostly composed of thin- to thick-bedded muddy and sandy turbidites that form upward-fining sequences with relatively uniform thickness. This association is characteristic of active overbank deposition and minor channel migration over an extended period of time. A sharp transition to finer-grained and more pelagic deposition (Core 117-720A-30X, ~277–290 mbsf) probably indicates a major shift in the distributary channel which may be related to differential tectonic motion between

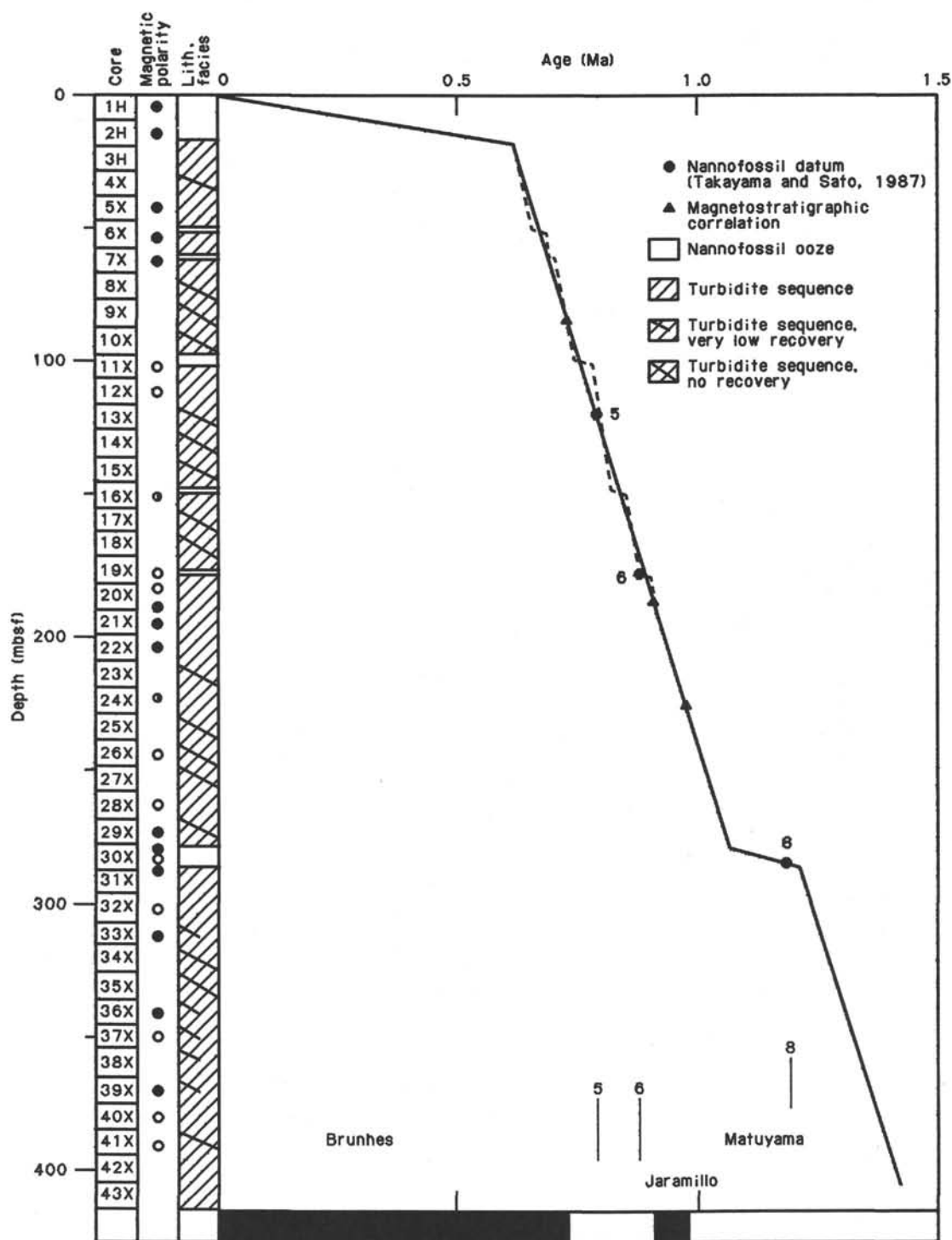


Figure 34. Depth-age diagram of Hole 720A. Vertical columns show core interval, magnetic polarity (solid circle: normal; open circle: reversed; half solid circle: intermediate) and lithologic facies. Bottom column shows standard magnetostratigraphic sequence. Numbers represent nannofossil datum number by Takayama and Sato (1987). Solid line shows average curve of sedimentation rate and dotted line shows changes inferred for pelagic intervals.

the Owen Ridge and the Indus Fan (see "Seismic Stratigraphy" section, this chapter). On the basis of sedimentation rates in similar sediments of lithologic Unit I, this quiescent interval of pelagic deposition may have lasted as long as 300,000 years.

The lower Pleistocene (~1.19 Ma) pelagic interval of Core 117-720A-30X is overlain by sandy thick-bedded turbidites that form both fining- and coarsening-upward sequences from about

277 to 188 mbsf in seismic Subsequence B-2 and B-3. The turbiditic interval is interrupted by at least four pelagic intervals; these are observed in the log data, but were not recovered in the cores. We interpret this interval to represent intermittent deposition by unchanneled sand sheets with occasional quiescent periods of pelagic deposition.

The interval from 188 to 103 mbsf of Subsequence B-1 is

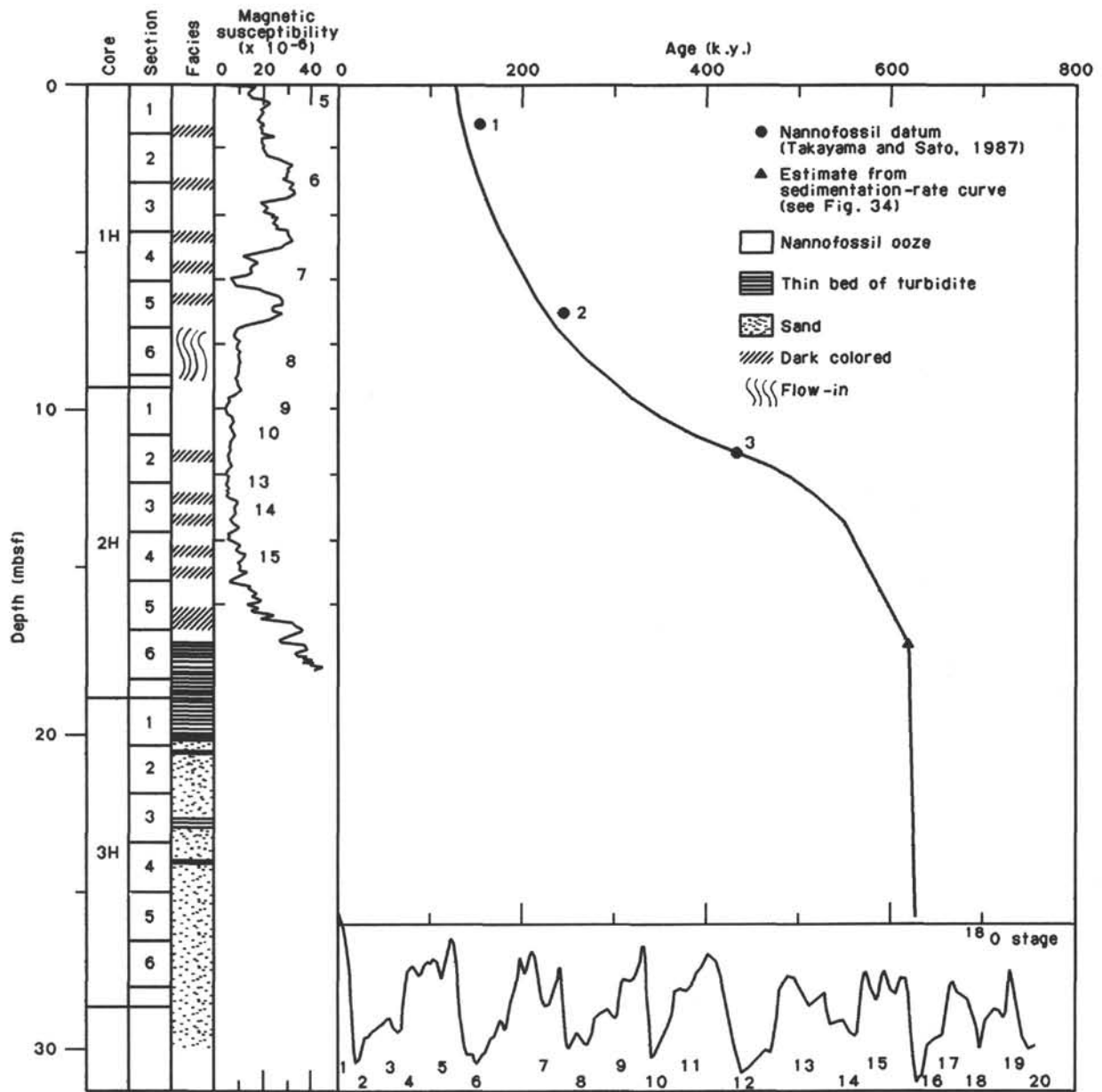


Figure 35. Depth-age diagram of the top part of Hole 720A. Vertical columns show core interval, section interval, lithologic facies, and magnetic susceptibility (number: correlative oxygen isotopic stage). Bottom column shows standard oxygen isotope stratigraphy. Numbers on the diagram represent nannofossil datum number by Takayama and Sato (1987).

characterized by turbidites of variable thickness, numerous thin pelagic intervals, and generally increasing clay content upsection. This interval forms the two large upward-fining sequences observed in the log data (see "Downhole Measurements" section, this chapter). The facies indicates that turbiditic deposition was dominated by large overbank events or sheet flow of thick sands, alternating with a normal overbank-levee environment that accumulated mud turbidites primarily. The upsection increase in clay content could alternatively indicate that the size and frequency of the turbidite events was decreasing.

The upper 100 mbsf at Site 720 (seismic Sequence A) is characterized by further channel switching and abandonment of active channels resulting in several pelagic intervals intercalated with turbiditic sediments. This seismic Sequence (A) thickens toward the Owen Ridge and has abundant buried channels that indicate a rapid infilling over the past 0.7 m.y. (Fig. 34 and "Seismic Stratigraphy" section, this chapter). The most recent

transition from predominantly turbiditic to pelagic deposition (lithologic Unit I) occurs at about 0.5 Ma (17 mbsf). On most submarine fans, late Pleistocene rates of turbidite deposition are generally related to changes in sea level; higher rates are usually observed during low sea-level stands. However, pelagic Unit I of Site 720 does not contain turbidites. Therefore, the temporary lack of terrigenous influx to the site is probably related to switching of the distributary channel away from the site rather than to a general decrease in turbidite deposition on the Indus Fan.

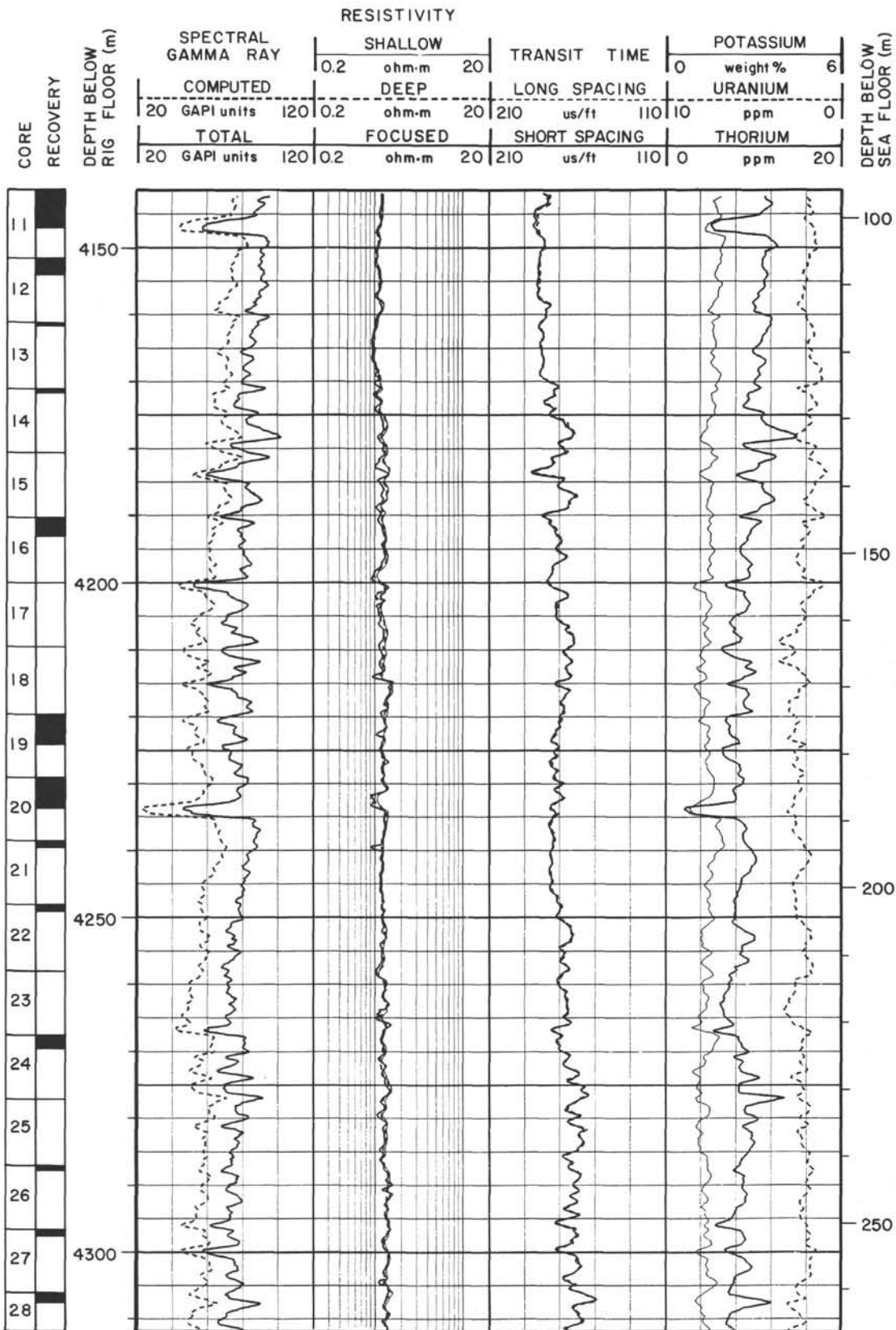
The high rates (> 500 m/m.y.) of Pleistocene turbidite deposition on the Indus Fan are more than twice the rates found by Leg 116 on the distal Ganges Fan. These high accumulation rates are consistent with accelerated uplift and erosion in the Indus source area. However, the lack of a longer record precludes any observations concerning longer-term relations between the rates of uplift and sedimentation on the Indus Fan at Site 720.

REFERENCES

- Archie, G. E., 1942. The electrical resistivity log as an aid in determining some reservoir characteristics. *Trans. Am. Inst. Min. Eng.*, 146: 54-63.
- Arthur, M. A., Srivastava, S., et al., 1987. Site 646. In Arthur, M. A., Srivastava, S., et al., *Proc. ODP, Init. Repts.*, 105: College Station, TX (Ocean Drilling Program), 419-674.
- Barron, J. A., Keller, G., and Dunn, D. A., 1985. A multiple microfossil biochronology for the Miocene. *Geol. Soc. Am. Mem.*, 163:21-36.
- Berggren, W. A., Kent, D. V., and Van Couvering, J. A., 1985. The Neogene: Part 2, Neogene geochronology and chronostratigraphy. In Snelling, N. J. (Ed.), *The Chronology of the Geological Record*: Geol. Soc. Mem. (London), 10:211-260.
- Blow, W. H., 1969. Late Middle Eocene to Recent planktonic foraminiferal biostratigraphy. In Bronnimann, R. and Renz, H. H. (Eds.), *Proceedings of the International Conference on Planktonic Microfossils*: Leiden (E. J. Brill), 1:199-421.
- Bode, G. W., 1974. Appendix II. Carbon and carbonate analyses, Leg 23. In Whitmarsh, R. B., Weser, O. E., Ross, D. A., et al., *Init. Repts. DSDP*, 23: Washington (U.S. Govt. Printing Office), 1131-1135.
- Broecker, W. S., and Peng, T. L., 1982. *Tracers in the Sea*: New York (Eldigio Press).
- Cochran, J. R., Stow, D. A. V., et al., in press. *Proc. ODP, Init. Repts.*, 116: College Station, TX (Ocean Drilling Program).
- Degens, E. T., and Mopper, K., 1976. Factors controlling the distribution and early diagenesis of organic material in marine sediments. In Riley, J. P., and Chester, R. (Eds.), *Chemical Oceanography* (Vol. 6): New York (Academic Press), 59-113.
- Drever, J. I., 1974. The magnesium problem. In Goldberg, E. D. (Ed.), *The Sea* (Vol. 5): New York (John Wiley Press), 337-357.
- Emeis, K., 1985. Particulate suspended matter in major world rivers—II: Results on the rivers Indus, Waikato, Nile, St. Lawrence, Yangtze, Parana, Orinoco, Caroni, and Mackenzie. *SCOPE/UNEP Sonderband*, Mitt. Geol.-Paläont. Inst., Univ. Hamburg, Heft 58:593-617.
- Fertl, H. H., 1979. *Gamma Ray Spectral Data Assists in Complex Formation Evaluation*: Dresser-Atlas.
- Hamilton, E. L., 1974. Prediction of deep-sea sediment properties: state-of-the-art. In Interbitzen, A. L., (Ed.), *Deep-Sea Sediments: Physical and Mechanical Properties*: New York (Plenum Press), 1-43.
- , 1976. Variations of density and porosity with depth in deep-sea sediments. *J. Sediment. Petrol.*, 46:280-300.
- , 1979. Sound velocity gradients in marine sediments. *J. Acoust. Soc. Am.*, 63:909-922.
- Jipa, D., and Kidd, R. B., 1974. Sedimentation of coarser grained interbeds in the Arabian Sea and sedimentation processes of the Indus Cone. In Whitmarsh, R. B., Weser, O. E., Ross, D. A., et al., *Init. Repts. DSDP*, 23: Washington (U.S. Govt. Printing Office), 471-495.
- Johnson, D. A., Nigrini, C., Caulet, J. P., Schneider, D., and Kent, D., in press. Pliocene-Pleistocene radiolarian events and magnetostratigraphic calibrations for the tropical Indian Ocean. *Mar. Micropaleontology*.
- Johnson, D. A., and Nigrini, C. A., 1985. Synchronous and time transgressive Neogene radiolarian datum levels in the equatorial Indian and Pacific Oceans. *Mar. Micropaleontology*, 9:489-523.
- Keller, G. V., 1982. Electrical properties of rocks. In Carmichael, R. S. (Ed.), *Handbook of Physical Properties of Rocks* (Vol. 1): Boca Raton, FL (CRC Press), 217-293.
- Kolla, V., Kostecki, J. A., Robinson, F., and Biscaye, P. E., 1981a. Distribution and origins of clay minerals and quartz in surface sediments of the Arabian Sea. *J. Sediment. Petrol.*, 51:563-569.
- Kolla, V., Ray, P. K., and Kostecki, J. A., 1981b. Surficial sediments of the Arabian Sea. *Mar. Geol.*, 41:183-204.
- Kolla, V., and Coumes, F., 1984. Morpho-acoustic and sedimentologic characteristics of the Indus fan. *Geomarine Lett.*, 3:133-139.
- , 1987. Morphology, internal structure, seismic stratigraphy, and sedimentation of Indus fan. *AAPG Bull.*, 71(6):650-677.
- McHargue, T. R., and Webb, J. E., 1986. Internal geometry, seismic facies, and petroleum potential of canyons and inner fan channels of the Indus submarine fan. *AAPG Bull.*, 70:161-180.
- Martini, E., 1971. Standard Tertiary and Quaternary calcareous nannoplankton zonation. In Farinacci, A. (Ed.), *Proc. II Planktonic Conf.*: Roma (Ed. Technoscienza), 2:739-785.
- Mercier, J.-L., Armijo, R., Tapponnier, P., Carey-Gailhardis, E., and Lin, H. T., 1987. Change from late Tertiary compression to Quaternary extension in Southern Tibet during the India-Asia collision. *Tectonics*, 6:275-304.
- Murray, J. W., 1976. Comparative studies of living and dead benthic foraminiferal distributions. In Hedley, R. H., and Adams, C. G. (Eds.), *Foraminifera* (Vol. 2): London (Academic Press), 45-109.
- Nigrini, C. A., 1971. Radiolarian zones in the Quaternary of the equatorial Pacific Ocean. In Funnell, B. M., and Riedel, W. R. (Eds.), *The Micropaleontology of Oceans*: Cambridge (Cambridge Univ. Press), 443-461.
- Sato, T., Takayama, T., Kato, M., Kudo, T., and Kameo, K., in press: Calcareous microfossil biostratigraphy of the uppermost Cenozoic formations distributed in the coast of the Japan Sea. Part 4: Conclusion. *Sekiyo Gijutsu Kyokaiishi*.
- Serra, O., 1987. *Fundamentals of Well-log Interpretation, (Vol. 2, Part 2; The Interpretation of Logging Data)*: Amsterdam (Elsevier).
- Shanmugam, G., and Moiola, R. J., 1982. Eustatic control of turbidites and winnowed turbidites. *Geology*, 10:231-235.
- Takayama, T., and Sato, T., 1987. Coccolith biostratigraphy of the North Atlantic Ocean, Deep Sea Drilling Project Leg 94. In Ruddiman, W. F., Kidd, R. B., Thomas, E., et al., *Init. Repts. DSDP*, 94, Pt. 2: Washington (U.S. Govt. Printing Office), 651-702.
- Vail, P. R., Mitchum, R. M., Todd, R. G., et al., 1977. Seismic stratigraphy and global sealevel changes. In Payton, C. E. (Ed.), *Seismic Stratigraphy*, AAPG Mem., 26:49-212.
- van Gorsel, J. T., and Troelstra, S. R., 1981. Late Neogene planktonic foraminiferal biostratigraphy and climatostratigraphy of the Salo River section (Java, Indonesia). *Mar. Micropaleontology*, 6:183-209.
- van Morkhoven, F. P., Berggren, W. A., and Edwards, A. S., 1986. Cenozoic cosmopolitan deep-water benthic foraminifera. *Bull. Cent. Rech. Explor.-Prod. Elf-Aquitaine*, Mem. 11.
- Weser, O. E., 1974. Sedimentological aspects of strata encountered on Leg 23 in the Northern Arabian Sea. In Whitmarsh, R. B., Weser, O. E., Ross, D. A., et al., *Init. Repts. DSDP*, 23: Washington (U.S. Govt. Printing Office), 503-519.
- Whitmarsh, R. B., 1974. Some aspects of plate tectonics in the Arabian Sea. In Whitmarsh, R. B., Weser, O. E., Ross, D. A., et al., *Init. Repts. DSDP*, 23: Washington (U.S. Govt. Printing Office), 527-535.
- Whitmarsh, R. B., Weser, O. E., Ross, D. A., et al., 1974. *Init. Repts. DSDP*, 23: Washington (U.S. Govt. Printing Office).
- Winsauer, W. O., Shearin, H. M., Jr., Masson, P. H., and Williams, M., 1952. Resistivity of brine saturated sands in relation to pore geometry. *AAPG Bull.*, 36:253-277.

Ms 113A-104

Summary Log for Hole 720A



Summary Log for Hole 720A (continued)

